Microcoleus* Aerial Monitoring User Guide

Prepared for Envirolink

November 2021

*Microcoleus autumnalis was formerly known as *Phormidium autumnale*

Prepared by:
 Hamish Biggs, NIWA
 Mark Heath, Aquanet
 Anika Kuczynski, NIWA
 Jo Bind, NIWA
 Oonagh Daly, NIWA
 Karl Safi, NIWA
 Susie Wood, Cawthron Institute (Technical Reference Group)

For any information regarding this report please contact:

Dr Hamish Biggs
Hydrodynamics Group
+64-3-343 7843
Hamish.Biggs@niwa.co.nz

National Institute of Water & Atmospheric Research Ltd
PO Box 8602
Riccarton
Christchurch 8011

Phone +64 3 348 8987

Revision	Description	Date
Version 1.0	Draft User Guide	1 December 2021
Version 1.1	Final User Guide	16 December 2021

Quality Assurance Statement		
(signature)	Reviewed by:	Cathy Kilroy
(signature)	Formatting checked by:	Rachel Wright
(signature)	Approved for release by:	Phillip Jellyman
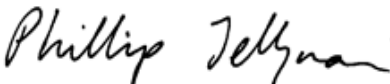
Contents

Tables

Figures

Executive summary

Toxic benthic cyanobacteria pose a significant management problem for regional and unitary councils around New Zealand. *Microcoleus* (formerly *Phormidium*) is widespread and poses a serious health risk to members of the public, pets, and livestock. Monitoring for *Microcoleus* is traditionally performed using underwater viewers for cover, or through biomass sampling. The increased availability of unmanned aerial vehicles (drones) and their use by councils around New Zealand prompted the request for a user guide to be developed, describing the methods required for aerial monitoring of *Microcoleus*. This work was championed by Greater Wellington Regional Council through the Envirolink programme.

This user guide details the equipment, field measurements, biomass ground truth samples, laboratory processing, aerial imagery processing, and data analysis required to perform this work. Most of the methods and equipment included in this user guide are applicable to other remote sensing tasks, and councils around New Zealand may use this guide as a starting reference for other classification and mapping work.

Detailed case studies included in this user guide in the Hutt and Waingawa Rivers demonstrate the potential of these techniques, but also highlight the challenges specific to remote sensing of patchy *Microcoleus* cover through water. Challenges include turbidity, depth, shadows, surface reflections, and the low spectral separability of *Microcoleus* compared to wet bed substrate. If this work is undertaken, then the use of multispectral cameras is recommended, with selection of band pass filters that target wavelengths between 500 and 650 nm.

Detailed aerial monitoring of *Microcoleus* is not trivial and is not expected to replace routine monitoring methods with underwater viewers. However, it does provide a valuable technique for mapping 2D distributions of cover and biomass at the reach scale and is recommended for scientific studies investigating the environmental drivers of *Microcoleus* growth and removal.

The use of drones for recording aerial imagery of *Microcoleus* (but without detailed processing and ground truth sampling) also provides a useful tool for communicating risks to the public, and it is possible to roughly estimate cover by comparing aerial imagery with reference images of cover levels.

This user guide describes techniques for combining biomass sampling and cover assessments (either from aerial imagery or distributed underwater views) to provide a more rigorous assessment of the abundance of *Microcoleus* at the reach or river scale. This information can help to inform overall risk to river users from either attached mats, or downstream risk from detachment, drift, and accumulation along riverbanks.

1   Introduction

The increased availability of unmanned aerial vehicles (drones), and their use by councils around New Zealand, prompted the request for a user guide to be developed describing the methods required for aerial monitoring of the benthic toxic cyanobacterium *Microcoleus autumnalis* (formerly *Phormidium autumnale*) (Oscillatoriales) in rivers. *Microcoleus* is problematic in rivers around New Zealand, but particularly so in the waterways managed by Greater Wellington Regional Council (notably the Hutt River). Preliminary progress on *Microcoleus* aerial monitoring was made by Hempel et al. (2014), however more detailed information was needed to apply these techniques at the river reach scale and to incorporate more advanced remote sensing methods and hardware. Further development was also needed to link measurements of *Microcoleus* cover to total *Microcoleus* biomass at the river scale. This is because *Microcoleus* cover is not only patchy in distribution, but mats are also variable thickness and variable taxonomic composition. Thus, this user guide provides detailed methods for assessing both *Microcoleus* cover and biomass at the river scale.

1.1   Why is *Microcoleus* a problem?

The benthic cyanobacterium *Microcoleus* (formerly *Phormidium*) (Oscillatoriales) forms brown/black benthic mats (Figure 1-1), which can be highly toxic. Proliferations of *Microcoleus* are widespread in New Zealand rivers and pose a significant management problem for regional and unitary councils (MfE and MoH, 2009; Heath et al. 2010; Quiblier et al. 2013; Wood et al. 2015; Heath and Greenfield, 2016; McAllister et al. 2016; Wood et al. 2018). Ingestion of *Microcoleus* has led to the death of more than 100 dogs (Hamill, 2001; Wood et al. 2007; Wood et al. 2017) and is a health risk to humans and livestock (Mez et al. 1997; Scott and Marcarelli, 2012; Quiblier et al. 2013).

Figure 1-1:   Left: *Microcoleus* cover in Hutt River. Right: Underwater image of a *Microcoleus* mat.

Microcoleus blooms are hard to monitor as they rapidly proliferate and can quickly transition from containing low levels of toxins to producing high quantities of potent neurotoxins (e.g., anatoxins) (Quiblier et al. 2013; McAllister et al. 2016; Wood et al. 2018; Wood et al. 2020). The risk due to *Microcoleus* is also not localised to where it grows. Large and small fragments from high biomass blooms can slough off the riverbed and drift downstream to accumulate at the river margins, where they are particularly accessible to dogs and children.

1.2   Limitations of current *Microcoleus* monitoring

Interim guidelines for managing cyanobacteria in recreational fresh waters were released in 2009 (MfE and MoH, 2009) and reviewed in 2018 (Wood et al. 2018). These guidelines recommended a 3-tier alert system for benthic cyanobacteria, requiring instream surveys of *Microcoleus* cover (usually at 'high risk' recreational sites). However, its effectiveness at identifying risks to recreational users has been questioned (Heath, 2018). Most of the problems arise from the patchy distribution of *Microcoleus* mats at the reach and river scales, as well as the variable of thickness mats (Wood et al. 2010; Heath et al. 2011; Heath et al. 2012; McAllister et al. 2018). As a result:

A.   The true extent of cover within sites can be missed during routine monitoring that is generally restricted to transect-based spot observations.

B.   The true extent of cover within longer river reaches can be missed because monitoring is restricted to wadable (or partly wadable) sections at selected recreation sites.

C.   Risks often arise from detachment and drift of upstream mats, which then accumulate on riverbanks where they are accessible to river users and dogs. Thus, the upstream biomass of *Microcoleus* is important, as well as localised cover.

D.   The thickness and taxonomic composition of *Microcoleus* mats is variable, with toxin production risks being dependent on total *Microcoleus* cells and biomass present (rather than just cover).

These issues can lead to significant over/underestimates of actual *Microcoleus* cover and biomass, with underestimates having potentially significant consequences for assessment of health risks (Heath, 2018). This variability in *Microcoleus* monitoring results, compared to actual cover and biomass at the river scale, can make it challenging to assess long term state and trends, or to determine relationships with abiotic and biotic factors (drivers). The development of monitoring techniques to assess *Microcoleus* cover at larger spatial scales and to quantify *Microcoleus* biomass are needed to address these issues.

1.3   *Microcoleus* Aerial Monitoring (MAM)

Aerial monitoring provides the ability to assess cover of classes of interest at larger spatial scales (Husson et al. 2016; Biggs, 2020). Aerial monitoring can also be an important communication tool, since aerial images, videos and orthomosaics can be shown to the public to inform them of the danger posed by *Microcoleus* and what to watch out for (e.g., *Microcoleus* segment on TV3 news 16/02/2019 - Dr Mark Heath).

The key steps of the process are to: (1) record aerial imagery, (2) process aerial imagery into a georeferenced orthomosaic (2D map), (3) classify aerial imagery to assess *Microcoleus* cover, (4) quantify the accuracy of classifications from ground truth data, (5) calculate *Microcoleus* biomass at the reach and river scale from ground truth data. Steps 1 to 3 are compulsory, while step 4 will be needed occasionally to verify classification accuracy, and step 5 is optional depending on the required outputs from the survey. Input imagery may be recorded with an entry level Red Green Blue (RGB) camera, mid-range multispectral camera, or high-end hyperspectral camera. Likewise, suitable aircraft vary from small consumer grade drones to manned helicopters. Selecting a suitable system for MAM is a trade-off between cost, complexity, and classification accuracy.

This user guide provides detailed advice on how to perform MAM with RGB, multispectral and hyperspectral cameras. It covers: aerial monitoring equipment selection and setup (Section 3); aerial monitoring missions to collect aerial imagery (Section 4); *Microcoleus* ground truth sampling and sample processing (Section 5); aerial imagery processing to generate georeferenced orthomosaics (Section 6); aerial imagery classification, interpretation and error analysis (Section 7); linking ground truth data with image classifications to calculate cover and biomass at larger spatial scales (Section 8); detailed case studies of *Microcoleus* Aerial Monitoring in Greater Wellington Regional Council (GWRC) rivers (Sections 9 and 10); future outlook for practical implementation of MAM and progressing MAM to routine monitoring (Section 11); conclusions and recommendations (Section 12); a glossary for acronyms and technical terms (Section 14). Supplementary appendices provide useful workflows for councils such as: a workflow for recording and processing RGB aerial imagery (Appendix A); a workflow for recording and processing multispectral aerial imagery (Appendix B); a workflow for recording and processing hyperspectral aerial imagery (Appendix C); reference images of *Microcoleus* cover and levels (Appendix D); and an example council decision tree for *Microcoleus* monitoring (Appendix E).

This user guide also provides advice on monitoring at a range of levels of detail and deployment complexity. For example, monitoring strategies using underwater viewers (Section 11.1), or by comparison of aerial imagery with reference images of cover levels (Appendix D).

1.4   *Microcoleus* cover and biomass

Currently *Microcoleus* risks are assessed based on estimates of percentage riverbed cover (MfE and MoH, 2009). Aerial surveying with drones is well suited to quantify cover, however downstream risks due to *Microcoleus* drift are also dependent on total upstream biomass. This is because *Microcoleus* will routinely slough off rocks, drift downstream and accumulate at river margins. A larger river (with suitable habitat) can grow more biomass than an equivalent smaller river, and this biomass can accumulate more densely at river margins, posing a greater risk to the public due to the increased possibility of exposure. For this reason, and to ground truth *Microcoleus* classifications in aerial monitoring, it can be very beneficial to collect samples and quantify biomass. Biomass sampling may also provide an early indication (forecast) of whether there may be a future high-risk public health problem (mass sloughing event). The limitation of biomass sampling is the time and cost to process the samples. Thus, biomass sampling is not likely to be part of routine (i.e., weekly) monitoring by councils but may be beneficial to undertake less frequently (i.e., monthly). For scientific studies quantifying *Microcoleus* abundance in detail, biomass sampling is highly recommended.

This user guide provides methods for collecting and processing *Microcoleus* biomass samples. Biomass samples are most commonly (affordably) analysed for ash-free dry mass (AFDM), or chlorophyll *a*. In situations where high accuracy is required (such as for scientific studies, or critical river management decisions), it is recommended to analyse the taxonomic composition of samples to determine what proportion of biomass is made up of *Microcoleus*. This user guide provides details of these methods, as well as field data on pigment analysis and reflectance spectra for selection of band pass filters for multispectral cameras, which may be useful for more detailed assessment.

2 Where, when, and how to use *Microcoleus* Aerial Monitoring

Microcoleus aerial monitoring is not a 'one size fits all' approach and will not replace transect based surveying. This is because there are many sites where aerial monitoring is not feasible (e.g., due to lack of water clarity, excessive depth, proximity to airfields, overhanging riparian vegetation, powerlines, high wind, lack of landowner permission and other issues). The collection of aerial imagery (and potentially ground truth samples) is relatively quick, however the time (and cost) of detailed data processing is substantial and likely beyond the scope of routine monitoring. Thus, MAM should be treated as one of several tools in the environmental monitoring arsenal of councils and scientists around New Zealand. Simplified variations of MAM are discussed in Section 11.1 and Section 11.2, which may be more practical to implement, but likely provide lower accuracy than the full workflow presented in this user guide. These alternatives include visual comparison with reference cover levels (Appendix D). The envisaged sites and scenarios suitable for MAM are detailed below.

2.1 Where to use MAM

- Sites with shallow (i.e., < 1 m deep) clear water where *Microcoleus* is easily visible;

- Sites that comply with Civil Aviation Authority (CAA) rules and restrictions on drone flights (e.g., more than 4 km from an airfield, and with landowner/administrator permission);

- Sites without substantial overhanging riparian vegetation;

- Sites where drones can be safely launched and landed, and operators are able to maintain continuous visual line of sight observation of the drone during the flights.

2.2 When to use MAM

- If *Microcoleus* cover is very spatially heterogeneous and routine monitoring transects are providing inaccurate/unrepresentative estimates of cover at the river scale;

- If detailed quantification of *Microcoleus* cover (and potentially biomass) is needed, such as for scientific studies, or possibly when approaching transitions in alert levels;

- If aerial imagery of *Microcoleus* cover is needed to better convey risks to the public (e.g., media releases, Land, Air, Water Aotearoa (LAWA) and social media channels);

- Deployments should occur when river levels are low and water is clear. There should also be minimal cloud cover to avoid reflections (Biggs, 2020) and maintain good illumination of the riverbed with minimal shadows. Deployment times between 10 am and 3 pm are recommended.

2.3 How to use MAM

- For rapid estimation of *Microcoleus* cover, it is recommended to fly the study reach with a RGB camera and compare the collected images with cover levels in Appendix D of this user manual;

- For detailed quantification of *Microcoleus* cover, it is recommended to follow the workflow in Appendix A (RGB Cameras) or Appendix B (multispectral cameras) of this user guide. In summary:

- Deploy Ground Control Points (GCPs) throughout the study reach, fly the study reach with a RGB or multispectral camera, collect ground truth samples, survey the locations of GCPs and ground truth samples, process the aerial imagery to generate a georeferenced orthomosaic, perform classifications of the orthomosaic to get cover, use the ground truth sample GPS coordinates to validate/check the accuracy of the *Microcoleus* cover classification;

- To obtain biomass, process the ground truth samples for AFDM (and potentially undertake microscopy work for taxonomic composition), combine the ground truth and cover data to estimate biomass throughout the study reach. Divide this by the length of the study reach to obtain biomass per unit channel length.

- The deployment of hyperspectral imaging systems is not recommended for routine monitoring and most scientific studies. These systems are expensive, challenging to deploy and require advanced post processing techniques for data analysis (see Section 6.3). However, they are useful for applications where reflectance spectra, or classifications of a wide range of classes are required.

3 Aerial monitoring equipment

3.1 RGB Cameras

3.1.1 RGB camera selection

Red Green Blue (RGB) cameras are the standard digital cameras used for photography. They are affordable and easy to use, however not all RGB cameras are suitable (and convenient) to use for aerial surveying. The objective of aerial surveying is to generate a georeferenced orthomosaic (basically a 2D photo map) of the site. To achieve this requires dedicated software (such as Agisoft Metashape, or Pix4D) and quality input imagery.

- Images should be well illuminated, crisp (not blurry) and have constant zoom (prime lens is preferable but fixing a zoom lens at a specific setting is also a viable option);

- Cameras should also be mounted in a gimbal to maintain a vertical orientation;

- Ideal cameras will have a large sensor, high quality rectilinear prime lens, and the ability to operate with wide aperture (for low lighting conditions);

- It is also critical that camera settings such as shutter speed can be controlled to avoid image blur (which will occur at slow shutter speeds);

- The use of action cameras, which often have fish-eye lenses and limited control of image settings, are not recommended (Figure 3-1a).

Light weight integrated camera/gimbal modules (Figure 3-1b,c) are the most convenient for aerial surveying, and offer many advantages over high end digital cameras such as the Fujifilm GFX100 (Figure 3-1d), even though it has a much larger 100+ Megapixel (MP) sensor. The problem with large, high-resolution digital cameras is their weight (plus the weight of a suitably large gimbal for them), which increases the size of drone needed to carry them, decreases flight times (and thus spatial coverage) for each battery set, and increases overall mission complexity.

Thus, simple integrated aerial surveying cameras such as the DJI Phantom 4 Pro Camera and DJI X5S are recommended (Table 3-1). For nadir aerial imagery (i.e., pointing straight down) the use of polarising filters for recording through water imagery is not recommended (Biggs, 2020). The cost of a DJI Phantom 4 Pro Unmanned Aerial Vehicle (UAV) and integrated RGB camera/gimbal module is less than $4,000 NZD.

Figure 3-1: **(a) GoPro Hero 7 Black Action Camera, (b) DJI Phantom 4 Pro Camera, (c) DJI X5S Camera, (d) Fujifilm GFX100.**

Table 3-1: **Examples of specifications for RGB cameras and which are appropriate for MAM.**

	GoPro Hero 7 Black	**DJI Phantom 4 Pro Camera**	**DJI X5S Camera**	**Fujifilm GFX100**
Sensor Resolution (MP)	12	20	20.8	101.7
Weight (g)	116	~300	461	1400 + Lens + Gimbal
Advantages	None	Affordable. Includes gimbal. Seamless integration with drone for aerial surveying.	Includes gimbal. Choice of lenses. Seamless integration with drone for aerial surveying.	Very high resolution. Selection of high-quality lenses.
Disadvantages	Fish-eye lens distortion. Needs gimbal. Not designed for external control of camera settings, capture triggering etc.	None	None	Weight of camera, lens and gimbal over 4 kg. Price.
Suitable for MAM?	No	Yes	Yes	Yes, but not recommended
Suitable quadcopters	-	DJI Phantom 4 Pro	DJI M200/210 DJI Inspire 2	DJI M600 Aeronavics Skyjib

---

3.1.2   RGB camera spectral response and colour spaces

For *Microcoleus* aerial monitoring with RGB cameras, it is important to understand the basics of sensor spectral responses and colour spaces. RGB cameras have a broad spectral response as a function of wavelength (Figure 3-2) with substantial overlap between channels. To derive 'colour' information from RGB data it is not possible to simply analyse one channel, but the relative values of all 3 channels must be considered. For example, white light is observed when the red, green and blue channels are all high, while the colour red will be observed when the red channel is high, but green and blue are both relatively low. For image analysis of RGB data it can be convenient to convert imagery to another colour space (such as HSV or CIELAB) where colour is separated from brightness (Schanda, 2007; Ibraheem et al. 2012; Richards, 2013). It is possible to undertake target specific detection from RGB data when a significant spectral difference occurs between objects of interest and the background, such as the detection of a red barn on a green field, however it can be challenging to resolve more subtle spectral differences and perform detection to species level.
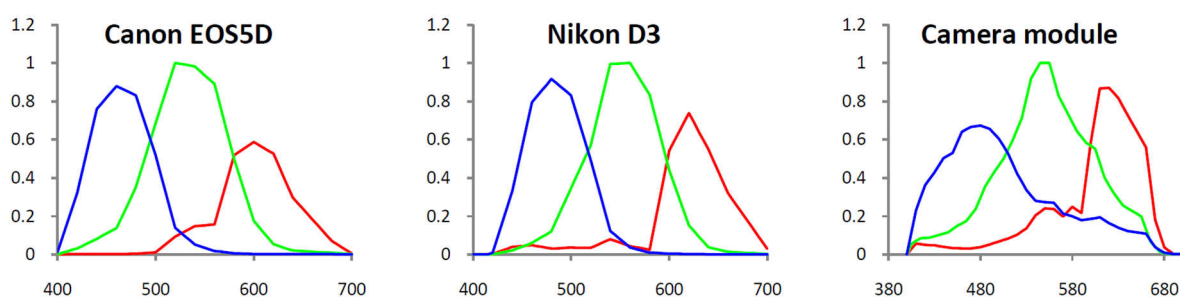
Figure 3-2:   Spectral responses of RGB cameras: Canon EOS5D, Nikon D3 and cell phone camera module (Cao et al. 2009).

3.1.3   RGB camera setup

In the last decade there has been a huge improvement in drone technology and integrated RGB cameras. Today, most RGB aerial surveying is performed with combined camera and gimbal modules, such as the DJI Phantom 4 Pro Camera, or DJI X5S Camera. These are very light weight (enabling long flight times) and integrate seamlessly with the drone hardware. This enables rapid system set up/assembly and easy to access camera settings in flight applications (such as DJI Go 4). These camera systems also integrate seamlessly with software for setting automated flight paths, for example DJI Ground Station and the '3D Map Area' feature.

To collect quality aerial imagery, it is critical to fly with suitable camera settings (Biggs, 2020). Failure to do this can result in motion blur, over/under exposed imagery, and out of focus imagery. The recommended camera settings are:

- Shutter priority mode with 1/1000 shutter (or 1/1600 in bright lighting conditions);

- Focus: auto, or manual infinity;

- Aperture: auto;

- ISO: auto.

Fast shutter speeds are the most critical parameter to avoid blurry imagery. Setting aperture to auto will allow the camera control software to adjust aperture to maintain sufficient sensor illumination

(incoming light) as ambient lighting conditions change (e.g., time of day, variable cloud cover etc). If the widest aperture setting is reached (i.e., in very low light conditions), the camera starts to increase ISO to compensate. For drone surveys (usually above 30 m) wide aperture does not result in depth of field issues (the river is approximately a 2D surface) and auto focus (or manual focus at infinity) is suitable. Flight speeds, altitudes, imagery overlap, and other relevant settings are discussed in Section 4.3.

3.2 Vis-NIR and multispectral cameras

3.2.1 Vis-NIR and multispectral camera selection

Visible to Near InfraRed (Vis-NIR) and multispectral cameras have much narrower spectral responses than the broad 'colour' bands of RGB cameras. This enables Vis-NIR and multispectral cameras to be selected that target specific absorption or reflection peaks of classes of interest. For example, pigments commonly present in cyanobacteria (i.e. phycobiliproteins) provide a potential means to identify cyanobacteria (Rowan, 1989). Specific absorption peaks can then be targeted for detection with multispectral cameras (Table 3-2). Vis-NIR cameras are also commonly known as Red Green Near-InfraRed (RGN) cameras.

Table 3-2: Absorption spectrum of common cyanobacteria pigments (Saini et al. 2019).

Pigment	Absorption maxima (nm)
Chlorophyll-*a*	430, 660
Phycoerythrin	550
Phycocyanin	610
Phycoerythrocyanin	560-600
Allophycocyanin	650–660
β-Carotene	425, 450, 480

When selecting Vis-NIR and multispectral cameras (Figure 3-3), there are several important considerations. Vis-NIR cameras typically have one sensor and lens, with a compound filter that restricts transmitted light to three narrow bands, rather than the three broad bands of RGB. This contrasts with multispectral cameras which typically have an array of camera sensors and lenses, with different band pass filters for each.

Since Vis-NIR cameras only have one lens and sensor they can be very light weight and cost effective (e.g., Mapir Survey 3W RGN Figure 3-3a). Having only one lens and sensor also provides image data with the same origin and orientation, which simplifies post processing and generation of georeferenced orthomosaics in software such as Agisoft Metashape, or Pix4D. RGN cameras provide data well suited for computing simple indices, such as Normalised Difference Vegetation Index (NDVI) and Normalised Difference Water Index (NDWI):

$$NDVI = \frac{\phi_{nir} - \phi_{red}}{\phi_{nir} + \phi_{red}} \qquad\qquad NDWI = \frac{\phi_{green} - \phi_{nir}}{\phi_{green} + \phi_{nir}}$$

where ϕ is the brightness of a pixel in a specific colour band. NDVI provides an indication of the presence of vegetation, while NDWI provides an indication of soil moisture (Richards, 2013). Metrics such as NDVI and NDWI can be convenient for general aerial surveying and broad scale classifications, however they are not suitable for finer scale classification tasks such as identification of a single species of vegetation.

The main downside of Vis-NIR cameras such as the Mapir Survey 3W RGN is that they only provide 3 channels of data and the specific wavelengths of light that are transmitted (through the internal band pass filters) are not usually selectable by the customer, limiting the development of target specific detection systems.

Multispectral cameras with arrays of sensors and filters (Figure 3-3b,c,d) provide more channels of data for aerial classification tasks. Cameras such as the Parrot Sequoia (Figure 3-3b) come with prescribed filters for detecting in specific spectral bands Table 3-3, while other cameras such as the Mapir Kernel (Figure 3-3d) are highly customisable and offer a wide range of band pass filters (Table 3-3, Figure 3-4). The Mapir Kernel also offers monochrome sensors with much higher resolution (3.15 MP) compared to the Parrot Sequoia and Hiphen Airphen (1.23 MP), plus a faster image capture rate (2 vs 1 Frames Per Second (FPS)) allowing surveys of much larger areas, since it can be flown at higher altitude and with faster flight speeds to obtain the same ground sample distance.

One downside of both Vis-NIR and particularly multispectral cameras is that the band pass filters let through less light (i.e., a narrow spectral band) compared to the broad bands of RGB. This means that these types of cameras are usually unable to use as a high shutter speed as RGB cameras, and hence may need to be flown at slower speeds to reduce motion blur. Whether this is an issue will depend on solar illumination (i.e., bright sunny day vs cloudy) and the specific model of camera flown.

To develop a multispectral target detection system, it is important to know the reflectance spectrum of the target of interest. This can be obtained with a handheld spectrometer, or an aerial hyperspectral camera system. The use of an aerial hyperspectral camera system is advantageous because it also captures data on other objects (or species) that commonly occur in close proximity to the target of interest. This enables the selection of specific wavelengths that provide a spectral response that is unique to the target of interest and will facilitate detection. Combining this information with the wide range of filters available for cameras such as the Mapir Kernel can enable the development of light weight and relatively affordable detection systems.

Some final considerations when selecting a suitable multispectral camera are: (1) GPS is highly recommended; (2) a downwelling irradiance sensor (or calibration tarpaulin) to obtain reflectance (invariant of lighting conditions) rather than radiance is recommended; (3) camera compatibility with software that will align the imagery and generate a georeferenced orthomosaic is essential (since multispectral cameras have multiple lenses and sensors, which all have a different origin and orientation). This issue is not trivial to solve and it is essential that suitable software is offered by the manufacturer or a partner organisation.
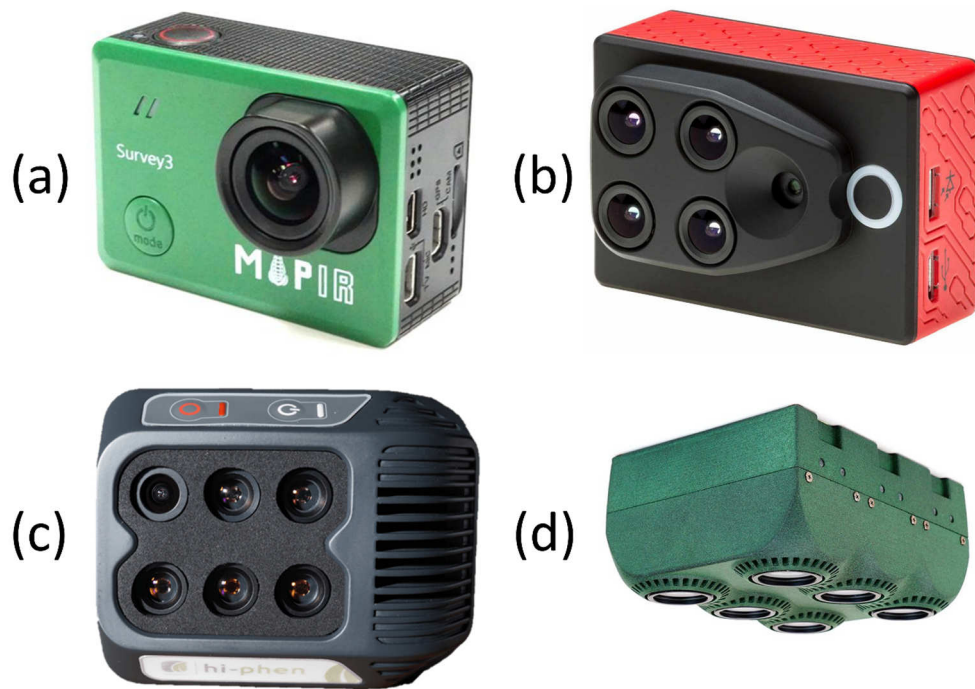
Figure 3-3: (a) Mapir Survey 3W RGN (Red, Green, Near Infrared), (b) Parrot Sequoia, (c) Hiphen Airphen, (d) Mapir Kernel.

Table 3-3: Key specifications of selected Vis-NIR (i.e., RGN) and multispectral cameras.

	Mapir Survey 3W RGN	Parrot Sequoia	Hiphen Airphen	Mapir Kernel
RGB Camera Included (Y/N)	N	Y	N	Y
RGB Sensor Resolution (pixels)	N/A	4608 × 3456	N/A	4384 × 3288
Number of multispectral bands	3	4	6	5 or 6 *RGB Camera is optional
Available bands (nm) ± Bandwidth (nm)	550 ± 20, 660 ± 20, 850 ± 30 *Bandwidth was not quoted for Mapir Survey 3W RGN, so was estimated from RGN filter for Mapir Kernel.	550 ± 20, 660 ± 20, 735 ± 5, 790 ± 20	450 ± 5, 530 ± 5, 570 ± 5, 622 ± 5, 675 ± 5, 710 ± 5, 730 ± 5, 750 ± 5, 850 ± 5 *Bandwidth quoted as FWHM, so functional bandwidth is likely >2x this value.	407.5 ± 7.5, 455 ± 10, 491 ± 41, 517 ± 19, 546.5 ± 11.5, 589.5 ± 25.5, 625 ± 49, 632.5 ± 7.5, 654 ± 11, 686 ± 12, 724.5 ± 7.5, 780 ± 30, 809 ± 9,850 ± 15, 878.5 ± 26.5, 935 ± 30, 945 ± 4 *Bandwidth quoted as FWHM, so functional bandwidth is likely >2x this value.
Bands user selectable	N	N	Y	Y

	Mapir Survey 3W RGN	Parrot Sequoia	Hiphen Airphen	Mapir Kernel
Sensor resolution of monochrome bands (pixels)	4000 × 3000	1280 × 960	1280 × 960	2048 × 1536
Mass (g)	75.4	72.0 (camera) + 35.0 (sunshine sensor)	200	~400
Max framerate (FPS)	0.67	1	1	1 (RGB), 2(Mono)
GPS tagging of images available	Y	Y	Y	Y
Downwelling irradiance sensor offered for reflectance spectra	N	Y	N	N
Extra features of interest	Single lens camera with GPS tagged images provides data that is simple to process into georeferenced orthomosaics.	Well integrated with Pix4D. Downwelling irradiance sensor offered for reflectance spectra. This is very significant.	Plugin offered for Agisoft Metashape to generate georeferenced orthomosaics.	14.3 MP RGB camera is optional. 4 filters are also offered for the RGB camera. Lenses/FoV user selectable. MAPIR work in partnership with Agisoft and Pix4D, however there is currently a lack of documentation about the methods for generating georeferenced orthomosaics from Kernel camera images.
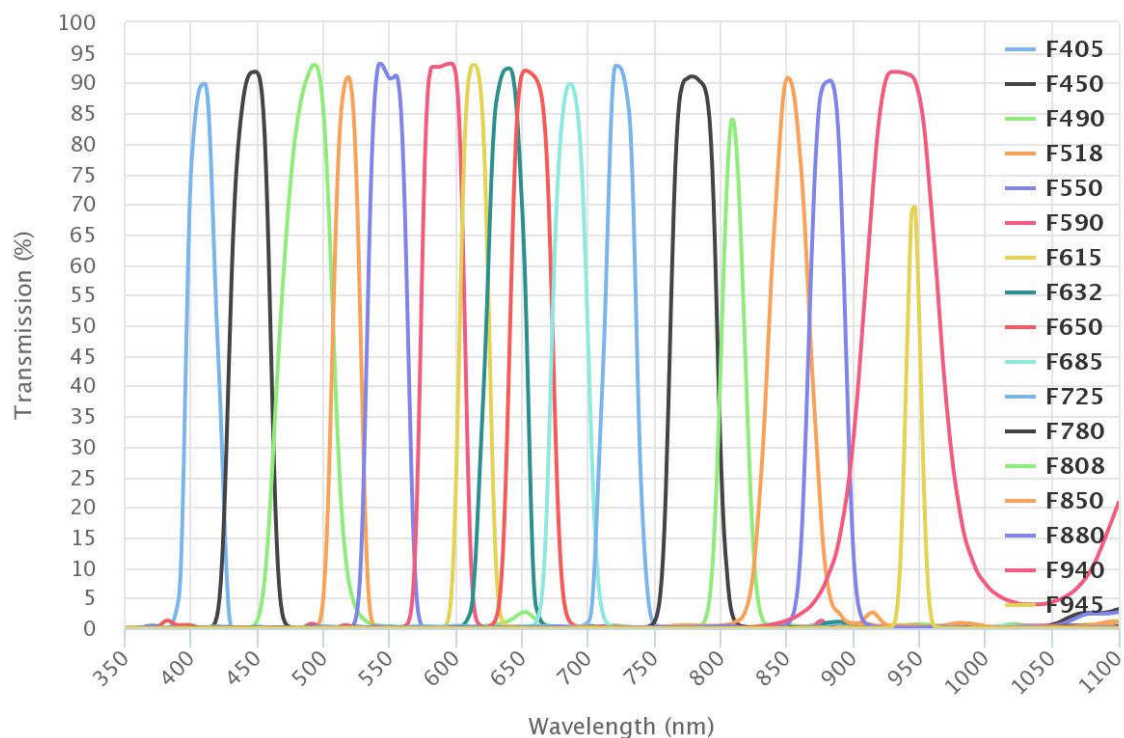
Figure 3-4: **Mapir Kernel: Transmission characteristics of the 17 available monochrome filters.**[1]

3.2.2 Vis-NIR and multispectral camera setup

Currently few Vis-NIR or multispectral cameras are available as integrated camera and gimbal packages. Likely this will change in the future, but for now these cameras are usually mounted in a generic gimbal. At NIWA, we fly our RGN and multispectral cameras together in a DJI Ronin MX Gimbal (Figure 3-5a) on a DJI Matrice 600 drone (Figure 3-5b). The cameras are both powered by the gimbal battery and log to internal SD cards. Both cameras are usually set up in time lapse mode and run independently from the drone. Flight speed, altitude, and flight line spacing are all set to match the field of view and frame rate of the cameras. An aerial imagery and flight parameter calculator written by the lead author of this user guide is freely available upon request.

It is also possible to trigger operation of some models of multispectral cameras from the drone flight controller. This has benefits such as only recording images at waypoints where necessary but adds to the overall hardware complexity.

---

[1] Reproduced from https://www.mapir.camera/pages/kernel-filters

Figure 3-5:   **(a) Mapir survey 3W and Airphen multispectral cameras mounted on a DJI Ronin MX Gimbal. (b) Ronin MX Gimbal and multispectral cameras deployed on a DJI M600 drone in the Hutt River.**

3.3   Hyperspectral cameras

3.3.1   Hyperspectral camera selection

Hyperspectral cameras (scanners) record aerial imagery in hundreds of narrow spectral bands. This is vastly different from the three broad spectral bands of RGB cameras (which usually have an overlapping spectral response), or the limited number of spectral bands (usually between 4 and 10) offered by multispectral cameras. However, hyperspectral cameras have a very different architecture from RGB or multispectral cameras. Hyperspectral cameras record only a single line of pixels and must be moved through space to create a 2D image. This type of imaging system is known as a push broom scanner and contrasts with RGB and multispectral cameras which collect a 2D image for every frame. The advantage of the hyperspectral camera system is high spectral sensitivity, providing data well suited for automatic classification of objects based on differences in reflectance at different wavelengths of light.

There are also disadvantages of hyperspectral cameras such as increased cost (e.g., $50k–$100k), complexity, and the inability to capture images of moving objects (which can be achieved easily with RGB and multispectral cameras). RGB and multispectral cameras are well suited for recording overlapping 2D images along flight paths, with these images able to be processed with structure from motion software (e.g., Agisoft Metashape) to generate georeferenced orthomosaics and Digital Elevation Models (DEMs). In contrast, hyperspectral cameras need high resolution Inertial Measurement Units (IMUs) to resolve their orientation, and high-resolution GPS to determine their origin (ideally Real-Time Kinematic (RTK) or Post-Processed Kinematic (PPK) GPS).

Post processing hyperspectral imagery to generate georeferenced orthomosaics is also non-trivial. For surveys of terrain that is not flat (i.e., with hills or trees) geo-correction of imagery involves projections onto a Digital Surface Model (DSM) (see Section 6.3). For this reason, it is often complementary to simultaneously fly a high resolution RGB camera and use Structure from Motion (SfM) to generate a DSM. It is also more challenging to remove sunglint and surface reflections from hyperspectral aerial imagery than RGB or multispectral, although it is possible if overlapping flight lines are used. For hyperspectral aerial imagery from UAVs, lightweight sensors are needed. Two appropriate systems are the Headwall Nano-Hyperspec and Resonon Pika L Airborne System (Figure 3-6).
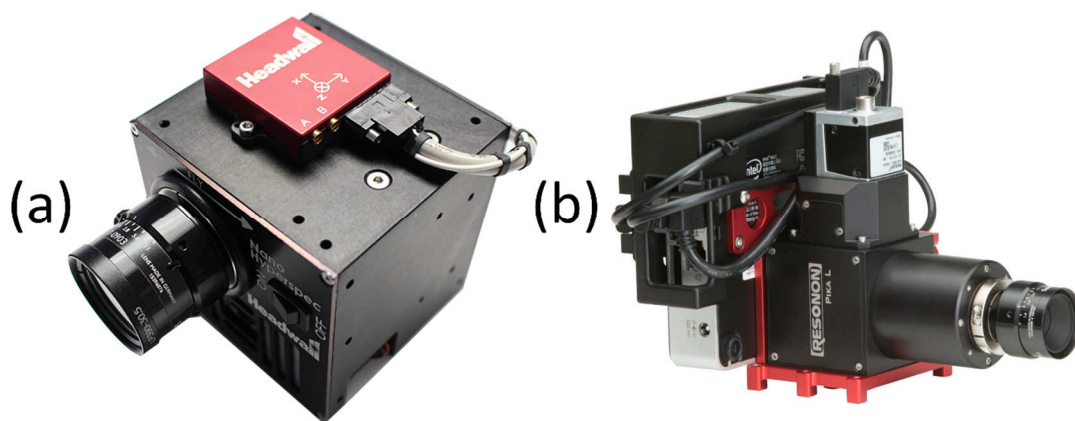
Figure 3-6: **(a) Headwall Nano-Hyperspec, (b) Resonon Pika L Airborne System.**

The specifications of the Headwall Nano-Hyperspec and Resonon Pika L cameras are similar (Table 3-4). The Resonon Pika L provides a slight advantage for aerial applications with 900 spatial bands rather than the 640 provided by the Headwall Nano-Hyperspec. This results in wider images and fewer flight lines. The Nano-Hyperspec is able to record at a higher maximum frame rate of 350 FPS, compared to 249 FPS for the Pika L. However, this difference is mainly advantageous for high velocity surveys such as those from a manned aircraft. For deployments from a UAV frame rates close to 100 FPS are more common and provide sufficient exposure time (i.e., incoming light to the sensor) to minimise the gain required and thus decrease signal noise.

Many auxiliary systems are required to generate high quality (and properly georeferenced) imagery. These systems are:

- A high resolution IMU and RTK GPS system (e.g., the SBG Systems Ellipse2D, or Ellipse3N; see Section 3.3.2 below);

- A ground calibration tarpaulin, and potentially also a downwelling irradiance sensor to enable conversion to reflectance spectra (e.g., the ocean optics flame spectrometer);

- Georectification software (e.g., the Resonon georectification plugin);

- Software for postprocessing/analysis of hyperspectral imagery (e.g., Resonon Spectronon Pro).

The ground calibration tarpaulin should have a flat spectral reflectance curve and size of at least 2.4×2.4 m. It is recommended to get a tarpaulin that has at least two different reflectance values (e.g., 12% and 24%). A tarpaulin with a single high reflectance value (e.g., 36%) can saturate the sensor when deployed on a dark background.

Anyone looking to purchase a hyperspectral imaging system should be aware that all systems are extremely expensive and time consuming to commission. While these systems are sold as 'turn-key solutions' this is far from accurate. Significant time should be allocated to installation, set up, and training before field operation of any hyperspectral imaging system. Although we have not had experience with Headwall products and service to compare, we have found that the training and ongoing customer support from Resonon are excellent.

Table 3-4:   **Hyperspectral camera specifications October 2019.**

	Headwall Nano-Hyperspec	**Resonon Pika L**
Spectral Range (nm)	400–1000	400–1000
Spectral Channels	270	281
Spectral Resolution (nm)	2.2	2.1
Spatial Bands (i.e., Pixel Swath)	640	900
Max frame rate (fps)	350	249
Bit Depth	12	12

3.3.2   Hyperspectral camera setup

The setup of hyperspectral camera will vary by manufacturer and the hardware purchased. Here an overview of the setup procedure for the Resonon Pika L is provided. During fieldwork for MAM, our hyperspectral camera was not optimally set up, and we have subsequently been working with the manufacturer to improve our deployment configuration. Here, we will provide recommendations on equipment set up following improvements.

The hyperspectral camera should be mounted on a gimbal (such as the DJI Ronin MX) and properly balanced. A single antenna GNSS receiver and IMU is recommended (e.g., SBG Systems Ellipse3N) rather than the dual antenna Ellipse2D which is very susceptible to Electro Magnetic Interference (EMI).

All USB connections and particularly the external Solid-State Drive (SSD) should be shielded with copper tape, and the SSD ideally placed inside a metal enclosure.

The downwelling irradiance sensor should be run independently from the hyperspectral camera and mounted on a tripod on the ground logging to a laptop. This ensures that the angle of the fibreoptic cable inlet relative to the sky is consistent. It also improves the balance of the gimbal and reduces the risk of damaging the fibreoptic cable when performing gimbal calibrations.

The system clock on the laptop and hyperspectral camera flight computer should be synchronised (usually in UTC time zone). The downwelling spectra can then be matched to the hyperspectral data cubes during post processing using python scripts provided by Resonon.

The calibration tarpaulin should be placed within the survey area, ideally on top of flat terrain that has similar reflectance to avoid saturation of the recorded pixels of the tarpaulin. The tarpaulin should be stretched flat (i.e., between waratahs with rachet straps) and may even benefit from being ironed prior to deployment if it is wrinkly or creased. The user manual should be read in detail and protocols followed to set up the GNSS receiver and IMU (i.e., calibration, lever arms, etc.).

Before a flight, the area to be surveyed should be defined in Google Earth as a polygon and exported as a .kml file. This file is then uploaded to the hyperspectral camera flight computer in the Resonon Ground Station software. The Resonon Airborne Calculator can be used to determine the flight line spacing, altitude, flight speed and frame rate required to achieve square pixels with the desired

dimensions and overlap. These parameters are then written to the hyperspectral camera flight computer using the Resonon Ground Station software.

Automated drone flights are planned and set up in software such as DJI Ground Station Pro to match the parameters specified by the Resonon Airborne Calculator. Flight lines should extend past the boundaries of the polygon defined in Google Earth, as a hyperspectral data cube will cease recording when the hyperspectral camera GPS location is outside of this polygon, and a new one will commence when it re-enters the polygon.

The drone and camera orientation must be aligned with the flight path (i.e., the drone rotates at the ends of each flight line to maintain 'forward' facing flight). This is because the hyperspectral camera is a push broom scanner and the scan line must pass over the terrain to be imaged.

More detailed information on camera settings and setup can be found in manufacturers user manual, and it is highly recommended to attend a training course run by the camera system manufacturer before use.

3.4   Aircraft (i.e., Drones/UAVs)

3.4.1   Multirotors

Multirotor aircraft are convenient for *Microcoleus* aerial monitoring and surveying in general. They can take off and land vertically and are a suitable deployment platform for many different camera systems. Multirotor aircraft can be flown manually, or easily programmed to fly repeatable paths. They are relatively inexpensive to purchase (generally less than $10K NZD) and are very inexpensive to operate compared to flights with manned aircraft. Selecting an appropriate multirotor aircraft depends on the required payload and flight time. For most RGB applications a small UAV is sufficient (e.g., the 20 MP camera on the DJI Phantom 4 Pro). The use of small UAVs is advantageous for battery life, equipment complexity, and operator safety. However, for more complex (and heavy) camera systems, larger UAVs (such as the DJI Matrice 600 Pro) are needed (Figure 3-7).

New models of drones, such as the DJI Phantom 4 Pro RTK and Matrice 210 RTK, are being released with Real Time Kinematic (RTK) or Post Processed Kinematic (PPK) GPS. This may enable accurate orthomosaics and Digital Elevation Models (DEMs) to be generated without the use of Ground Control Points (GCPs) (Tomaštík et al. 2019; Štroner et al. 2020). This is highly beneficial for surveying wide river sites where it is not possible to deploy GCPs within the river, and/or where dense riparian vegetation makes deployment of GCPs on riverbanks problematic. Where new multirotor aircraft are purchased, it is recommended to obtain RTK/PPK GPS models if the available budget allows. The use of GCPs is still recommended for scientific studies that require validation of the spatial accuracy of orthomosaics and DEMs. However, for routine monitoring applications they may not be necessary.
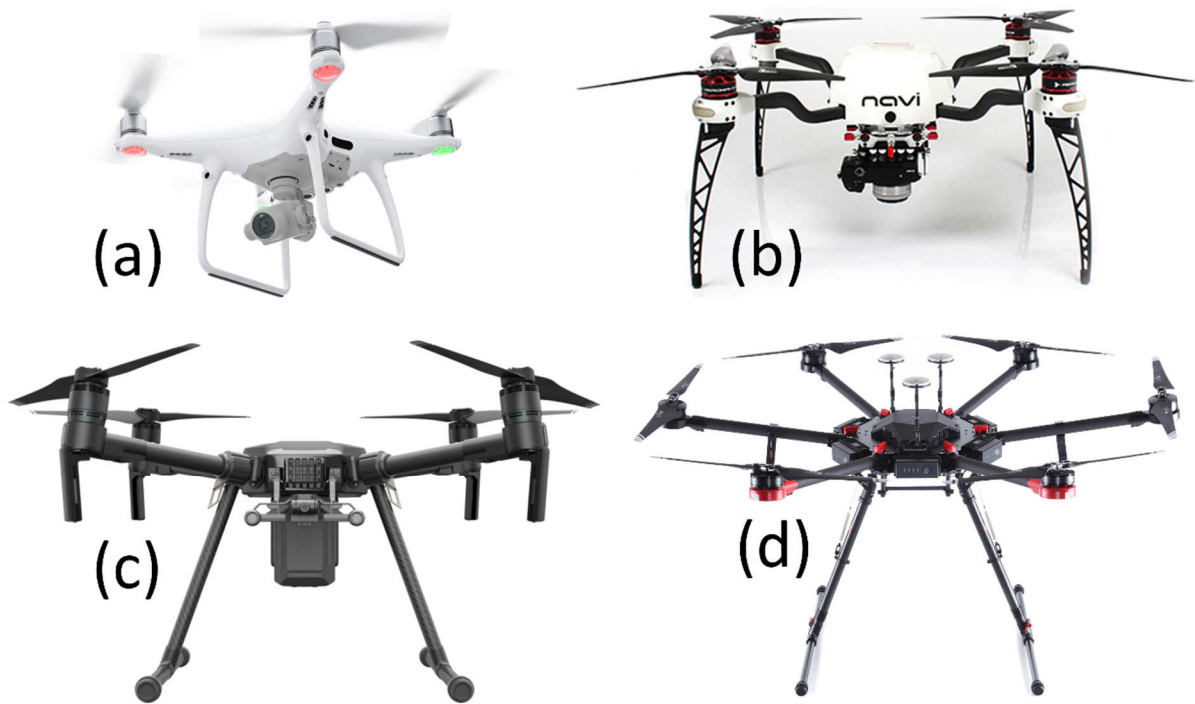
Figure 3-7: Examples of multirotor UAVs and suitable camera payloads: (a) DJI Phantom 4 Pro (RGB), (b) Aeronavics Navi (RGB, RGN, Multispec), (c) DJI Matrice 200 (RGB, RGN, Multispec), (d) DJI Matrice 600 Pro (RGB, RGN, Multispec, Hyperspec).

3.4.2   Fixed wing UAVs

Fixed wing UAVs are more energy efficient than multirotor aircraft. This allows them to stay airborne for longer and cover larger areas (Klemas, 2015). Fixed wing UAVs can be advantageous for some large survey jobs such as mapping farms, lakes, or wetlands (Husson et al. 2014). However, most fixed wing UAVs have fundamental disadvantages over multirotor aircraft for high resolution river surveying. For example:

- Lack of vertical take-off and landing (most fixed wing UAVs need a suitable field or runway near the survey site);

- Lack of availability of gimbals, and mounting challenges;

- Gimbal/payload interference with: centre of pressure (wind resistance), centre of mass, and landing wheels;

- Few safety factors compared to multirotor aircraft (i.e., no motor/propeller system redundancy);

- Difficulty in maintaining flights within visual line of sight;

- Risk to cargo/camera systems when landing.

In most cases only turnkey RGB fixed wing UAV systems should be considered, and only for very large 2D mapping tasks. River reaches for MAM are generally far longer than they are wide and are better suited to multirotor UAVs. For larger spatial coverage with high end camera systems (i.e., hyperspectral) it is much more prudent to use manned aircraft than fixed wing UAVs. Fixed wing UAVs also cannot be safely flown at the low altitudes achievable with multirotor UAVs, due to risks of crashing into trees and other obstacles, this limits the resolution of the imagery that can be collected with them, making it challenging to identify *Microcoleus.*

3.4.3   Manned aircraft

Microcoleus aerial monitoring requires high pixel resolution since *Microcoleus* can occur in small patches. This generally precludes the use of fixed wing aircraft due to restrictions on minimum flight altitude and high flight speed (e.g., large pixels and motion blur). Surveying with manned helicopters may be possible, however the high cost of flight time makes their use not recommended. It is also challenging to use manned aircraft to obtain imagery with sufficient overlap for processing with SfM software and less accurate image mosaicking techniques may be required.

3.5   Surveying equipment and ground control points

For qualitative aerial surveys to observe *Microcoleus* cover detailed surveying is not necessary; however, for quantitative *Microcoleus* aerial monitoring Real-Time Kinematic (RTK) GPS surveying equipment is essential. There is a wide range of RTK GPS surveying equipment available that is suitable for MAM. The equipment used by NIWA is a Trimble R10 base station (Figure 3-8a) and two Trimble R10 Rovers (Figure 3-8b). Most large organisations that will undertake MAM will already have their own RTK GPS equipment, however for those that do not, the equipment can be rented from providers around New Zealand.

Figure 3-8:   **(a) Trimble R10 RTK GPS base station, (b) 2x Trimble R10 Rovers.**

To georeference aerial imagery it is important to use Ground Control Points (GCPs). GCPs can be made from weatherproof canvas and should have a clearly defined centre (Figure 3-9). Temporary GCPs can be held down with rocks and collected after flights. Sites where repeated monitoring occurs may benefit from the installation of more permanent GCPs that only need to be surveyed once.
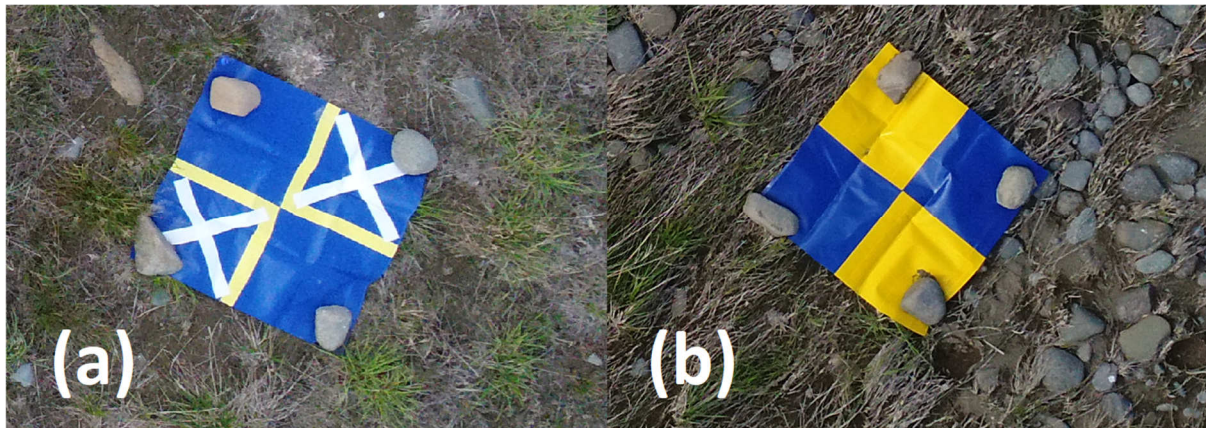
Figure 3-9: Ground control points that are easily visible in aerial imagery and have a clear centre to survey (Biggs, 2020).

For surveys of wide rivers, it may also be necessary to deploy GCPs within the wetted channel, to ensure that an accurate georeferenced orthomosaic is produced. White painted rocks work well as underwater GCPs. However, they do take time to paint and can be unsightly if left at a river site following a survey. For reusable underwater GCPs we recommend stainless steel plates (150 × 150 mm) with circular holes to let water through. These sit nicely on the riverbed and can be easily stacked for transport to and from the field site. We tested a range of colours (Figure 3-10a) and found that white was generally the brightest and best (Figure 3-10b). It is important to paint the underwater GCPs, rather than leaving them as polished stainless steel. If left unpainted they act as a mirror and reflect the light and colours of objects around them (rather than diffuse white light) making them much harder to see. Painting them is easy, with a base coat of grey metal etching primer applied first, then a topcoat of white paint. Once deployed, they can be surveyed with RTK GPS the same way as GCPs deployed on land. Underwater GCPs can also be deployed to mark the locations where *Microcoleus* covered rocks have been removed for biomass sampling.
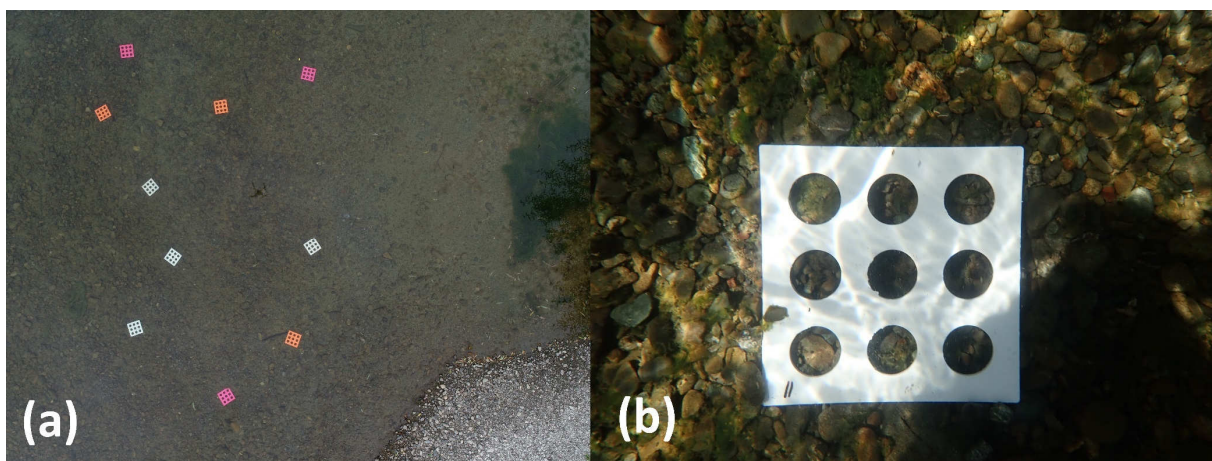
Figure 3-10: (a) Tests to select underwater Ground Control Point (GCP) colour. (b) Underwater GCP deployed in the Hutt River.

4   Aerial monitoring missions

This section of the user guide provides methods and recommendations for detailed aerial monitoring missions. For simple recording of aerial imagery for communication purposes, or comparison with reference cover levels (Appendix D) then the deployment of GCPs is not required and flights are simplified (i.e., overlapping aerial images are not required).

4.1   Mission planning

4.1.1   Site selection

Microcoleus aerial monitoring is suitable for shallow river reaches, with clear water and some *Microcoleus* cover (e.g., >5%). Selected sites should be representative of the river at larger spatial scales and cover a selection of geomorphic features (i.e., riffles, runs and pools). Selected sites also need to be practical for UAV operations, with consideration given to airspace restrictions, land ownership/administration and overflying members of the public (see Section 4.1.2). Other practical constraints are overhead powerlines, bridges, and dense riparian vegetation. The site must have open spaces to place ground control points and the UAV operator must be able to keep the aircraft within visual line of sight during the survey. Finding suitable monitoring sites is usually straightforward for braided gravel bed rivers but can become problematic for rivers in densely populated areas.

4.1.2   CAA regulations

UAVs must be operated by competent pilots who have been well trained (ideally to CAA level 102) and are familiar with CAA regulations https://www.caa.govt.nz/rules/rule-part/show/101. Examples of important restrictions for MAM are:

- Not to fly higher than 120 metres above ground level;

- Not to fly within restricted airspace;

- Not to fly above people without their consent (such as members of the public);

- Not to fly over land without the consent of the property owner or administrator;

- To keep the aircraft within visual line of sight at all times.

Information on airspace restrictions can be found on https://www.airshare.co.nz/maps and it is prudent to log all flights on the airshare website. It is recommended that organisations undertaking MAM implement an internal mission planning system, where flight plans are reviewed and approved by a nominated chief pilot (particularly for new survey sites). This provides an extra layer of oversight that safe operating practices will be followed, and flights comply with CAA regulations.

4.1.3   Deployment conditions

Weather conditions, lighting and river clarity are critical for the success of aerial monitoring. Weather reports and published flow data should be monitored in the days prior to the MAM deployment, then conditions should be reassessed upon reaching the survey site. To obtain clear through-water imagery it is important for the riverbed to be well illuminated, but to minimise reflections off the water surface. In our experience the optimal deployment conditions for New Zealand are to perform flights close to solar noon, with no cloud cover and minimal wind (Biggs, 2020). Reflections of the sun off the water surface (sunglint) is dependent on the angle of the sun, angle of the water surface and field of view of the camera. Sunglint due to specular reflection is more problematic at latitudes closer to the equator

where the sun is directly overhead. Sun path diagrams provide a convenient estimate of solar angle at different locations around New Zealand, times of the year, and times of day https://www.victoria.ac.nz/architecture/centres/cbpr/resources. As discussed in Section 6, one of the important benefits of recording aerial imagery with high overlap (i.e., 80% front and 60% side) and processing it with structure from motion software, is that sunglint and other transient phenomena that are not fixed in space are usually filtered out of the final georeferenced orthomosaics. If problems with sunglint still occur, then survey time of day, camera angle and flight direction should be adjusted (Overstreet and Legleiter, 2017), however, this provides a trade-off with illumination of the bed. In our experience, reflections of low altitude clouds pose a more serious problem than sunglint to the visibility of the riverbed in through-water aerial imagery. This is because clouds provide a diffuse source of sunlight, where light rays from all angles are reflected off the water surface back to the camera (Biggs, 2020).

4.2   Ground control points and surveying

GCPs (if used) should be placed at locations where they are easily visible in aerial imagery (i.e., away from trees and bushes). The number of GCPs required depends on the size of the reach, with longer reaches requiring more GCPs. The current recommendation from the SfM software provider Agisoft is to use 10–15 GCPs https://www.agisoft.com/index.php?id=31. For surveys requiring highly accurate orthomosaics, more than 15 GCPs can be used, and should be spread throughout the reach, ideally with a stratified random distribution (Martínez-Carricondo et al. 2018). GCPs must be placed before flights commence and should be secured with rocks to avoid movement by wind gusts. For most MAM operations, the length of the survey reaches will not necessitate the use of a RTK GPS base station repeater. GCPs can be surveyed at any time during the deployment, but it is prudent to survey them as soon as possible following flights to ensure they are not accidentally moved by a member of the public or the wind.

4.3   Flight planning

The complexity of flight planning will depend on the purpose of the mission. For example, a flight for rapid visual assessment of cover will require less rigorous planning and preparation than a detailed quantitative survey of an entire river reach. For flights to record images and video for visual assessment of cover (or media releases) drones/UAVs can be rapidly deployed and flown manually, whereas for quantitative surveys automated flight paths are necessary.

Flight paths for UAVs are created in applications such as 'Mission Planner' or 'DJI Ground Station Pro'. To obtain imagery suitable for generating georeferenced orthomosaics (2D photo maps), a high degree of image overlap is required. Flight paths providing at least 80% front overlap and 60% side overlap are recommended (Agisoft, 2021). Selecting an appropriate altitude for flights is a trade-off between pixel resolution (ground sample distance) and flight time. For example, halving the aircraft height requires four times longer flights (since images now cover only ¼ of the ground area). When performing low altitude flights, it is important to check the heights of tall trees near the study site (e.g., poplars). This can be achieved with a laser range finder such as a Nikon Forestry Pro (Biggs, 2020). Common sense is required for assessing potential hazards, and flights at altitudes of less than 50 m should generally be avoided.

To obtain quality aerial imagery, appropriate camera settings are critical. Camera settings are discussed in detail in Section 3, but it is reiterated here that a fast shutter speed must be used to avoid blurry images. For RGB, RGN (i.e., Vis-NIR), and multispectral cameras, the recommended settings are:

shutter priority mode with 1/1000 shutter (or faster in good lighting conditions); focus set to infinity or auto; aperture set to auto; and ISO set to auto. In poor lighting conditions, or when using cameras with narrow apertures, it may be necessary to use slower shutter speeds (indicated by ISO exceeding 400). In these situations, both shutter speed and flight speed should be reduced. It is recommended to fly slower rather than stopping and hovering at each image capture location. This is because the UAV flies much more stably through clean air than when hovering, which causes orientation instabilities that result in more significant blur than those arising from translational motion. For more detailed information on image blur, please refer to Biggs, (2020).

Mission planning with RGB cameras is relatively easy, as the camera hardware parameters are usually pre-loaded into appropriate software (i.e., in DJI Ground Station Pro there will already be a Phantom 4 Pro camera to select). For multispectral and RGN cameras, custom cameras will need to be created in the mission planning software, or the camera will need to be run in time-lapse mode (i.e., standalone), and flight parameters adjusted to provide the required image overlap, flight speed, ground sample distance etc. The lead author of this user guide has created a camera flight parameter calculator that is freely available upon request and can be easily adjusted to include other camera models.

Hyperspectral cameras have a different mode of operation from RGB or multispectral cameras, in that they record pixels in a line (i.e., pushbroom) and the line needs to be flown across the landscape to build up an image (see Section 3.3). They also require an underlying DSM which can be obtained from RGB aerial imagery and SfM software such as Agisoft Metashape. It is also necessary to calculate flight parameters for hyperspectral cameras based on lenses, Field of View (FoV) and framerate. This can be achieved in the camera flight parameter calculator provided by the author, or an alternative calculator if provided by the hyperspectral camera manufacturer. One major difference when flying hyperspectral cameras (compared to RGB cameras, for example) is that the drone (and thus camera) orientation needs to remain consistent with the flight direction. For example, when the drone is flying a zigzag pattern, it needs to turn at the end of each flight line, such that the image acquisition line sweeps the landscape and is orthogonal to the drone flight path. This can be achieved in the mission planning software (i.e., DJI Ground Station Pro) by setting the drone and camera alignment follow the flight path (i.e., so that the drone is always flying forward).

4.4   Summary

The sections above provide a basic overview of mission planning for RGB, multispectral and hyperspectral camera systems. As a rule of thumb, expect recording and processing RGB aerial imagery for quantitative surveys (i.e., orthomosaics and DEMs) to be ~10× more difficult than RGB aerial imagery for visual assessments and media releases. Then, expect recording and processing multispectral aerial imagery to be ~10x more difficult than quantitative RGB, and hyperspectral to be ~10× more difficult than multispectral. Thus, multispectral remote sensing should only be undertaken by those familiar and comfortable with RGB aerial monitoring first, while hyperspectral should be reserved for specialist applications.

Finally, here are some tips for flight planning:

- Start flying upwind and zigzag downwind. This enables a safe return to home if wind speeds increase, or batteries get low;

- Return to home when the battery is below 35–40% and land with at least 30% remaining. This is important for LiPo battery life and equipment safety;

- Use a spotter to keep a look out for aircraft, members of public etc. Members of the field team may also carry walkie talkie radios if they are scattered around the study site;

- Members of the field team should leave the river when the drone is overhead, so they do not obscure aerial imagery;

- For large surveys, bring generators for battery charging and pick landing sites along the study reach for battery swapping;

- Bring a rolled-up carpet (or similar) for landing on rough/uneven terrain;

- Launching (and particularly landing) in windy conditions can be risky for drones tipping over and breaking propellers. This is particularly true when they are at partial throttle, as the spinning blades create more wind resistance, but there is less weight force holding them down. Try to select launch/landing sites shielded from the wind (e.g., behind a stand of trees, or vehicle);

- Plan flight paths so that the drone is always within visual line of sight. Always ensure flights are within CAA regulations (Section 4.1.2), log flight plans, check Notices to Airmen (NOTAMs);

- Always check aerial imagery on a computer before leaving a study site (i.e., imagery not blurry, full site coverage) and transfer it to the computer hard drive as a back-up.

5 Periphyton ground truth sampling and sample processing

Microcoleus cover estimates can be obtained from aerial imagery classifications and user judgement to select training pixels for image classification (Section 7). However, to evaluate the accuracy of *Microcoleus* cover maps, or to quantify *Microcoleus* biomass, ground truth measurements are required. The following sections describe field sampling procedures and the required laboratory analyses.

5.1 Cover sampling and ground truth

5.1.1 GPS ground truth

GPS point samples are a convenient way to obtain ground truth measurements of *Microcoleus* cover. To achieve high spatial accuracy RTK GPS should be used, as is the case for surveying in ground control points for aerial imagery (Sections 3.5 and 4.2). One field team member should walk throughout the survey reach and record 200–500 GPS points covering different classes of visually distinctive objects. Examples of visually distinct classes are: *Microcoleus*, green algae, dry sediment, wet sediment, other vegetation, man-made objects, shadows and miscellaneous. Each survey point is assigned a class when recorded. Points can be grouped later if needed, for example into the binary (presence/absence) classes of *Microcoleus* and Not *Microcoleus*. It is important that survey points also cover areas with no periphyton (i.e., a negative control), with these being recorded in similar proportion to the number of *Microcoleus* samples.

5.1.2 Visual cover estimates with a bathyscope

Average cover of *Microcoleus* within an area of interest can also be estimated using a bathyscope (i.e., underwater viewer, or aquascope, Figure 5-1). Usually, 20 views along four transects of a river reach are obtained and averaged (i.e., five views per transect) (NEMS Periphyton, 2020). If the river reach has heterogenous cover and habitat types (i.e., pools, riffles, and runs) then more transects may be needed. This provides a spatially averaged cover estimate, rather than point values of presence/absence obtained with RTK GPS. While somewhat subjective, visual cover estimates are an inexpensive and widely used technique to estimate cover. Bathyscopes can be obtained from multiple manufacturers and retailers globally, such as Envco or Nuova Rade[2].

---

[2] Envco bathyscope: http://envcoglobal.com/catalog/water/limnology/field-equipment/bathyscope-underwater-viewer
Nuova Rade bathyscope: https://www.nuovarade.com/product.php?productId=5519&categoryId=267

Figure 5-1: **A bathyscope is used to view the riverbed in wadeable rivers.**

Quadrats are marked on the circular bottom of the bathyscope to facilitate percent cover estimates (Figure 5-2). To only monitor *Microcoleus*, the binary categories of *Microcoleus* and Not *Microcoleus* can be used. For routine visual monitoring of periphyton in New Zealand, the categories in NEMS Periphyton, (2020) are recommended, which are based on Kilroy et al. (2008; 2013). For targeted monitoring of *Microcoleus* that still quantifies total periphyton cover the recommended categories are: no periphyton (i.e., bare substrate), film (very thin cover), mats – *Microcoleus*, mats - other, and filaments (which can be split into green filaments and other filaments if needed).

Figure 5-2: **Left: Underwater view with predominantly *Microcoleus* and bare substrate, Right: Underwater view with a predominantly filamentous green algae and bare substrate.**

When making underwater views, the location of the view (centre of the bathyscope) should be recorded with RTK GPS (Table 5-1). Usually the RTK GPS surveyor will work alongside the team member who is making underwater views to record the view locations. Alternatively, coloured and numbered markers (Section 3.5) can be placed on the riverbed and surveyed later. Where possible a camera image should also been taken through the bathyscope (Figure 5-2), with the image number recorded (Table 5-1). Camera images provide a valuable resource for additional image analysis, or to check the correspondence of cover estimates between team members.

Table 5-1:   Example table for recording underwater viewer data.

Site location: _____ Team member: _____
Date: _____ Notes: _____

View Number	View Time	GPS Point Name	Camera Image Number	*Microcoleus* Cover %	Not *Microcoleus* Cover %	Add other columns if estimating cover of more than two classes
1	08:24	Hutt-0092	DSC072	30%	70%	
2						
3						

A bathyscope is always recommended (particularly in shallow water), however, if one is not available (and water is deep), georeferenced underwater camera images may be used (Figure 5-3). Cover estimates can then be made after returning from the field.

Figure 5-3:   Underwater camera images with: *Microcoleus* dominated cyanobacterial mats (left) and filamentous green algae (right).

When collecting data from underwater views, it is important that they are distributed throughout the study reach (i.e., randomly distributed, or at least 20 underwater views from 4 transects), so that they are spatially representative of average cover, and do not specifically target *Microcoleus* patches. Target bias is a big problem for this type of sampling, since it is easy to subconsciously gravitate towards finding patches of *Microcoleus* or other periphyton, rather than making views of bare substrate. This is critical for both GPS presence/absence surveying and underwater views, since negative control data are key for training (and ground truthing) the aerial cover classification algorithms, with average cover throughout the study reach being the output parameter of interest. The approach of randomly walking a certain number of steps and then looking down is recommended (similar to Wolman counts for sediment size measurement), or a structured grid/cross section approach (e.g., NEMS Periphyton, 2020). However, unlike NEMS Periphyton (2020) views should also occur in riffles and pools, such that underwater views are representative of the entire study reach. This is particularly important for *Microcoleus* since it tends to colonise riffles first.

5.2   Biomass sampling

Microcoleus cover provides a useful metric for regulators and applying thresholds for warnings to the public, where it is better to err on the side of caution. However, to accurately quantify *Microcoleus* abundance, ground truth biomass sampling is required. *Microcoleus* abundance is the product of spatial extent (area), mat thickness (biomass), and the proportion of *Microcoleus* in the mat. The total biomass of *Microcoleus* in a river is important, because the risk of toxin production is proportional to the number of toxin producing cells, which is a function of mat thickness (i.e., three-dimensional biomass), rather than cover (which could be a thin film). Toxin production by *Microcoleus* cells is irregular; it can vary between cells in the same mat and it can vary in time, making it very hard to predict (Quiblier et al. 2013; McAllister et al. 2016). Thus, it must be assumed that any *Microcoleus* mat has the potential to produce potent neurotoxins, with the amount of neurotoxin that can be produced being proportional to the number of *Microcoleus* cells (and thus biomass) that are present. The risks due to *Microcoleus* are not localised to the site where *Microcoleus* grows, as mats can slough (detach), drift downstream, and accumulate on riverbanks, where they may be eaten by dogs or come into contact with people. The following sections detail the equipment, fieldwork and laboratory analysis needed to quantify *Microcoleus* biomass.

5.2.1   Equipment for biomass sampling

The recommended equipment for biomass sampling is:

- Spray paint (white) or coloured (white) numbered metal markers (Section 3.5);

- Tubs/trays to hold sample rocks;

- Intermediate collection containers (e.g., clean ice cream tubs);

- Brushes (toothbrushes);

- Squirt bottles;

- Sample containers (Elkay pottles);

- Permanent markers and/or pottle labels;

- Chilly bin(s) with ice or ice packs;

- Waders and gloves if necessary;

- Sturdy nonslip shoes (ideally steel cap boots if carrying rocks);

- Radios (walkie-talkies) to communicate with drone pilot and other ground team members;

- Clipboard and pens, with underwater viewer (Table 5-1) and biomass sampling sheets (Table 5-2).

Table 5-2: Example table for recording biomass sample data.[3]

Biomass Sample Number	Pottle Number	Ground Target Number	Sample Time	GPS Point Name	Camera Image Number	Notes on sample contents
1	1	1	08:37	Hutt-0095	DSC075	Mainly *Microcoleus*
2	2	2				
3	3	3				
….	….	…				

Site location: _____ Team member: _____

Date: _____ Notes: _____

---

[3] Ideally biomass sample number, pottle number and ground target number will all match, however pre-numbered targets and pottles may be distributed amongst multiple team members.

5.2.2   Recommended workflow for biomass sampling during aerial surveying

River reaches provide heterogenous habitat conditions for periphyton growth (e.g., riffles, runs, pools, shade, variable depth, and velocities). The goal of biomass sampling is to characterise the distribution (and ideally taxonomic composition) of periphyton growth throughout the study reach, such that the biomass areal density metrics (g/m^2) for each class of interest can be determined (e.g., *Microcoleus* class). Biomass samples are spatially referenced with GPS and marker rock locations recorded in secondary drone flights, so that sample locations can be accurately tied to aerial imagery. For example, aerial imagery pixel *A* at sample location *B* corresponds to class *Microcoleus*, with measured biomass areal density *C*. The biomass areal density metrics for all the samples of each class can be averaged later, to provide reach averaged biomass areal density metrics for each class, which can be multiplied by cover to estimate total biomass of that class in the study reach. The approach of collecting and processing individual georeferenced biomass samples (compared to bulk sampling of each manually identified class, Section 5.2.3) allows for more options with data post processing, such as subdivision of classes, or geographic groups. For example, if denser mats are distinguishable in the aerial imagery, or mats are thicker in riffles, then these can be demarcated and processed with separate calibration factors.

Before commencing sampling, it is recommended that the ground truth team walk the length of the study reach to determine the overall distribution of *Microcoleus* growth, then team members are allocated different areas of the river to work in by the biomass sampling team leader. Ground Control Points for the aerial survey (Section 4.2) can also be distributed throughout the study site at this time.

The recommended workflow for biomass sampling is as follows:

1. **Drone survey #1**: Aerial imagery is collected for the undisturbed river reach (i.e., without any team members in the river, or stones removed).

    A.   During drone survey #1, the biomass sampling team should prepare labelled pottles, trays, scrubbing equipment, chilly bins, and labelled rocks/markers (Section 3.5), then distribute them throughout the study reach in preparation for biomass sampling.

    B.   Where possible, the numbering scheme for biomass samples, pottles and markers should match (Table 5-2). This can be achieved by placing matching pottles and markers into trays before distributing them throughout the study reach.

2. **RTK GPS ground truth surveying**: Following drone survey #1, the surveyor can commence RTK GPS ground truth measurements (Section 5.1.1) throughout the study reach (Figure 5-4).

    A.   The surveyor must cover the full range of visual object classes present throughout the study reach. Negative control points (i.e., Not *Microcoleus*) must be collected in similar proportion to targeting *Microcoleus* patches.

Figure 5-4: Surveyor performs RTK GPS ground truth measurements of cover classes throughout the study reach, then measures the locations of labelled markers (where biomass samples were taken).

3. **Periphyton sampling – Rock collection**: Following drone survey #1, collect periphyton-covered rocks and replace them with painted, numbered markers (Figure 5-5). Sample rocks are then carried to the riverbank, where they are placed in trays (Figure 5-6, Section 3.5).

   A. Each team member should select a range of rocks that are representative of the spatial distribution of periphyton and mat thicknesses found in their assigned area.

   B. Care should be taken that periphyton mats on the sampled rocks are not damaged or removed when the rocks are collected and carried to the riverbank.

   C. Health and safety: care should be taken by the sampling team that they are adequately warmed up, only carry rocks within their safe lifting capabilities, wear appropriate footwear (ideally steel cap boots), and take care when carrying rocks if the riverbed is slippery or unstable.

Figure 5-5: Labelled markers placed in the exact location where rocks were removed for biomass samples.

Figure 5-6: Sample rocks removed from the river and placed into trays with their respective Elkay pottles.

4. **Periphyton sampling – Rock recording**: First, take a photo of the sampled rock (Figure 5-6), then record the rock number, marker number, Elkay pottle number, camera image number and a description of the periphyton on the rock (Table 5-1). Add the GPS point number later after surveying.

5. **Periphyton sampling – Rock scrubbing**: The lid of an Elkay pottle is used to cover periphyton on the selected rock (Figure 5-7: Left) and all periphyton and other debris is scrubbed and rinsed off the rock (i.e., from the area surrounding that of the pottle lid, using a brush and river water in a squirt bottle). Then the pottle lid is removed, revealing the periphyton to be sampled Figure 5-7: Right). This periphyton is then scrubbed off (with a clean toothbrush) into a wide rim container (i.e., a clean ice-cream container). A squirt bottle is used to rinse residual periphyton from the rock and toothbrush into the wide rim container. The contents of the wide rim container are then tipped into the Elkay pottle. The squirt bottle can again be used to rinse the contents of the wide rim container into the Elkay pottle. The Elkay pottle should then be stored in a cool dark place (such as a chilly bin with ice or ice packs).

6. **Sample labelling**: Each pottle (not just the lid) should also be labelled with the sample number and further information, such as: the date and time of sample collection; the name or initials of the person who collected the sample; and the site name. This information is important to avoid samples being mixed up or lost during subsequent storage. If more than one Elkay pottle is required to store the sample, label each pottle to indicate that it is one of several (e.g., 1 of 3, 2 of 3, etc.). For more information, refer to NEMS Periphyton, (2020).
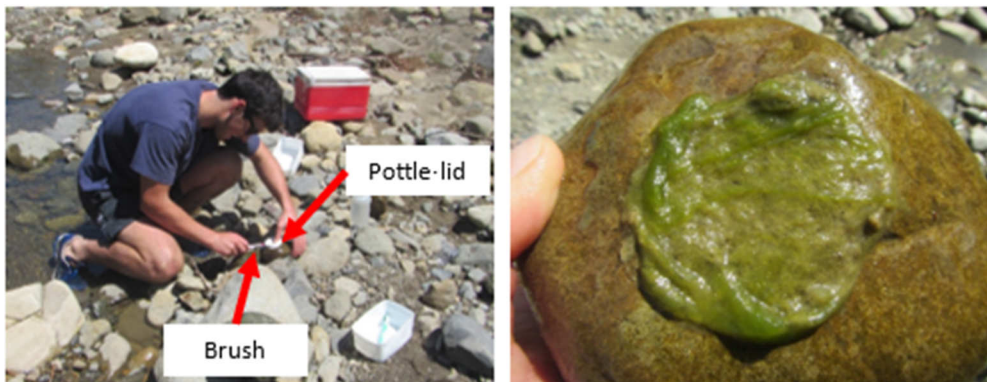
Figure 5-7: Biomass sampling using a sample container (pottle) and toothbrush.

7. **Marker location surveying**: After all ground truth sample rocks have been removed from the river, the surveyor can walk through the study reach and record the RTK GPS location of each marker. The surveyor must record the marker ID number when recording each GPS point.

8. **Drone survey #2**: After all ground truth sample rocks have been removed from the river, the second drone survey can be completed.

The purpose of the second survey is to identify the exact locations from which the biomass samples were taken, by comparing the georeferenced orthomosaic from survey #1 with the georeferenced orthomosaic from survey #2, which has markers distributed throughout the study reach.

9. **Underwater views:** If underwater views (visual cover estimates) are required (Section 5.1.2), then it is recommended that these are obtained following the second drone survey. The surveyor and underwater viewer operator can work together to record the RTK GPS location and details of the underwater view.

   It is important that underwater views are representative of the distribution of periphyton throughout the study reach. For example, it is important to also make views in areas with no periphyton (or *Microcoleus*) cover.

10. **Clean up:** Collect all markers, ground control points, and remove all sampling equipment from the site.

5.2.3   Method variations: Bulk sampling

A bulk *Microcoleus* (or periphyton) biomass estimate in the study reach may be obtained by averaging multiple single rock samples that are representative of cover throughout the study reach. For example, 10 rocks with representative cover can be selected from around the study reach, then scrubbed (one Elkay lid for each rock) all into one sample container, which is then analysed to obtain the average biomass (grams of chlorophyll *a*, DM or AFDM) per 10 sample areas (i.e., 10× Elkay lid area).

5.3   Biomass storage and transportation

Immediately after collection in the field, scrubbed periphyton samples are stored in river water in polyethylene containers (Elkay pottles) on ice and in the dark (NEMS Periphyton, 2020). After transport to the laboratory, samples are kept at 4°C (for immediate analysis) or frozen at -20°C until laboratory analysis. If samples are frozen, some free air space must be left in the container to allow for expansion as the sample water freezes, to prevent the container from breaking. It is not advisable to keep samples for more than three months if they are to be analysed for chlorophyll *a* (chl *a*), but AFDM is not significantly affected (NEMS Periphyton, 2020). As a precaution against the presence of didymo, all sampling equipment and protective gear such as waders and the outside of vehicles driven into rivers or close to the water on river banks are to be thoroughly checked, cleaned, and dried before visiting the next water body[4].

5.4   Laboratory analysis for Dry Mass (DM), Ash-Free Dry Mass (AFDM) and chlorophyll *a*

The biomass sample is poured from the pottle into a beaker and non-periphyton material such as stones, leaves, invertebrates, and moss are removed. Samples are then diluted (if needed) and homogenised using a blender, a beaker, and a squirt bottle. This is particularly important for samples containing filamentous algae. Distilled water is used to rinse the sample out of the container and off the blender blades after blending. Homogenised samples are then diluted up to a convenient target volume V_T (e.g., 250 mL), which is recorded. Subsamples are taken from the homogenised mixture and processed for DM, AFDM, and/or chl *a*. Dry mass is obtained by drying a known volume of the sample V_{SS} on a pre-weighed glass fibre filter (47 mm Whatman GFC or GFF) at 60–100 °C for at least 2 hours (overnight is common). Ash-free dry mass is obtained by ashing a known volume V_{SS} of the subsample on a pre-weighed, pre-ashed glass fibre filter (47 mm Whatman GFC) at 400–550°C for 2–4 h. Chlorophyll *a* is obtained by extraction using one of several possible solvents: acetone, methanol, ethanol, or dimethyl sulfoxide (DMSO). Ethanol extraction is commonly used in New Zealand and is recommended by Biggs and Kilroy, (2000) and NEMS Periphyton, (2020). Spectrophotometry,

---

[4] Biosecurity New Zealand, https://www.mpi.govt.nz/travel-and-recreation/outdoor-activities/check-clean-dry/

fluorometry, or high-performance liquid chromatography (HPLC) may be used to determine chl *a* in algae. At NIWA, the ethanol extraction method and spectrophotometry are used to determine chl *a*. The subsample biomass is obtained, and the full sample biomass is calculated by multiplying it by the ratio of the total sample volume V_T to the subsample volume V_{SS}.

$$Full\ sample\ biomass\ = Subsample\ biomass \times \frac{Total\ sample\ volume\ (V_T)}{Subsample\ volume\ (V_{SS})}$$

To obtain areal biomass (in g/m^2 or mg/m^2), the full sample biomass is divided by the area the sample was taken from (i.e., the area A_S of the pottle lid in Section 5.2.2).

$$Areal\ biomass\ (g/m^2) = \frac{Full\ sample\ biomass}{Sample\ area}$$

These equations are the same regardless of the biomass metric used (i.e., Areal AFDM, Areal DM, or Areal chl *a*). The procedures and equations in this section provide bulk periphyton biomass metrics (i.e., whole of periphyton mat). For taxon-specific biomass metrics (as needed for *Microcoleus*) please see the following Section 5.5.

Following sample dilution, it is recommended that all volumes (particularly subsamples) are determined by weight on a high precision scale (rather than by volume) as volume is notoriously difficult to measure accurately (even with pipettes) and can introduce significant percentage errors. Since the initial sample is heavily diluted, the assumption that the density of the diluted sample is 1 g/cm^3 at 4°C is valid. This assumption also holds for slightly warmer samples, since there is very little thermal expansion of water up to 25°C. If pipettes are used, they should be regularly calibrated (by weight), and routine QA procedures with multiple replicates used.

More detailed steps, and procedures for DM, AFDM and chl *a* are found in Annex F and G of NEMS Periphyton, (2020).

5.5   Biomass metrics for *Microcoleus* abundance using cell counts

Aerial imagery and visual observations provide a useful indication that cyanobacterial mats dominated by *Microcoleus* are present. This information and associated cover estimates may be suitable for routine monitoring and issuing warnings, where it is better to be conservative and err on the side of caution. However, for scientific studies, or accurate MAM, it is important to confirm the presence and abundance of *Microcoleus* within periphyton samples. This is critical, since periphyton mats usually comprise multiple taxa, and there may be other cyanobacteria with similar visual appearance to *Microcoleus*. Quantification of *Microcoleus* abundance within mixed periphyton samples requires specialised microscopy work, and it is recommended to send samples to an expert for processing and taxonomic identification.

The measurements that are required (and accuracy needed) will depend on the desired output biomass metric and what the data are being used for (i.e., routine monitoring, or detailed scientific studies). There are two recommended metrics for *Microcoleus* biomass, with the required processing steps differing slightly between them:

- Metric 1: Cell count of *Microcoleus* per m^2 (Section 5.5.1);

- Metric 2: Ash-free dry mass of *Microcoleus* per m^2 (Section 5.5.2).

Metric 2 has multiple advantages over Metric 1, since it is not sensitive to sample dilutions, the area of the microscope chamber analysed, the homogenous distribution of cells across the microscope chamber, or the complete resuspension and mixing of cells within the sample volume before subsampling (i.e., no settling of cells before subsampling), all of which introduce significant uncertainty in Metric 1. Metric 2 is sensitive to: homogenisation of all cells within the full sample before subsampling (i.e., cells are well mixed and not excessively clumped); the accuracy of species-specific mean biovolumes; and any variations in the relationship between biovolume and AFDM between species. For most practical purposes (unless extremely high accuracy is needed) the relationship between biovolume and AFDM can be assumed to be constant between species (i.e., X volume of species A corresponds to Y grams of AFDM, which also corresponds to X volume of species B). Details of the measurements and calculations required for each metric follow. The words taxon or taxa are used throughout the following sections to refer to different organisms at the species level, genus level, or any higher-level taxonomic grouping.

5.5.1   Metric 1: Cell Count Areal Density (CCAD) of *Microcoleus* (cells/m^2)

The periphyton sample is collected from a known area A_s (i.e., pottle lid area) following the procedure in Section 5.2.2. This sample is then homogenised and diluted to a full sample volume V_{FS}. This sample volume is then subsampled to a volume V_{MC} that is suitable for use in a microscope chamber (Utermöhl chamber or Sedgewick Rafter). Subsamples (volume V_{MC}) are stirred (i.e., cells resuspended and well mixed), then placed into a counting chamber where cells are left to settle, with settling times depending on the volume V_{MC}. The settling times for Utermöhl chambers are 0.5 hours per millimetre of settling column depth (Edler and Elbrächter 2010). The settled chambers are then analysed using an inverted microscope at 100x to 600x magnification. A sub area of the microscope chamber $A_{SA,MC}$ is then analysed for the algal taxa present (this may include groups such as cyanobacteria, diatoms and green algae as required). The count of *Microcoleus* cells $CC_{M,SA}$ is then performed in the sub area of the chamber $A_{SA,MC}$. The total number of *Microcoleus* cells in the original sample is then calculated as $CC_M = CC_{M,SA} \frac{A_{MC}}{A_{SA,MC}} \frac{V_{FS}}{V_{MC}}$, where A_{MC} is the full cross sectional area of the microscope chamber. The Cell Count Areal Density (CCAD) of *Microcoleus* is then found as $CCAD_M = \frac{CC_M}{A_S}$ with units of cells of *Microcoleus* per m^2.

As discussed previously, this method is sensitive to errors in the measurement of many parameters (two volumes, two areas, homogenisation and resuspension of the full sample before subsampling, and the homogenous distribution of cells across the microscope chamber, such that the sub area is representative of the whole chamber area). It is prudent to perform multiple counts (replicates) per sample and average them to get a more robust estimate of CC_M.

5.5.2   Metric 2: Ash-Free Dry Mass Areal Density (AFDMAD) of *Microcoleus* (g/m^2)

The periphyton sample is collected from a known area A_s (i.e., pottle lid area) following the procedure in Section 5.2.2. This sample is then homogenised and diluted to a full sample volume V_{FS}. This sample volume is then subsampled to a volume V_{SS} and AFDM is determined following the procedure in Section 5.4. AFDM of the full sample is then determined as $\text{AFDM}_{FS} = \text{AFDM}_{SS} \frac{V_{FS}}{V_{SS}}$. This corresponds to the total ash-free dry mass of the periphyton sampled from the area A_s. The AFDM Areal Density is then found by $\text{AFDMAD} = \frac{\text{AFDM}_{FS}}{A_S}$ and has units of grams of AFDM per m^2. The AFDMAD of *Microcoleus* can then be found as $\text{AFDMAD}_{Microcoleus} = \text{AFDMAD} \times RA_{Microcoleus}$, where $RA_{Microcoleus}$ is the relative abundance (as a proportion) of *Microcoleus* in the sample by biovolume.

In the literature it is common to find AFDM already reported as an areal density (g/m^2), however in some cases it is not and simply refers to the total ash-free dry mass of a sample (g); for this reason the slightly cumbersome, but more clear acronym of AFDMAD has been used.

The relative abundance of *Microcoleus* to other periphyton taxa in the sample by biovolume $RA_{Microcoleus}$ can be found via microscopy and is invariant of sample dilution, subsample volume and chamber area measurements. The homogenised full sample volume V_{FS} is subsampled to a volume V_{MC} that is suitable for use in a microscope chamber. The volume V_{MC} is then evenly distributed across the microscope chamber and cells left to settle (when using an inverted light microscope). The N most common taxa (e.g., $N = 10$) are then identified and cell counts CC_i are recorded for each taxon (with index from $i = 1$ to $i = N$). The sub area of the chamber, from which the cell counts are made, should be representative of the taxa distribution across the entire chamber. The cell counts for each taxon must be obtained from the same sub area of the chamber.

The biovolume for each taxon BV_i in the sub area of the microscope chamber is then found by multiplying the number of cells of that taxon CC_i by the mean cell volume for that taxon CV_i.

$$Species\ Biovolume, BV_i = CC_i \times CV_i$$

Taxon-specific mean cell volumes CV_i are obtained by measuring 10–15 cell widths W, thicknesses T and lengths L, then calculating cell volume based on an appropriate geometric formula to represent the cell shape. For example, the volume of an ellipsoid is $V = \frac{4}{3}\pi \frac{W}{2}\frac{T}{2}\frac{L}{2} = \frac{1}{6}\pi WTL$ and the volume of a cylinder with ellipse (or circular) cross section is $V = \pi \frac{W}{2}\frac{T}{2}L = \frac{1}{4}\pi WTL$ (Hillebrand et al. 1999). The 10–15 volumes are then averaged to represent a taxon-specific mean cell volume CV_i. Likely mean cell volumes for most taxa will already be known from previous biovolume work and can be looked up in a database or reference text (e.g., MfE and MoH, (2009) – Appendix 4), enabling this step to be skipped in many cases.

The total biovolume BV_T in the sub area of the microscope chamber is then found by summing the biovolume of each taxon.

$$Total\ biovolume, BV_T = \sum_{i=1}^{N} BV_i$$

The relative taxon abundance RA_i in the sub area of the microscope chamber is then found by dividing the taxon biovolume BV_i by the total biovolume BV_T.

$$Relative\ Species\ Abundance, RA_i = \frac{Species\ Biovolume, BV_i}{Total\ Biovolume,\ BV_T}$$

The relative taxon abundance RA_i in the sub area of the microscope chamber will be representative of the relative taxon abundance in the whole sample (assuming adequate homogenisation of cells of all taxa). If greater accuracy is needed, then more sub areas should be sampled from each chamber, and/or multiple independent subsample replicates taken from the original sample. In this case, the total cell count for each taxon CC_i will be comprised of a summation of cell counts from M sub areas (or independent sub sample replicates in new microscope chambers).

$$CC_i = \sum_{j=1}^{M} CC_{i,j}$$

In practice, whether multiple replicates are needed depends on how well samples are homogenised. For the first processed sample, it would be prudent to perform multiple replicates and check for variability within at least three independent estimates of RA_i. If the observed variability is outside of the bounds of allowable experimental uncertainty (which depends on the application for which the data is collected) then multiple independent cell counts, $CC_{i,j}$ should be obtained for each sample.

Care should be taken if samples include large algae (e.g., filamentous greens) which can easily be missed when looking at just a few fields in an Utermohl chamber. In this case large filaments can be counted at low magnification (×100), then smaller cells can be counted at high magnification (×400) with the two counts combined with appropriate calculations (Stancheva et al. 2012).

For further details of microscopy techniques and periphyton taxa identification, please refer to the *Stream Periphyton Monitoring Manual* (Biggs and Kilroy, 2000).

5.6   Further options for sample analysis

Additional sample analysis may be undertaken, depending on the objective of the study and reason for aerial monitoring. For routine monitoring for cover and biomass, it is unlikely that further analysis will be needed. However, if information on pigment and phycobiliprotein concentration is needed, then samples can be sent to specialised laboratories for analysis. High Performance Liquid Chromatography (HPLC) and fluorescence methods can be used to determine the concentrations of the pigments phycocyanin, phycoerythrin, alpha-carotene, beta-carotene, chlorophyll *a*, chlorophyll *b*, alloxanthin, canthaxanthin, diadinoxanthin, diatoxanthin, echinenone, fucoxanthin, lutein, peridin, violaxanthin, and zeaxanthin. HPLC pigment analysis can also be used to define the proportion of different algal groups present (Schlüter et al. 2006). If information on toxin concentrations or the proportion of toxin-producing cell is needed, then further specialist analysis will also be required.

6 Aerial imagery pre-processing to generate georeferenced orthomosaics

Once fieldwork has been completed, the next step is aerial imagery processing to generate georeferenced orthomosaics (2D photo maps). This can be skipped if the imagery is only being used for visual cover assessments (Appendix D); however, it is essential for accurate quantification of cover and supervised classifications. The images from the survey should be collated and cleaned up before processing. Usually this involves copying them to a new folder, removing any images from outside the survey area, and sometimes renumbering the images if there are duplicate image names (this may occur with large surveys). The imagery should ideally have GPS coordinates stored in the EXIF information (image meta-data), which will greatly help with image alignment and production of the georeferenced orthomosaic. The recommended software for creating georeferenced orthomosaics from RGB, RGN, and multispectral aerial imagery is Agisoft Metashape (or Pix4D). For hyperspectral aerial imagery, the recommended software for creating orthorectified and georeferenced hypercubes is Spectronon Pro (for cameras from Resonon) or Spectral View (for cameras from Headwall). In the following sections we will provide an overview of image processing procedures for Agisoft Metashape and Spectronon Pro.

6.1 RGB and RGN Cameras

To generate georeferenced orthomosaics in Agisoft Metashape from cameras with single lenses (RGB or RGN) the general steps are:

- Add photos;

- Align photos;

- Add markers (i.e., Ground Control Points if they are used);

- Optimise camera alignment;

- Build dense point cloud;

- Build digital elevation model (DEM);

- Build orthomosaic;

- Export DEM:

  - NZTM2000 with 10 cm pixels in .tiff format (not layered) is recommended;

  - If also analysing hyperspectral imagery from Resonon cameras, export a DEM in UTM59S or UTM60S that covers the part of New Zealand where measurements occurred;

- Export orthomosaic:

  - NZTM2000 with 5 cm pixels (or higher resolution) in .tiff format (not layered) is recommended for classifications;

  - WGS84 is recommended for visualisation in Google Earth.
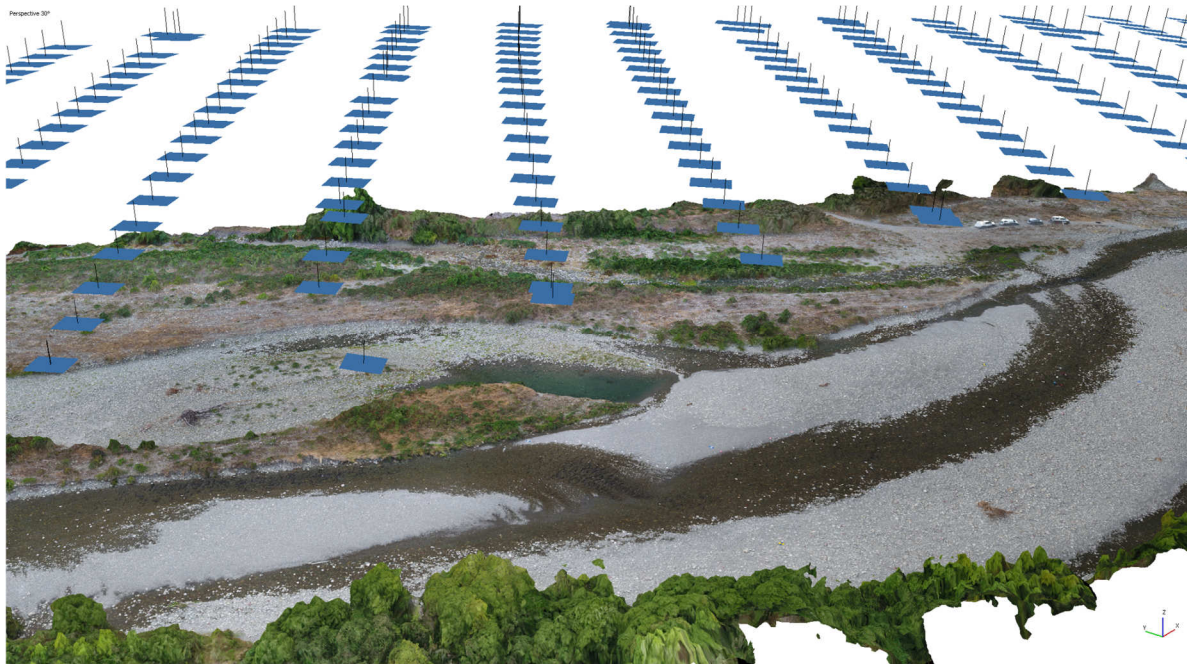
Figure 6-1: **Aerial imagery processing with Agisoft Metashape (Waingawa River). Visualisation of river 3D model, with aerial image locations as blue rectangles.**

The documentation provided by Agisoft for generation of DEMs and orthomosaics is detailed and easy to follow, please consult the user manual (Agisoft, 2021), or the following tutorials:

- For DEMs and orthomosaics without GCPs: https://agisoft.freshdesk.com/support/solutions/articles/31000157908-orthomosaic-dem-generation-without-gcps-

- For DEMs and orthomosaics with GCPs: https://agisoft.freshdesk.com/support/solutions/articles/31000153696

There are also many informative video tutorials on YouTube for creation of DEMs and orthomosaics.

Are ground control points necessary?

The use of GCPs surveyed with RTK GPS will create more accurate maps (georeferenced orthomosaics) and DEMs; however, there is a significant time penalty with GCP deployment, surveying, and data processing. The table below provides a general rule of thumb for when GCPs must be deployed, or could be skipped if there are time (or equipment) constraints:

Table 6-1: **Situations where ground control points must be used, or can be skipped.**

GCPs must be used	GCPs can be skipped
Aerial imagery does not have GPS information attached in EXIF information (i.e., GPS metadata).	Aerial imagery has GPS information attached in EXIF information (i.e., GPS metadata). **And:**
There will be comparison between aerial imagery and georeferenced ground control measurements.	Aerial imagery is only being used for visual cover estimation from reference images. **Or:**
There will be pixel by pixel comparison between different aerial imagery types (i.e., RGB vs Multispec).	Classifications are only being used to compute percentage cover, rather than absolute cover in m^2 (or biomass).

GCPs must be used	GCPs can be skipped
There will be ongoing monitoring at a study site, where change over time is being investigated on a pixel by pixel basis.	
Classifications are being used to compute absolute cover in m^2 or to estimate biomass.	
A digital elevation model (DEM) is required.	

6.2 Multispectral cameras

Processing of multispectral camera data is similar to RGB or RGN, but the complexity is increased since multispectral cameras comprise multiple cameras and lenses that have slight differences in origin and orientation. For example, a six-camera system such as the Airphen will not produce six images that perfectly overlap. Thus, they must be processed with a different workflow from single camera RGB or RGN images. For the most up to date workflow, please consult the 'Multispectral Imagery' and 'Rigid camera rigs' section of the latest Agisoft Metashape user manual (Agisoft, 2021). Alternatively consult the specific advice from the multispectral camera manufacturer, about orthomosaic generation. Some may be processed natively in Agisoft Metashape, or PIX4D, while others may need custom scripts from the manufacturer for processing and alignment.

6.3 Hyperspectral cameras

Hyperspectral cameras require different processing software than that used for RGB, RGN and multispectral imagery. As discussed in Section 3.3.2 this is because they record a line of pixels (rather than a 2D image) and must be moved across the landscape to build up an image (this is why they are sometimes called 'hyperspectral scanners'). They require GPS and IMU information for the origin and orientation of the camera in space, as well as an underlying digital surface model to project the recorded imagery onto (for orthorectification). Each image 'hypercube' from a hyperspectral camera is usually stored in a separate folder, along with other files used for processing (e.g., GPS and IMU data, and downwelling irradiance data). Hypercubes contain a lot of data (some can be 1 GB per 'image') and are usually batch processed with the following general workflow:

- Add all hypercubes to the batch processor;

- Convert the raw hypercubes to radiance using the imager calibration file;

- Convert the radiance hypercubes to reflectance by either:

  – Using the spectrum derived from a calibration tarpaulin with known reflectance;

  – Using downwelling irradiance measurements (for example, with the Ocean Optics flame spectrometer available for purchase with Resonon hyperspectral cameras). However, this does not have a good response in the near infrared part of the spectrum (i.e., >900 nm) so if this information is needed for classifications, it is recommended to use the tarpaulin. The continuous record of downwelling irradiance data is still useful for monitoring overall lighting changes due to time of day and cloud cover;

- Georectify the reflectance hypercubes in the batch processor, using an input digital surface model (in UTM59S or UTM60S for hyperspectral data collected in New Zealand with a Resonon hyperspectral camera);

- The georectified reflectance hypercubes are now ready for analysis, classification, or further pre-processing. Some further pre-processing methods that can make them easier to work with are:

  - Spectral averaging (to reduce file size and noise);

  - Principal component analysis to find the most spectrally distinctive channels (maximise variance), which reduces file size and removes redundant (i.e., correlated) channels;

  - Averaging and resampling of overlapping hypercubes from neighbouring flight lines.

This provides an overview of the usual steps required for hyperspectral image pre-processing to generate georeferenced reflectance hypercubes (the hyperspectral equivalent of georeferenced orthomosaics). Working with hyperspectral data is non-trivial, and the latest version of the camera manufacturers user manual should be consulted for up to date (and detailed) data processing procedures (Resonon, 2021a,b). It is also recommended to attend a training workshop from the camera manufacturer (e.g., Resonon or Headwall) to learn hyperspectral data collection, processing and analysis. After the hyperspectral aerial imagery has been processed, reflectance spectra can be extracted from user defined polygons around classes of interest and exported.

7 Aerial image classification

7.1 Choose image analysis program

Image classification is commonly divided into supervised and unsupervised classification.

- Supervised classifications usually consist of defining the classes comprising an image, then selecting polygon Regions of Interest (RoI) for each class, from which pixels are extracted for training data;

- Unsupervised classifications usually consist of automatic delineation of an image into spectrally distinct classes, with user adjustable parameters such as thresholds, or the number of output classes. These classes can then be merged or assigned physical meaning through user interpretation, or ground truth data.

Classification can either be performed on a pixel basis (which is convenient for multispectral and hyperspectral imagery), or using Object Based Image Analysis (OBIA) techniques which utilise spatial information such as texture (Blaschke, 2010). For our application of classification of sparsely distributed *Microcoleus* cover, we will focus on supervised classification algorithms on a pixel basis, with the selection of training and ground truth data, from either user judgement, or RTK GPS ground truth surveys.

Several software programs are suitable for classification of drone-captured remote sensing data (i.e., georeferenced orthomosaics). Common examples are, ENVI, Erdas Imagine, eCognition, Matlab, ArcGIS and QGIS. Some of these programs are very expensive and may require the purchase of additional toolboxes or packages (e.g., ENVI, Erdas Imagine, Matlab and ArcGIS). Some are very powerful and flexible but have a steep learning curve and programming-based interface (i.e., Matlab), or are designed for processing a specific manufacturers hyperspectral data (e.g., Spectronon Pro for Resonon hyperspectral scanners). To provide a practical workflow for councils around New Zealand to analyse individual georeferenced orthomosaics (i.e., from RGB and multispectral imagery) and perform supervised classifications, we used, and recommend, the open-source software QGIS (Congedo, 2021).

7.2 Installing QGIS and importing data

QGIS can be downloaded and installed from https://qgis.org/en/site/forusers/download.html. The version used at the time of writing was 3.22.1. The next step is to install the Semi-Automatic Classification Plugin (Figure 7-1). Detailed information about the Semi-Automatic Classification Plugin can be found here https://fromgistors.blogspot.com/p/semi-automatic-classification-plugin.html.
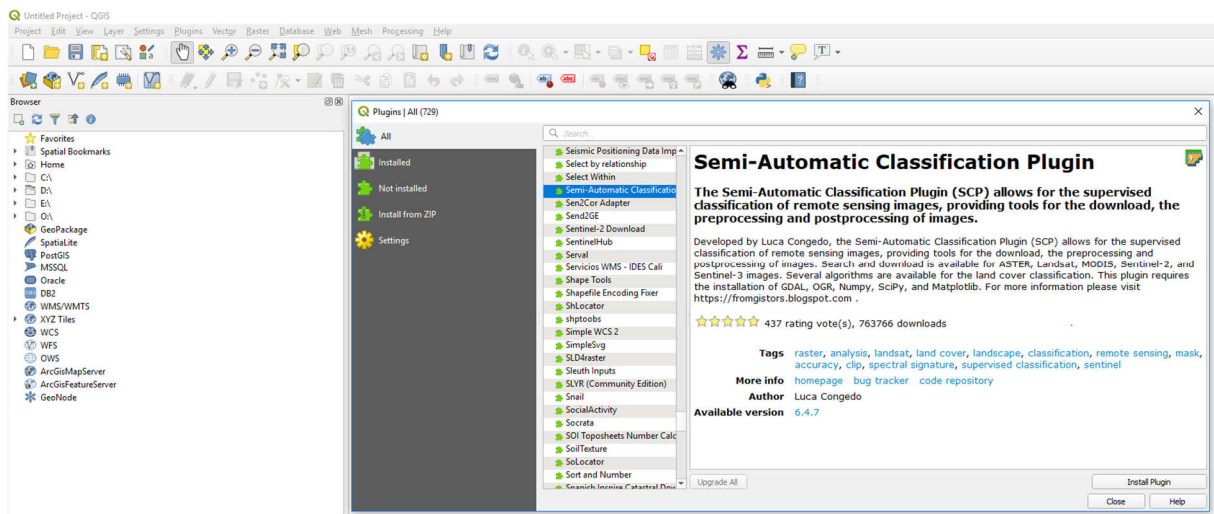
Figure 7-1:   Install the Semi-Automatic Classification Plugin for QGIS.

Load the georeferenced orthomosaic (i.e., .tiff file) of the RGB (Figure 7-2) or multispectral imagery.
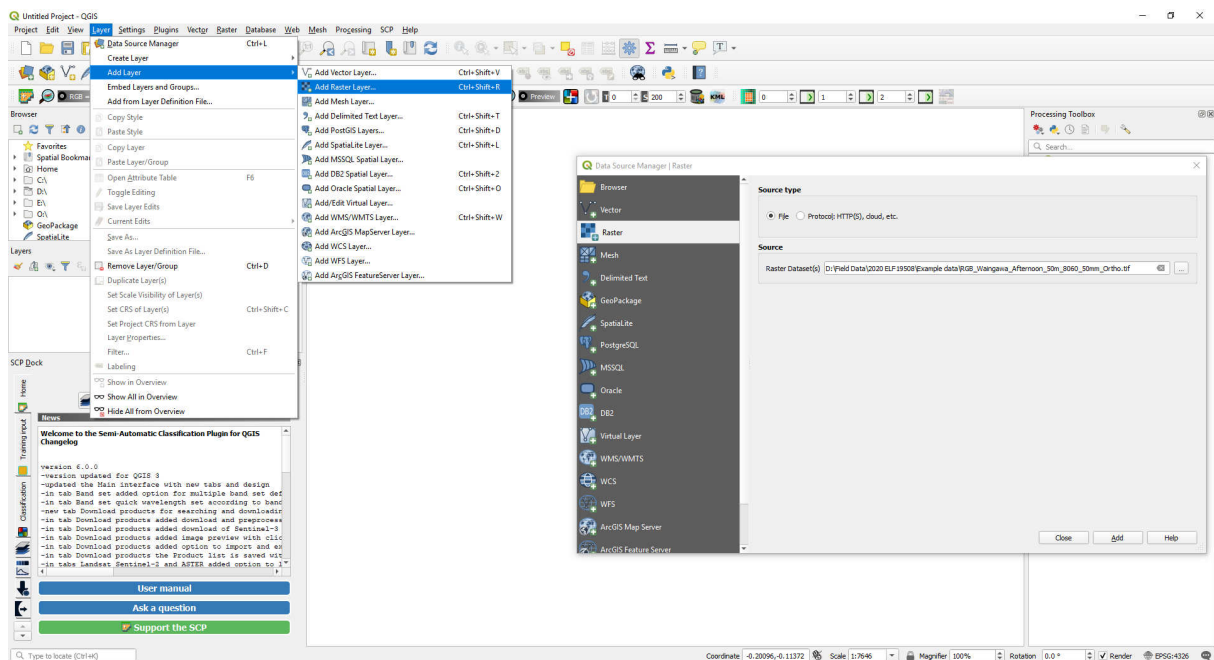
Figure 7-2:   Load the georeferenced orthomosaic (usually in NZTM2000).

If GPS data is available it can also be loaded as a delimited text layer (Figure 7-3).
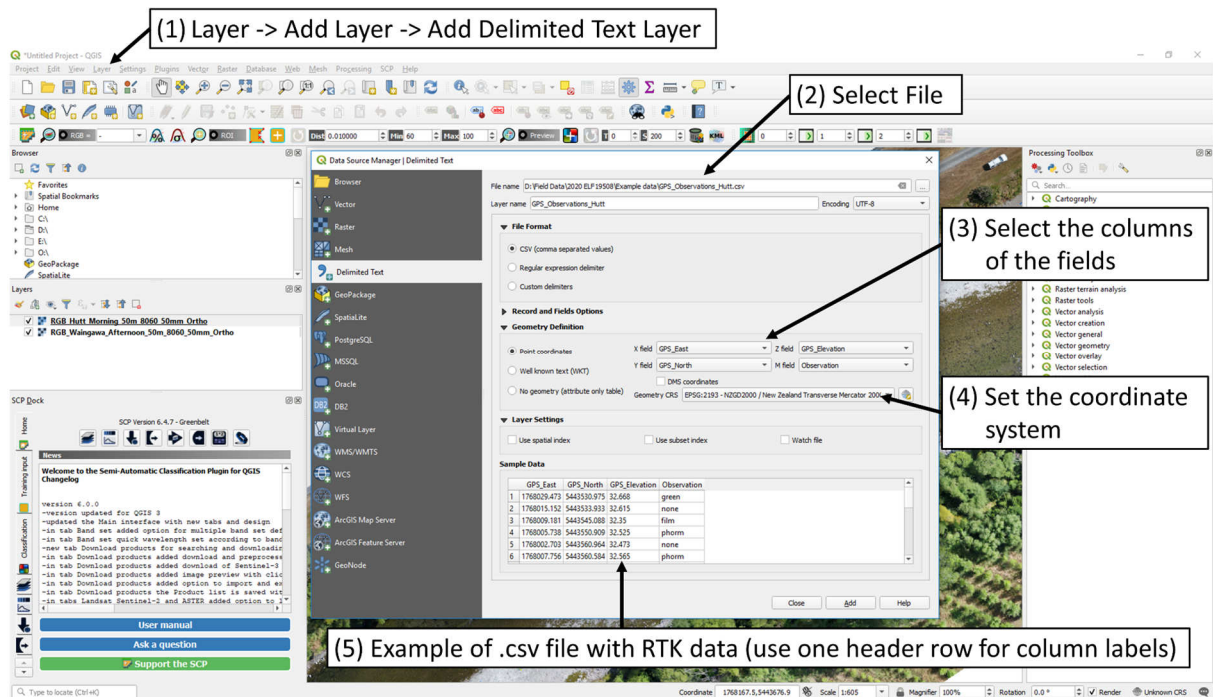
Figure 7-3: Load GPS data if available.

Then set the symbols to representative colours for the observation classes (Figure 7-4).
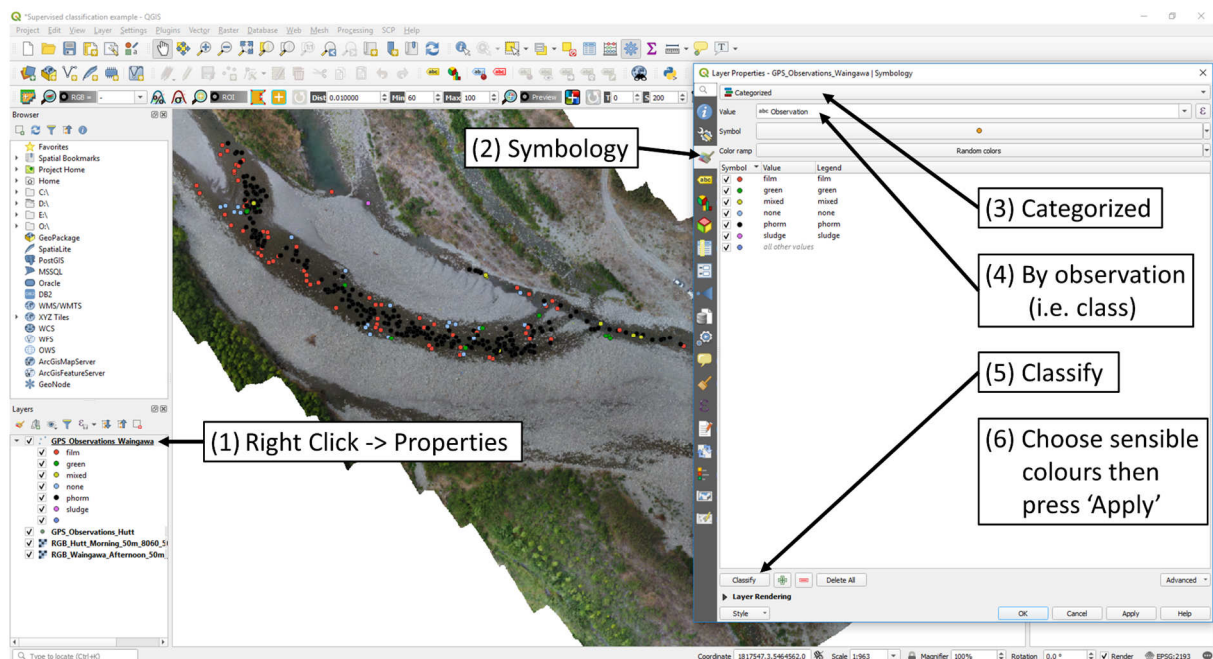
Figure 7-4: Visualise GPS observations by class and set observation colours.

7.3   Visualising multispectral raster data and creating band ratios

To visualise multispectral data more effectively, it is useful to know information about the spectral responses of the band pass filters of the camera, and the absorption (or reflection) characteristics of

the target class of interest. For example, the Airphen multispectral camera has bands 10 nm wide at band centres of: B1=530, B2=570, B3=622, B4=675, B5=710, B6=750 nm. These correspond to some of the absorption peaks of the pigments phycoerythrin, phycocyanin and chlorophyll *a* (Figure 7-5).
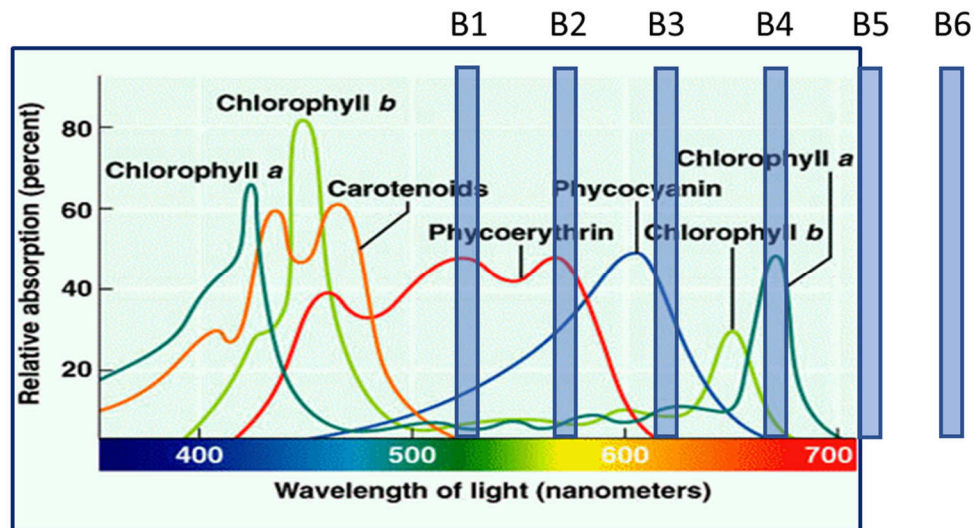
Figure 7-5: **Photosynthetic pigments with an overlay of the spectral bands of the Airphen multispectral camera.**[5]

Pigments with high relative absorption will appear dark, for example *Microcoleus* appears black since it is high in phycoerythrin and phycocyanin and hence absorbs most of the visible light, compared to most plants and green algae that reflect green light. Thus, it can be convenient to use band ratios to differentiate between *Microcoleus* and other chlorophyll-containing classes of interest. Since chlorophyll also has high reflectance in the near infrared, convenient ratios to differentiate between *Microcoleus* and green algae are Band6/Band2 or similar. Band ratios can be calculated in most software packages suitable for image analysis of remote sensing data. In QGIS, this is performed using the raster calculator (Figure 7-6), with data being saved into a new geotiff file, to be used for further processing. This is essentially a form of feature engineering to maximise class separation based on known spectral responses.

---

[5] Image reproduced from https://www.simply.science/images/content/biology/cell_biology/ photosynthesis/conceptmap/Photosynthetic_pigments.html and amended to show six Airphen bands.
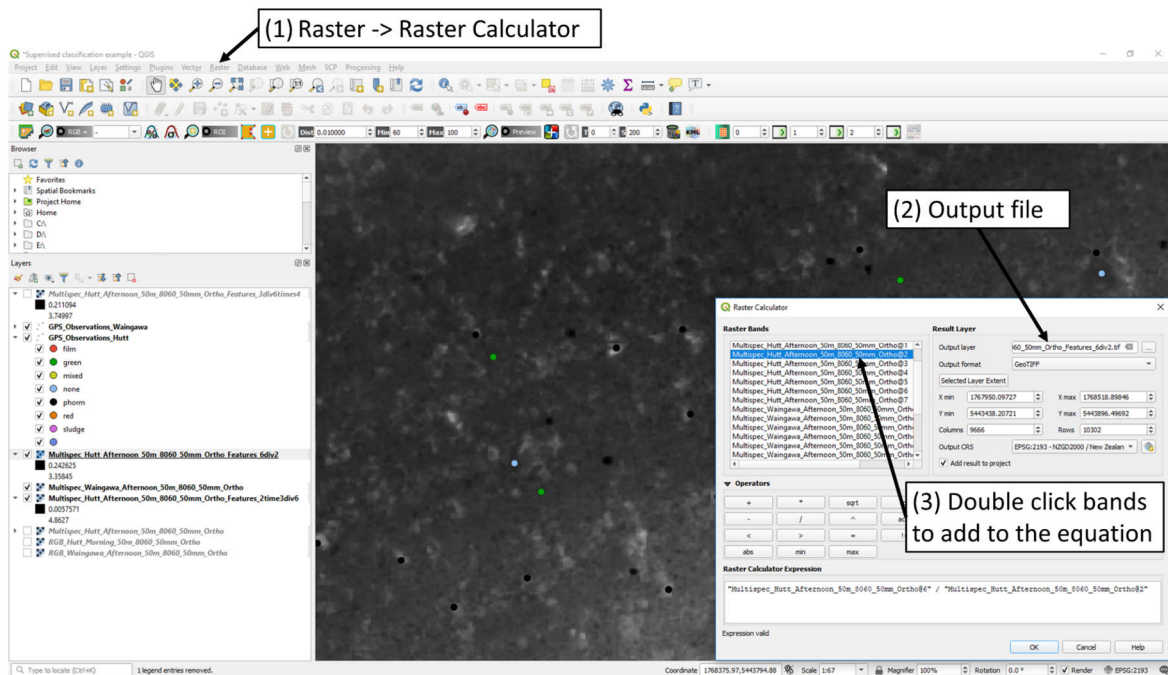
Figure 7-6: **Creating new raster layers using band ratios in QGIS.**

Newly created raster layers can be used with the existing multispectral imagery to provide further predictive power. Raster layers can be combined by using the merge tool in QGIS (Figure 7-7). It is important to click the 'Place each input file into a separate band' if you would like bands to be 'stacked', otherwise they will be averaged together.
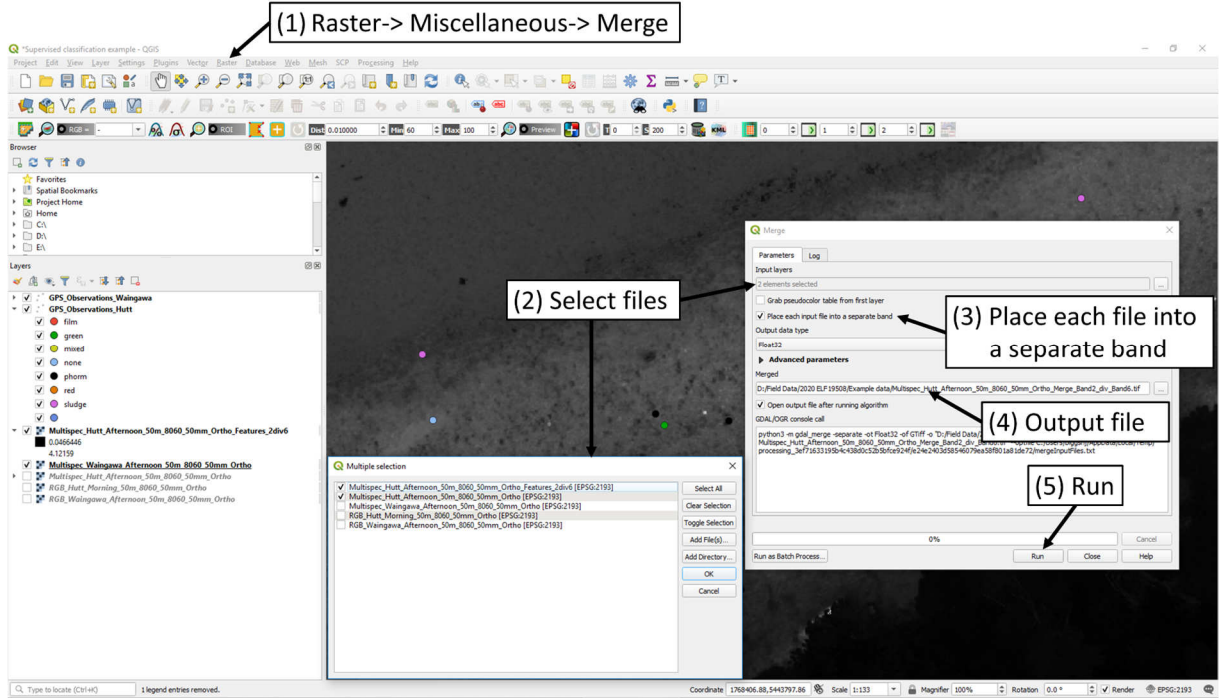
Figure 7-7: **Example of merging raster bands in QGIS, where the multispectral orthomosaic has the band ratio of Band6/Band2 appended to the end.**

7.4   Demarcating river boundaries and cropping raster imagery

The next pre-processing step is to demarcate the boundary of the river, then clip the georeferenced orthomosaic to match this region. This will speed up classifications by focussing on the data of interest in the river. To do this in QGIS, create a polygon shapefile (Figure 7-8) then draw the boundaries of the river (Figure 7-9). This polygon shapefile is then used to clip the georeferenced orthomosaic to the river region (Figure 7-10).
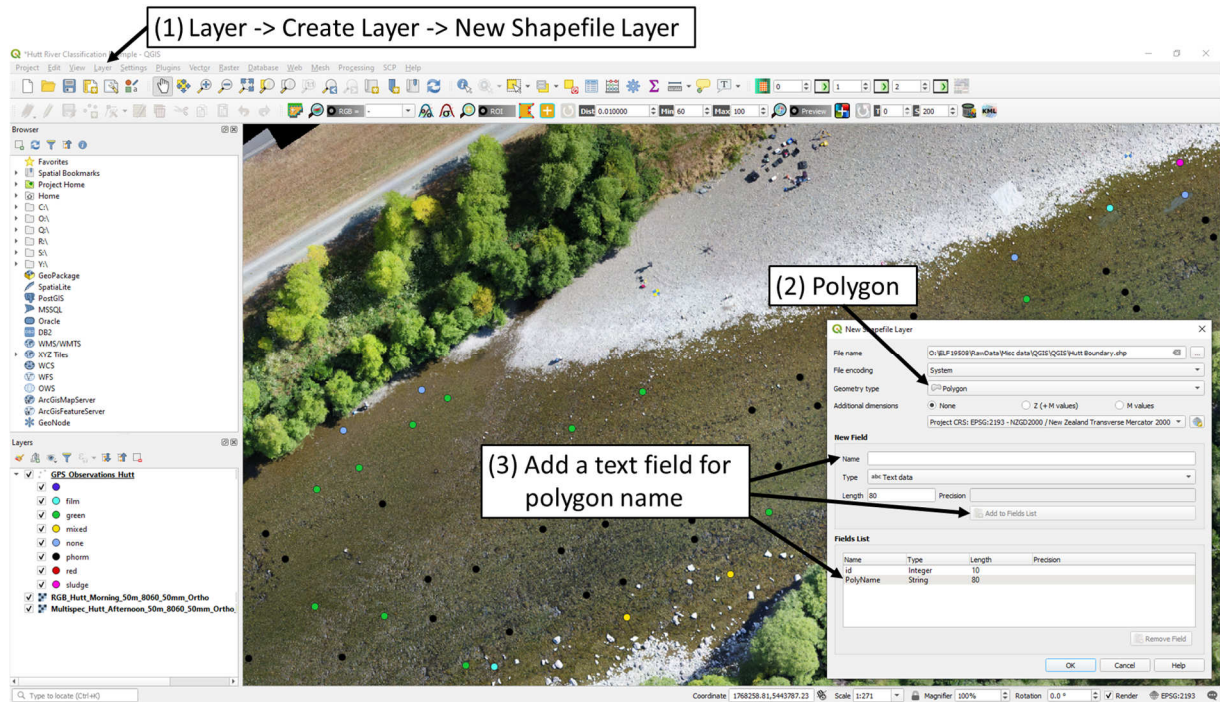
Figure 7-8:   Create polygon shapefile in QGIS.
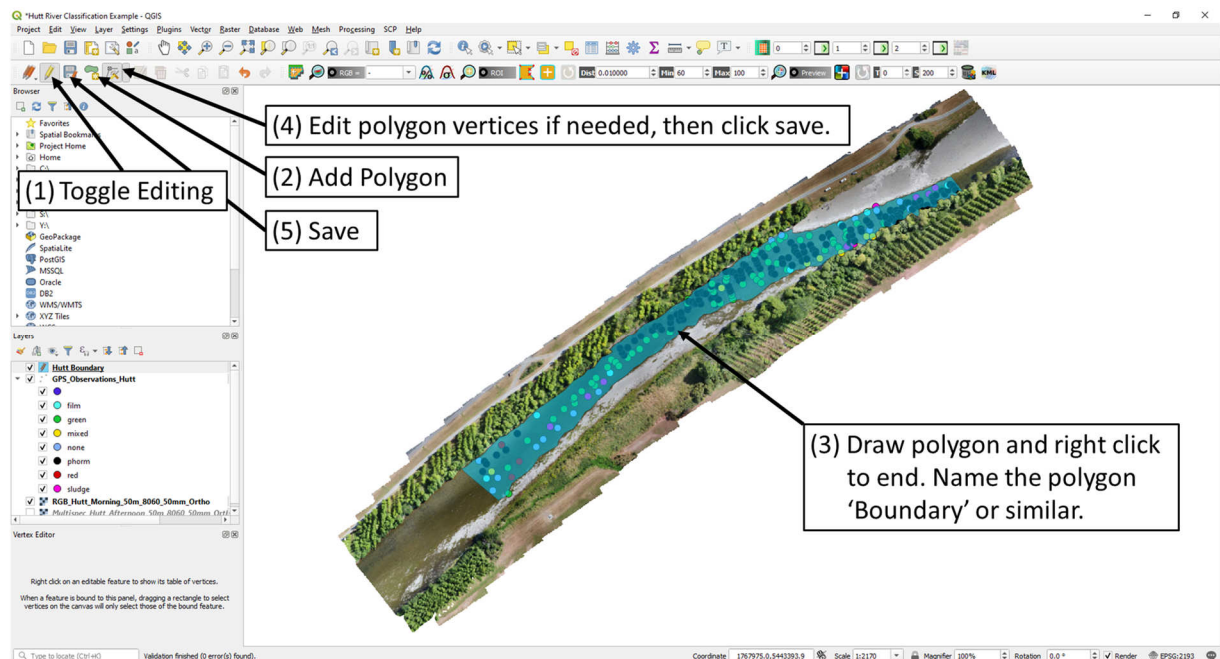
Figure 7-9:   Draw the boundary of the river reach in QGIS.

Microcoleus* Aerial Monitoring User Guide
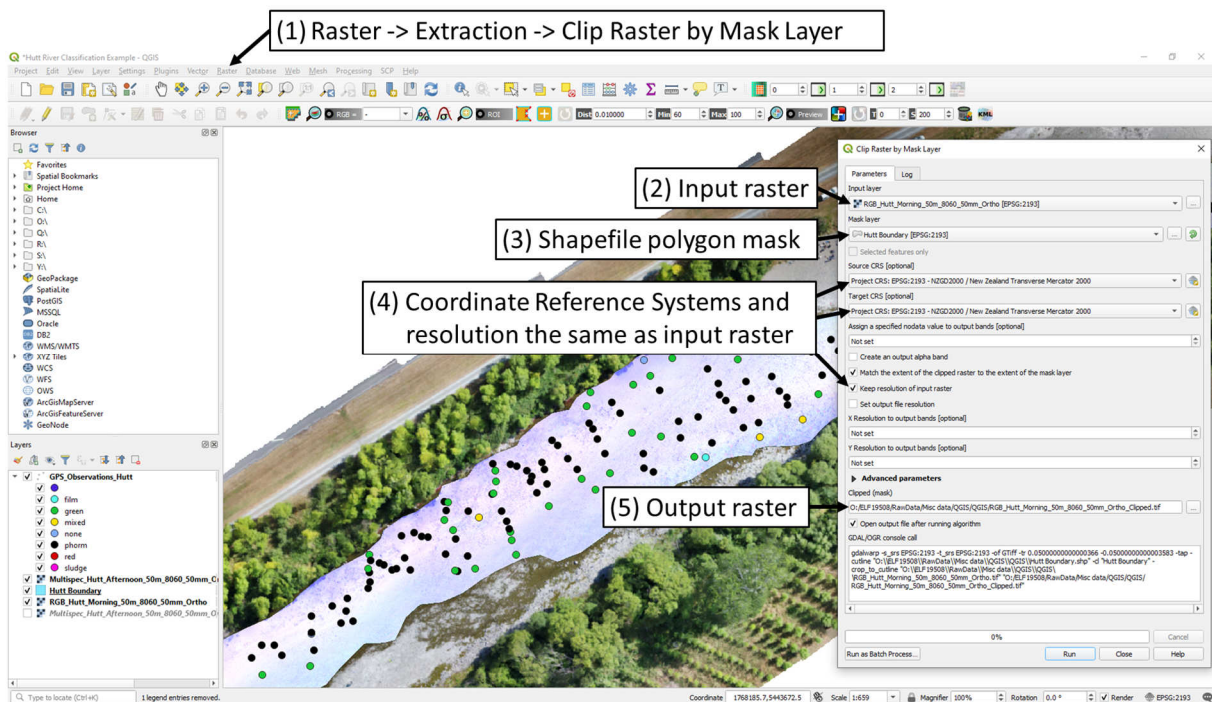
Figure 7-10: Clip the raster data (georeferenced orthomosaics) by the polygon shapefile of river boundaries in QGIS.

7.5   Removing alpha layer (if needed)

In QGIS, maximum likelihood classifications are not possible when alpha (i.e., transparency) layers are present. This problem can be avoided by not exporting georeferenced orthomosaics from Agisoft Metashape (or Pix4D) with an alpha layer. However, this band can also be removed in QGIS before starting to select training pixels (Figure 7-11).
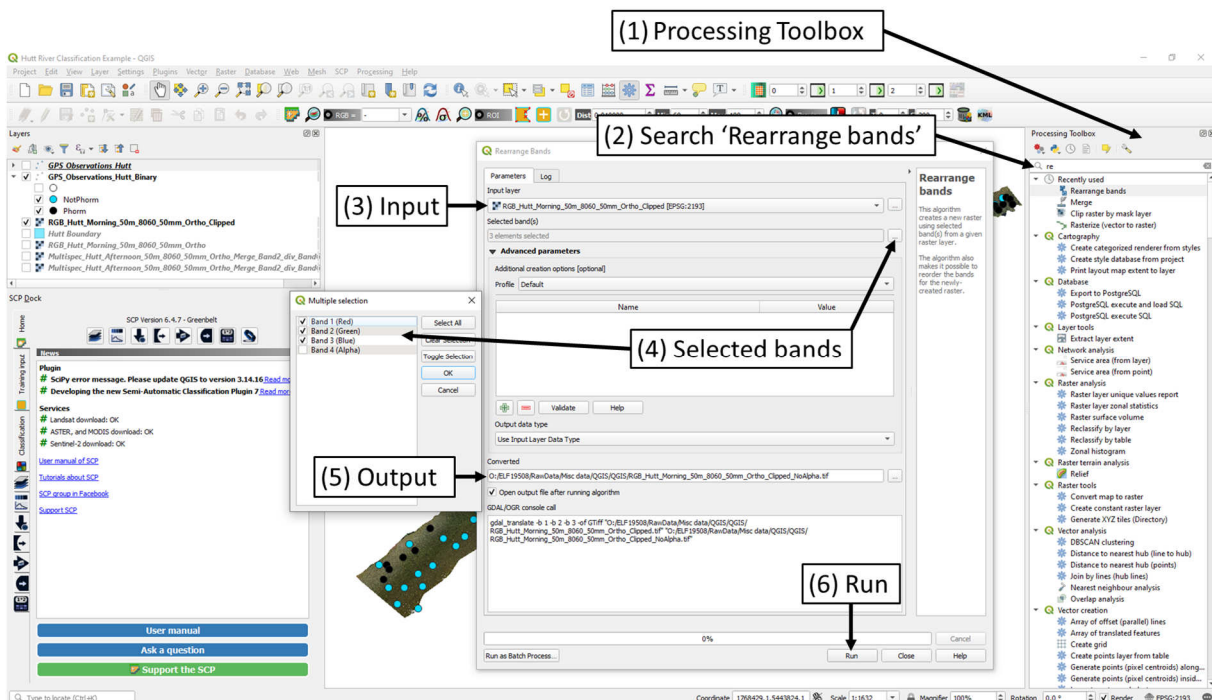
Figure 7-11:   Removing the alpha band from orthomosaics before classifications.

7.6   Fixing georeferencing (if needed)

The spatial accuracy of georeferenced orthomosaics output from Agisoft Metashape is dependent on sufficient overlap of aerial images (e.g., 80% front overlap, 60% side overlap), and a good distribution of ground control points throughout the study reach. Sometimes there may be an insufficient number of ground control points in one part of a study reach, or there may be no GCPs within the wetted river region. This can result in discrepancies between surveyed GPS ground truth measurements (i.e., *Microcoleus* locations) and where these ground truth measurements appear in the georeferenced orthomosaic (Figure 7-12). For most image classification tasks the objects of interest and classes are large, such that these small discrepancies are not problematic (e.g., identification of buildings, cars, trees etc). However, for the fine spatial resolution required for *Microcoleus* Aerial Monitoring, small discrepancies in the correspondence of image and ground truth coordinates are very problematic for classifications (i.e., correctly selecting training and validation pixels).

Figure 7-12: Example of spatial discrepancies between objects apparent coordinates in georeferenced orthomosaics and their actual coordinates from RTK GPS ground truth surveys.

To correct this problem in QGIS, the Georeferencer plugin can be used to refine the georeferencing of imagery. Open the Georeferencer plugin window and resize it so that it occupies half the screen (Figure 7-13). Load the orthomosaic that will be corrected and set the transformation settings and output. For smooth georeferencing and correction of the orthomosaic throughout the study reach (as in this example) the recommended transformation type is 'Polynomial 2' with 'Nearest neighbour' resampling. If the majority of reference points are correct and only a small area of the orthomosaic requires correction, then 'Thin Plate Spline' with 'Nearest neighbour' resampling is recommended.
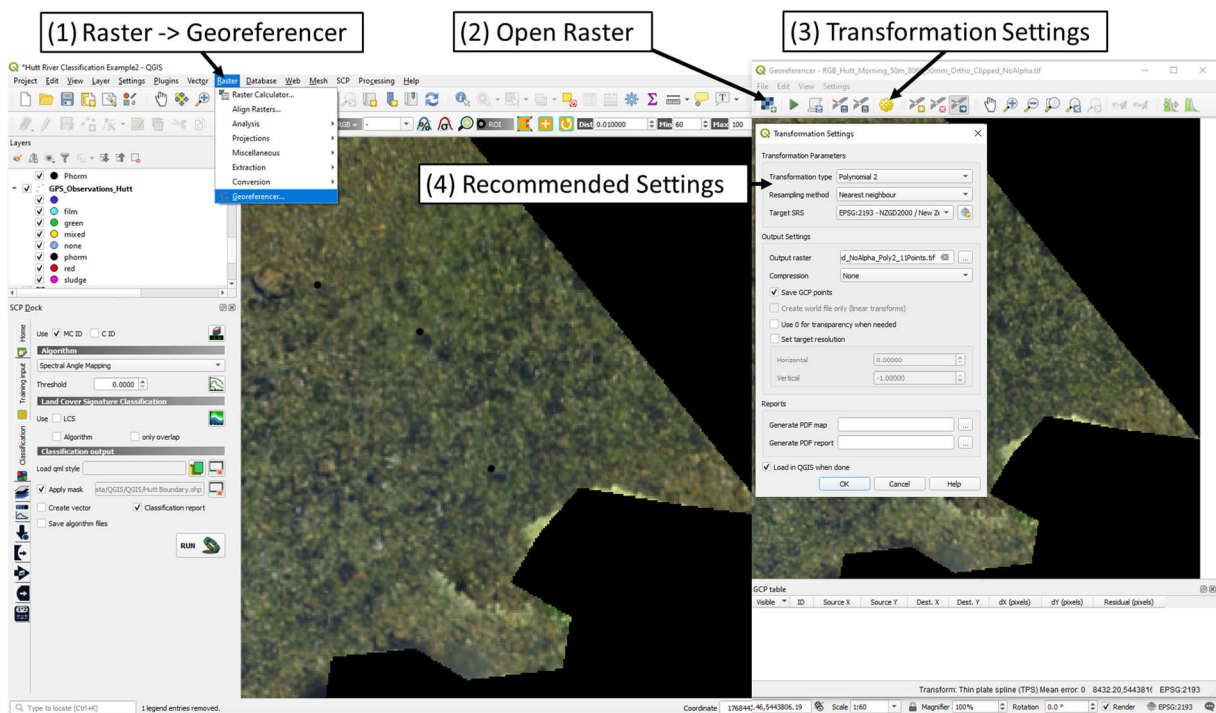
Figure 7-13:   Georeferencer plugin in QGIS.

The next step is to start selecting points that will be used for georeferencing the orthomosaic (Figure 7-14). Suitable points are GPS measurements that can be visually distinguished as being in incorrect locations. For our example, this was possible with some of the '*Microcoleus*' ground truth locations, but not points from the 'Not *Microcoleus*' class as they cannot be pinpointed to a specific location.
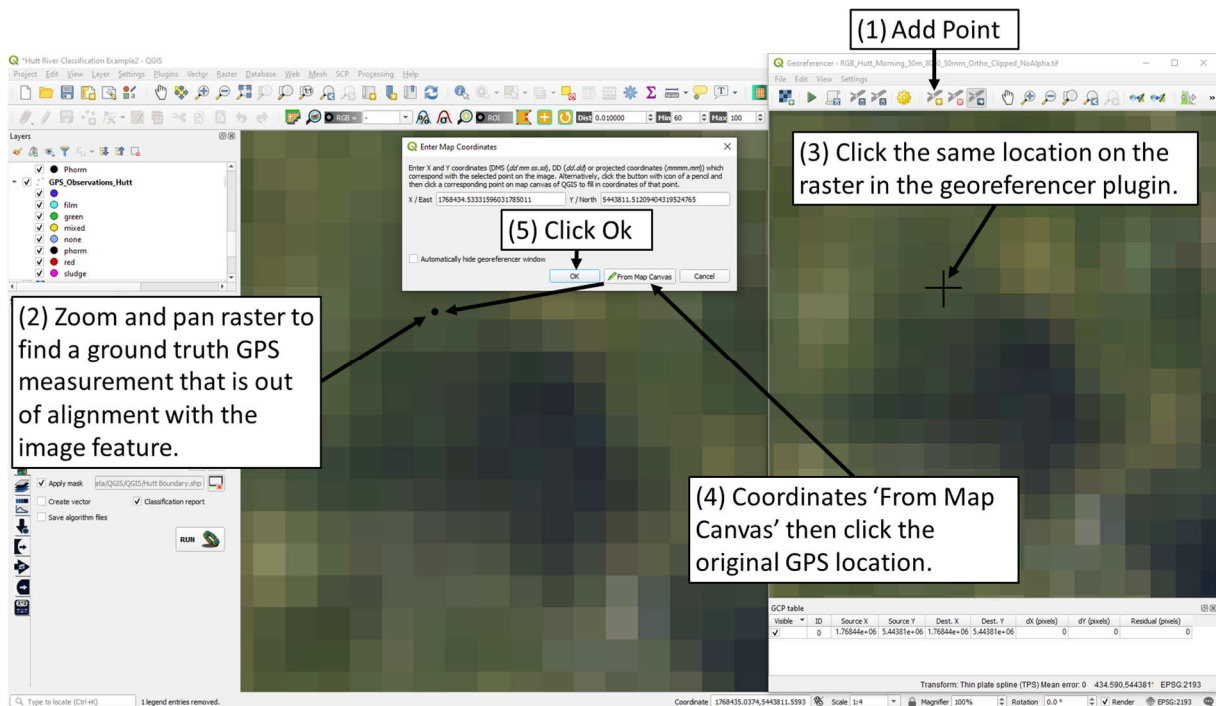
Figure 7-14:   Selecting reference points in the Georeferencer plugin in QGIS.

After points are selected in the Georeferencer plugin, the point ID and coordinates should be visible in both the Georeferencer window and the main QGIS window (Figure 7-15). The coordinates of the point will also appear in the GCP table.
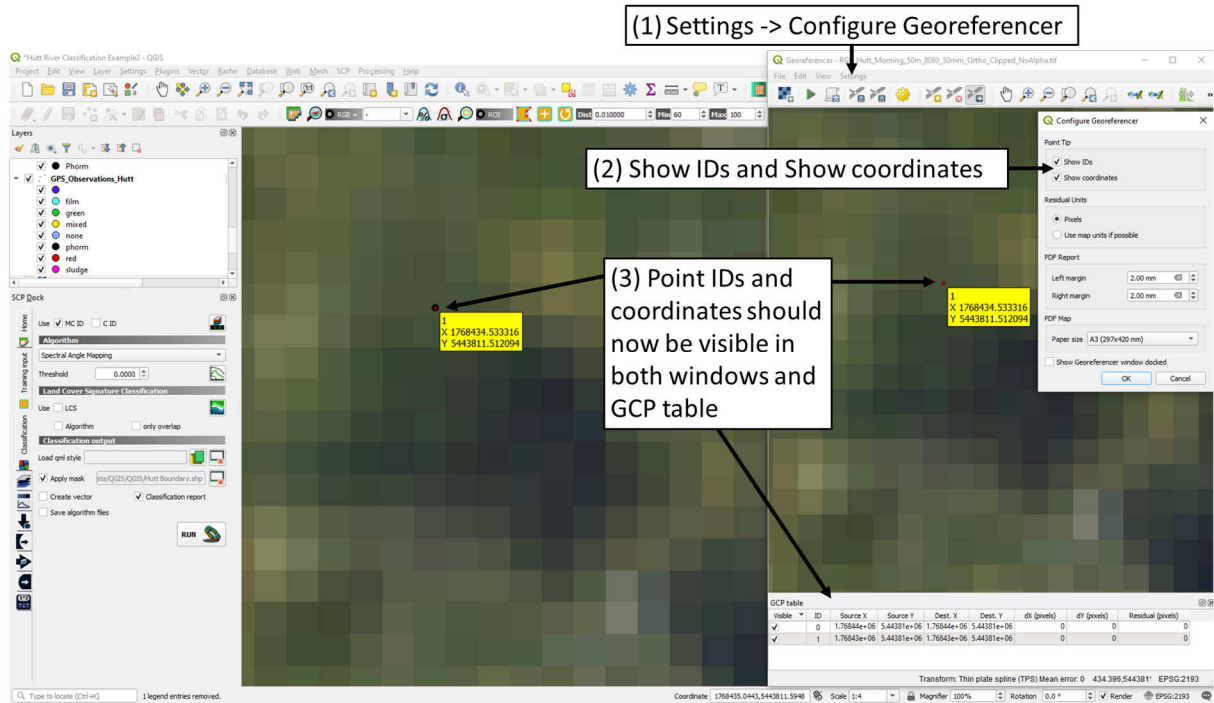
Figure 7-15: Viewing selected reference points in the Georeferencer plugin in QGIS.

Reference points should be selected from throughout the study reach (Figure 7-16).
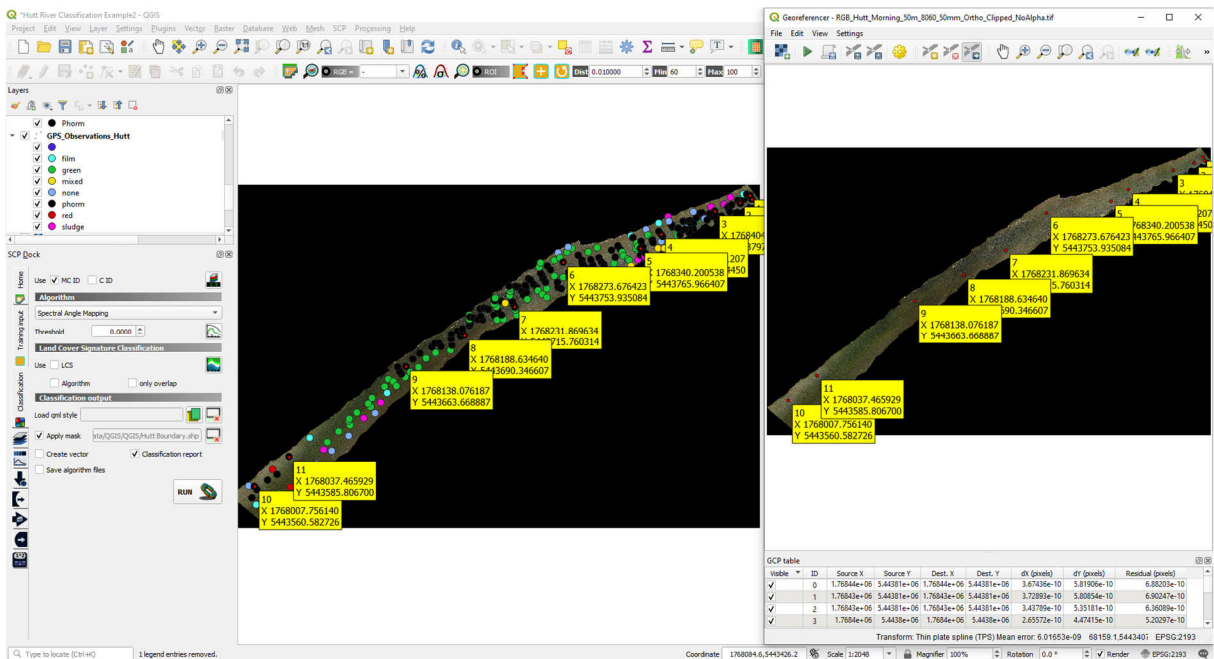
Figure 7-16: Reference points selected from throughout the study reach in the Georeferencer plugin in QGIS.

The next step is to move the points from their original inaccurate location to a more accurate location (Figure 7-17).

Microcoleus* Aerial Monitoring User Guide
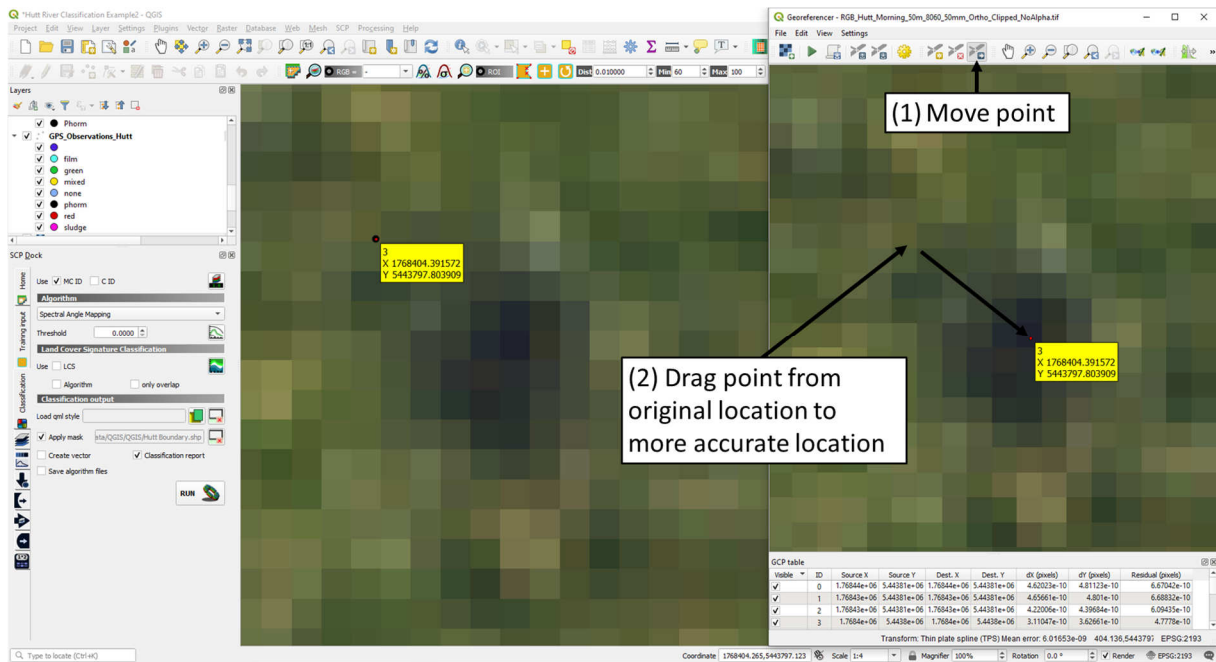
Figure 7-17: Moving reference points in the Georeferencer plugin in QGIS.

The process of moving points is repeated for all the selected reference points, then the points are saved and the georeferencing is run (Figure 7-18).
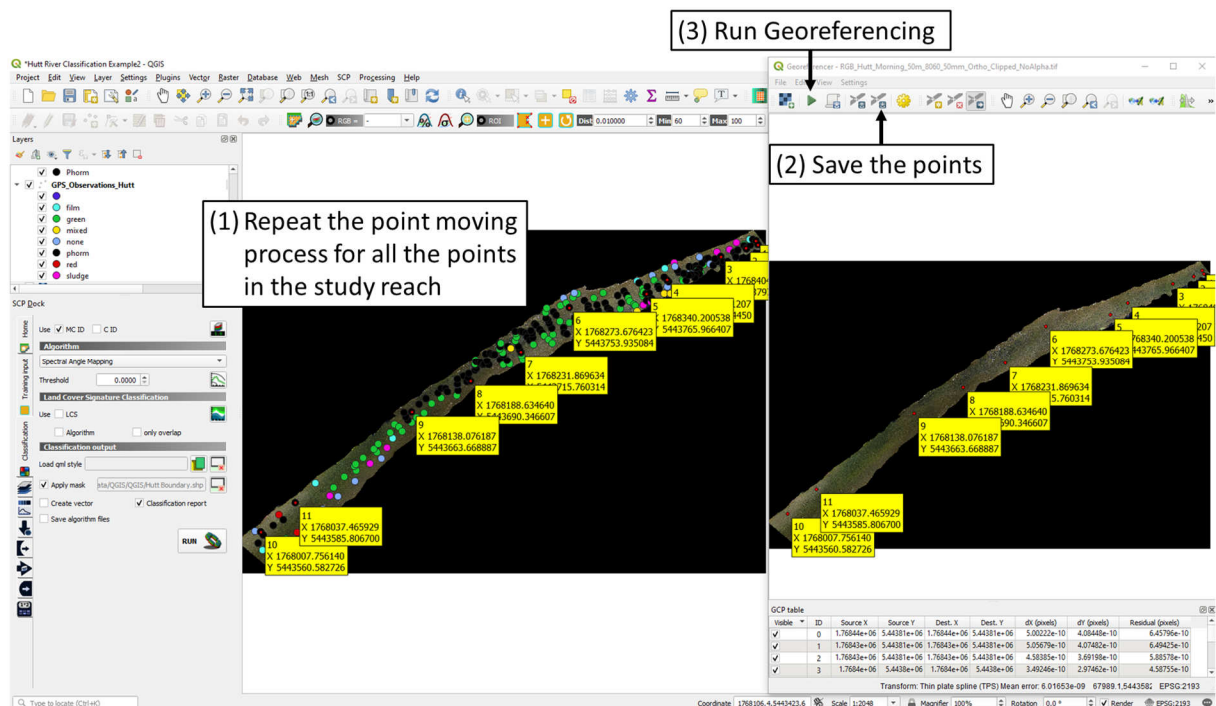
Figure 7-18: Move all the selected reference points, then save the points and run georeferencing in the Georeferencer plugin in QGIS.

Next, load the geo-corrected orthomosaic in QGIS and visually compare it with the original orthomosaic and GPS ground truth locations to ensure that the georeferencing and resampling were successful (Figure 7-19, Figure 7-20).
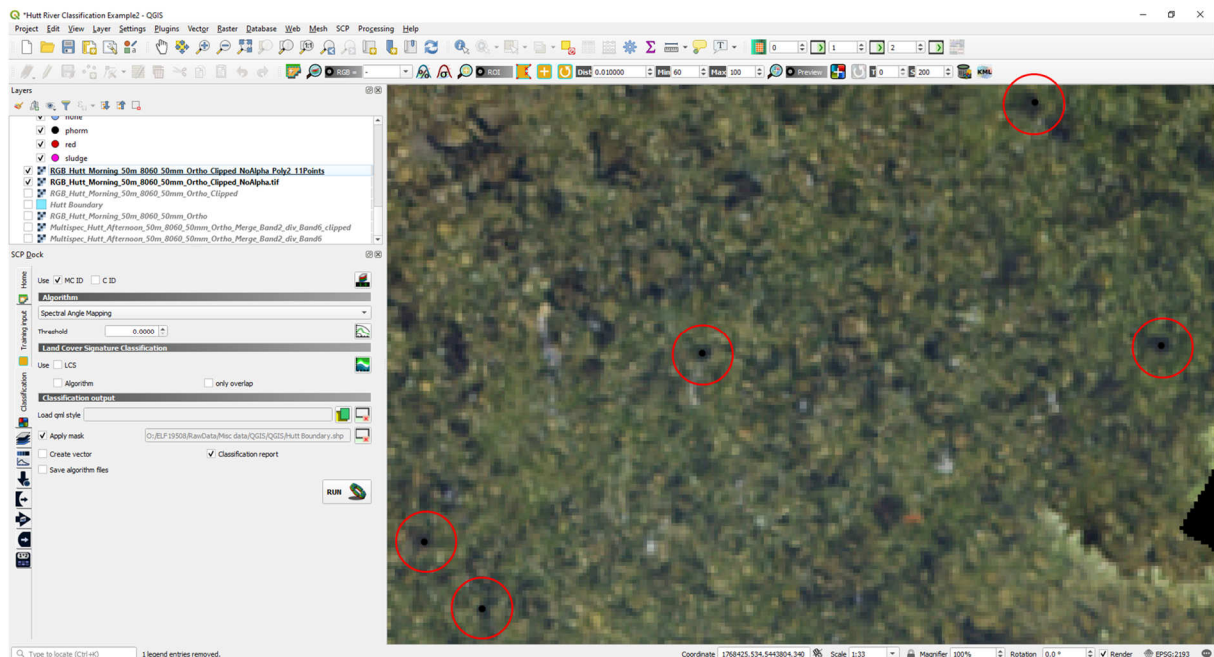
Figure 7-19: Geo-corrected orthomosaic with good alignment of *Microcoleus* patches and RTK GPS ground truth measurements.
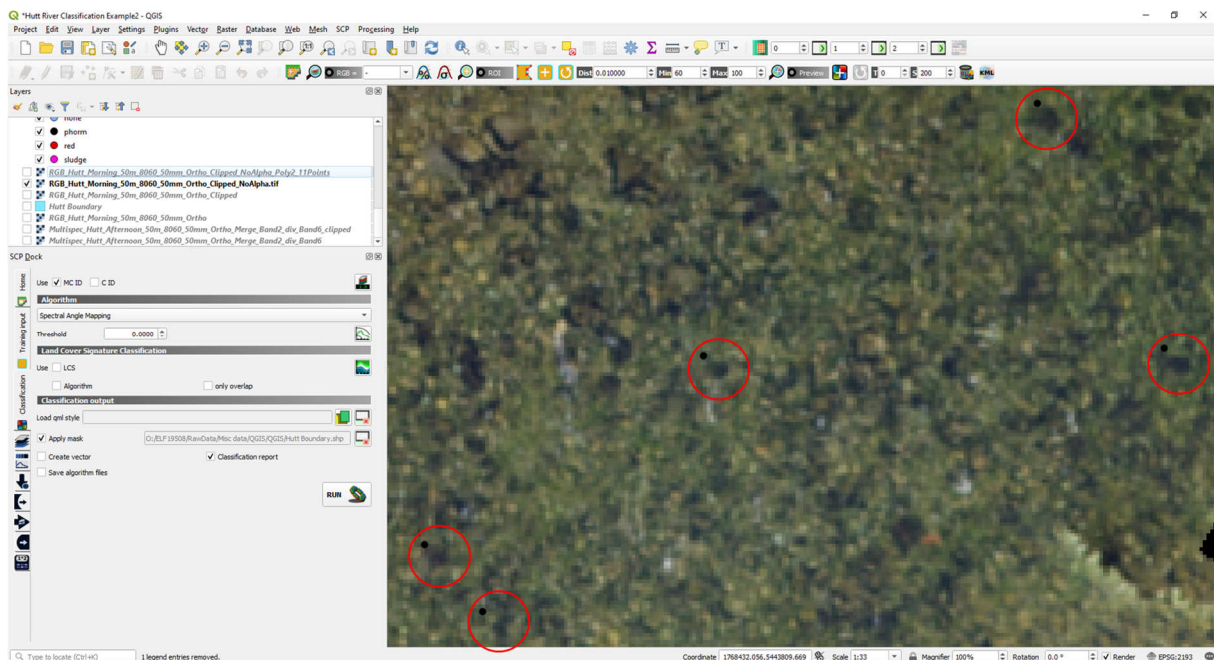
Figure 7-20: Original orthomosaic with small displacement errors between *Microcoleus* patches and RTK GPS ground truth measurements.

7.7   Define classes (supervised classification)

If RTK GPS ground truth data was collected, classes should have already been defined at the time of surveying. For example, we observed the classes 'film', 'green', 'mixed', 'none', 'phorm' (i.e., *Microcoleus*), 'red' and 'sludge'. Classes can be combined into the simpler classification scheme of macro classes '*Microcoleus*' and 'Not *Microcoleus*' in the QGIS classification workflow. However, the granularity of individual classes within each macro class is important to retain since it allows for much

more narrowly defined spectral properties. Any RTK GPS observations that span both output classes such as 'mixed' will need to be discarded. If classes can be easily distinguished by a human operator from aerial imagery, then it is possible to define them after collecting the imagery; however, this is not recommended compared to the collection of ground truth data.
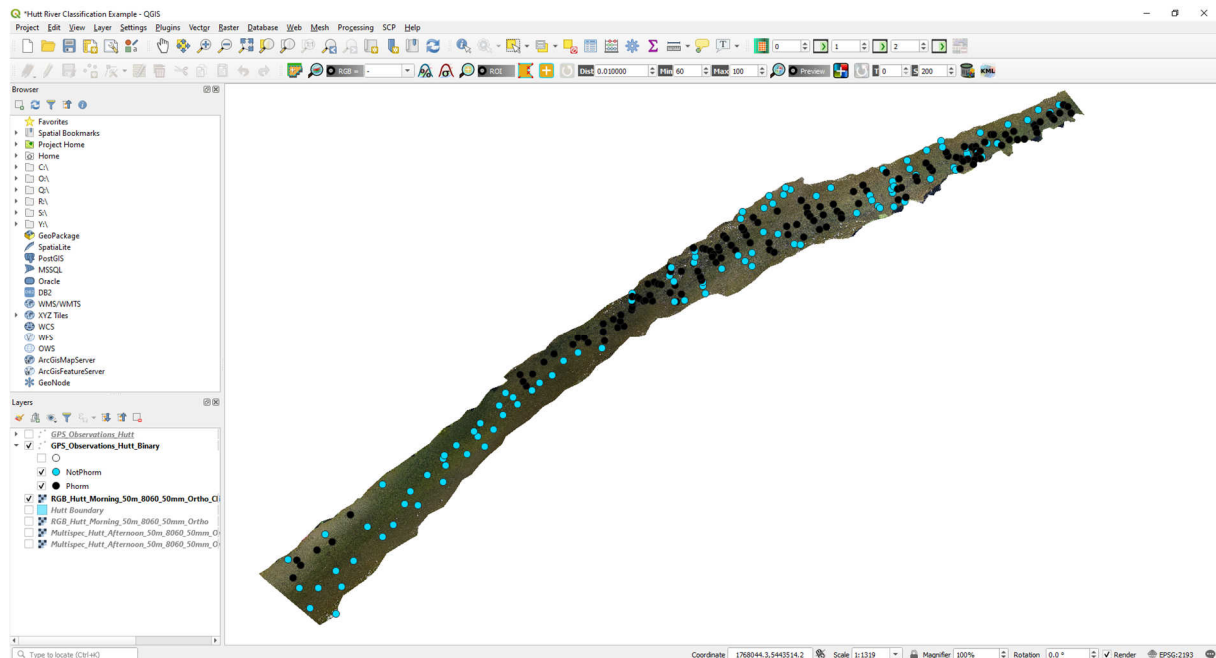
Figure 7-21:   RTK GPS ground truth measurements of the binary classes of *Microcoleus* and Not *Microcoleus* in the Hutt River.

7.8   Select training pixels for each class

Training pixels can be selected by users manually by creating a polygon of the region surrounding RTK GPS ground truth measurements. Although this is a time-consuming process, it is recommended to manually select training regions, rather than use automated extraction techniques, since the spatial heterogeneity of *Microcoleus* cover makes it challenging to define reliable rules for pixel extraction distances from RTK GPS ground truth measurements (i.e., a defined radius from a point). Also, there are commonly small-scale georeferencing issues in the orthomosaics (Section 7.6) resulting in imperfect alignment of RTK GPS ground truth measurements and imagery pixels. These issues can persist even after correction (although to a lesser degree). For classifications of larger scale terrestrial objects (i.e., trees and bushes) this is not an issue, but for *Microcoleus*, where cover changes are on the scale of 5-10 cm, high accuracy (and user judgement) in selection of neighbouring training pixels is needed. Manually selecting training pixels also allows user judgement to add any spectrally distinct regions of interest to individual classes in the 'Not *Microcoleus'* macro class (i.e., near bank shadows and other features).

The supervised classification process commences by opening the 'SCP Dock Panel', then selecting the input raster data file (Figure 7-22).
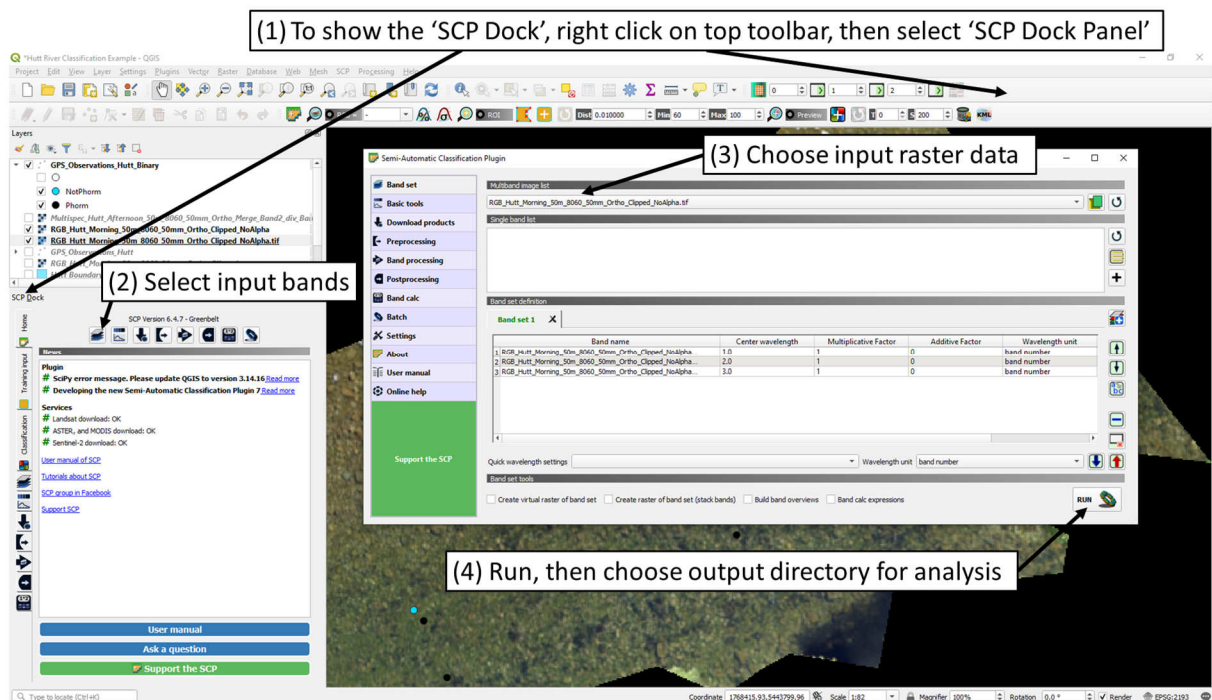
Figure 7-22: Open the Semi-Automatic Classification Plugin Dock and add the raster data in QGIS.

If RTK GPS ground truth measurements are available, they should be displayed on top of the orthomosaic to help with selection of training regions using user best judgement. Start by creating a new training file (Figure 7-23), then selecting regions of interest as polygons containing pixels of each class. For our example the top-level classes are *Microcoleus* and Not *Microcoleus,* with subclasses such as 'green' (algae), 'film', 'dry stones' etc. In QGIS the main parent classes are called MacroClasses, while subclasses can store each polygon of the individual classes making up the MacroClass. Polygons should be selected from throughout the study reach (Figure 7-25) and cover the range of spectral signatures visible in the imagery (i.e. in the Not *Microcoleus* macro class it is important to select regions with shadows, riparian vegetation, brightly exposed rocks that are above the water, ground control points, green algae etc).
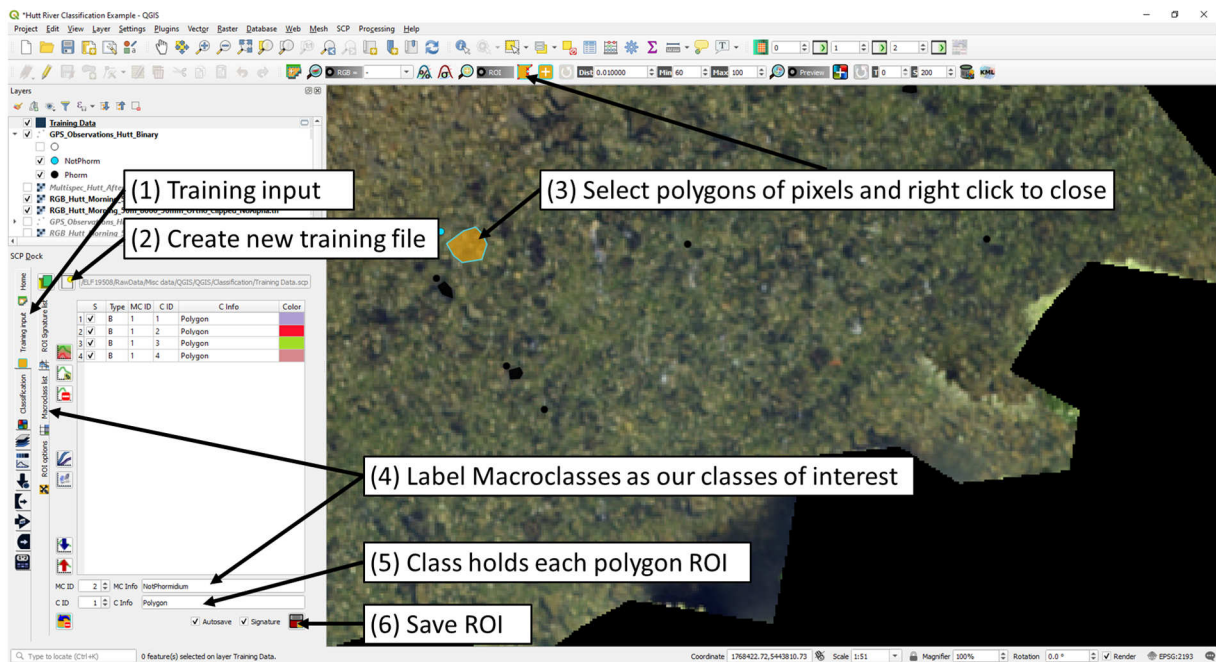
Figure 7-23: Create a training file and select Regions Of Interest in QGIS.
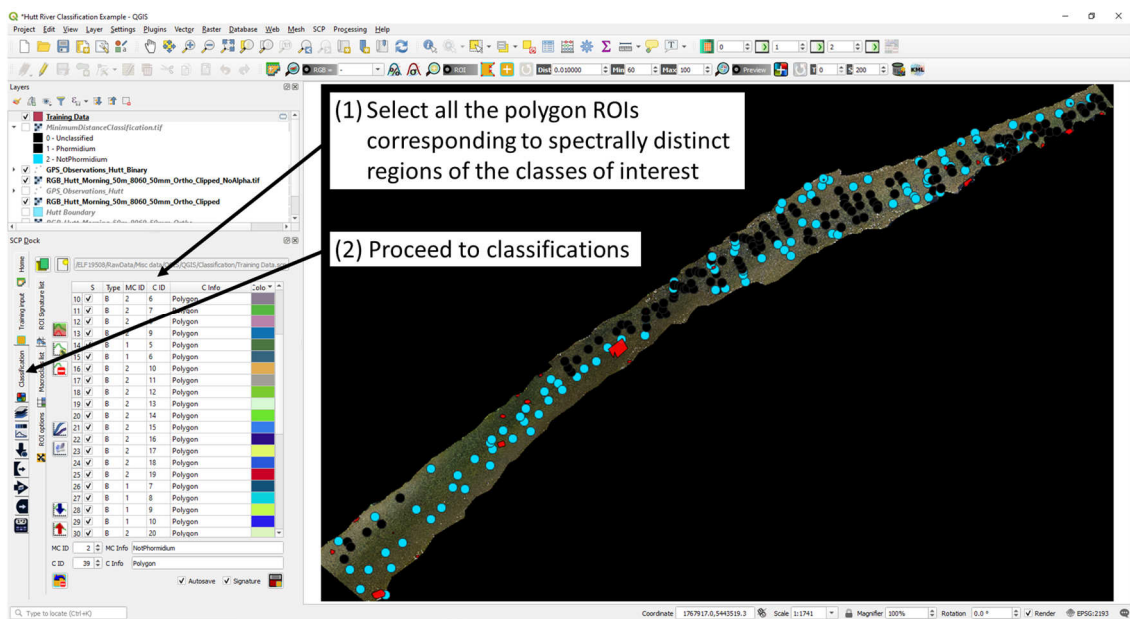
Figure 7-24: Polygon ROIs selected to cover the spectrally distinct regions of each class.

7.9   Select supervised classification algorithm and perform classification

QGIS supports the 'Minimum Distance', 'Maximum Likelihood' and 'Spectral Angle Mapper' algorithms. These are some of the most common and well-established classification algorithms. Expensive proprietary software packages provide a wider range of analysis algorithms (e.g., ACE, CNN, SVM), however testing, training and tuning algorithms to find the optimal for classifications can be a very time-consuming task. Selecting a well-established technique such as 'Minimum Distance' is usually suitable for pixel-based classifications. In the SCP plugin in QGIS, classifications are performed on the 'MacroClass', such as our case of *Microcoleus* vs Not *Microcoleus*. Outputs are then saved as

.tiff files (Figure 7-26) for visualisation and further analysis. Classification reports are saved as tab delimited .csv files to open in notepad or excel.
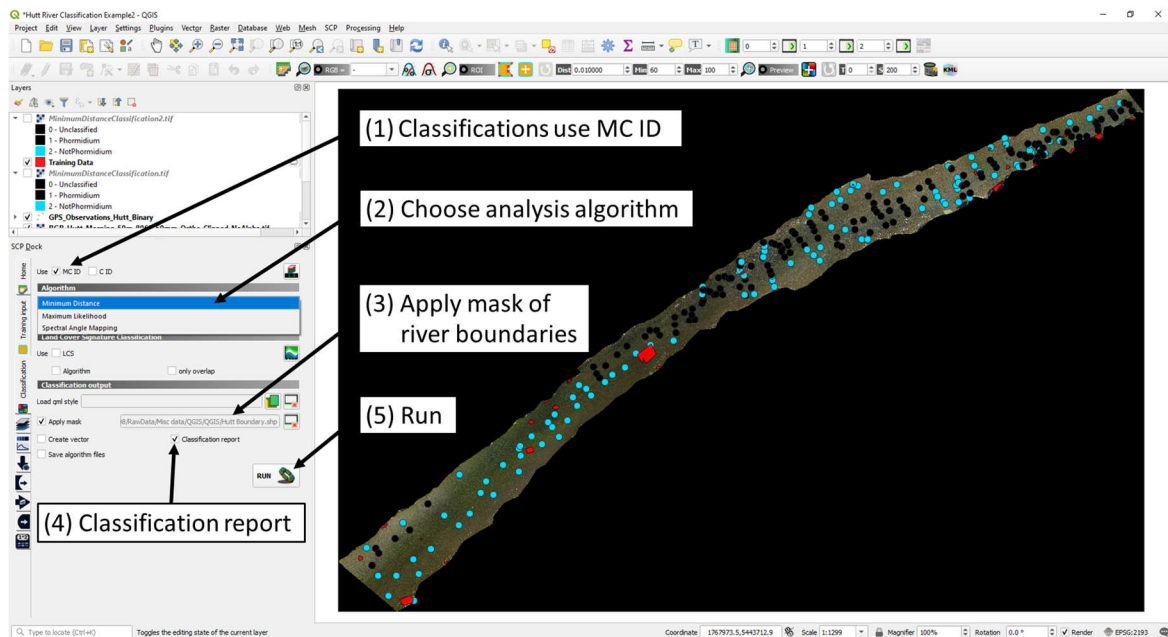
Figure 7-25:   Polygon ROIs selected to cover the spectrally distinct regions of each class.
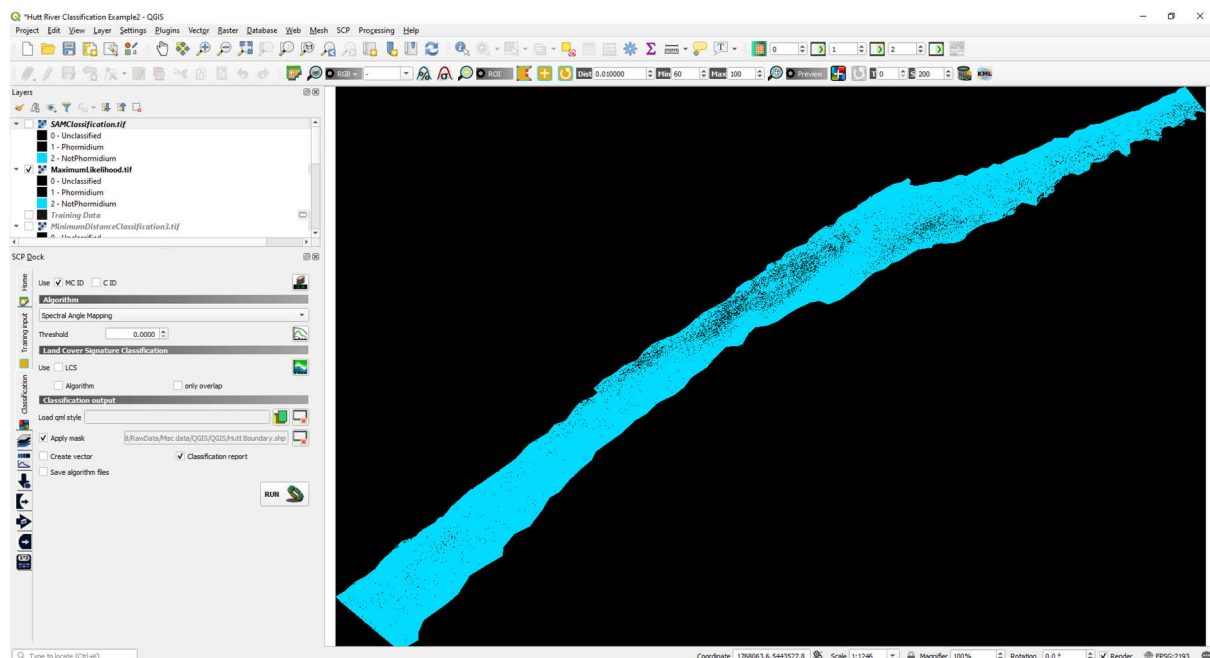
Figure 7-26:   Maximum likelihood classification of the Hutt River into classes '*Microcoleus*' [black] and 'Not *Microcoleus*' [blue] in QGIS.

It is prudent to visually inspect classification maps after they are produced and identify any areas where substantial misclassification is occurring. Further training polygons can then be selected in these areas (Section 7.8) and assigned to their correct class, then the classification re-run. This is an important step, as it can be easy to miss a spectrally distinctive class when performing ground truth measurements and selecting training polygons. The accuracy of classifications is highly sensitive to correct selection of training polygons/pixels.

7.10   Interpreting classification results

After performing the classification and exporting a classification report (Section 7.9) the data is ready for interpretation. The classification report is a table with the 'MacroClass' ID (i.e., *Microcoleus* or Not *Microcoleus*), the number of pixels of each class, the percentage cover of each class, and the area in m^2 of each class (Table 7-1). It contains the estimated percentage cover of *Microcoleus* in the study reach, which is the key metric of interest for determining alert levels and responses.

Table 7-1:   Example classification report from QGIS for the binary classification of *Microcoleus* and Not *Microcoleus*.

Class	PixelSum	Percentage [%]	Area [m^2]
Microcoleus	1493459	25.05	3733.65
Not *Microcoleus*	4467905	74.95	11169.76

If biomass ground truth data has been collected, then further parameters of interest can also be calculated. For example, by multiplying the area of *Microcoleus* by the Ash-Free Dry Mass Areal Density (AFDMAD) of *Microcoleus* (Section 5.5.2) it is possible to estimate the total biomass (i.e., AFDM) of *Microcoleus* in the study reach. Likewise, if estimation of total cell counts of *Microcoleus* in the study reach are needed, then the Cell Count Areal Density (CCAD) of *Microcoleus* (Section 5.5.1) can be multiplied by the area of *Microcoleus*, to estimate the total cell count in the study reach. See Section 8 for post processing classification maps and combining with ground truth data for reach and river scale biomass estimates.

7.11   Determining classification accuracy from ground truth data

There are many ways to assess the accuracy of aerial imagery classifications (Congalton and Green, 2009). One of the most common methods is through the creation of an error matrix (also known as a confusion matrix), then assessment of the 'user accuracy', 'producer accuracy' and 'overall accuracy'. In practice, this is achieved by creating validation polygons throughout the study reach where RTK GPS ground truth observations are made (Figure 7-27) in the same way as selecting training pixels (Section 7.8). Different RTK GPS observation points are used for these validation polygons, than those that were used for the training data. By selecting polygons throughout the study reach and covering a distribution of polygons of each class, this is a form of 'stratified random sampling'. After selecting the validation polygons for each class, navigate to the accuracy assessment through SCP → Postprocessing → Accuracy (Figure 7-27). Then select the classification to assess, with validation points as the reference and MC_ID as the vector field (Figure 7-28).
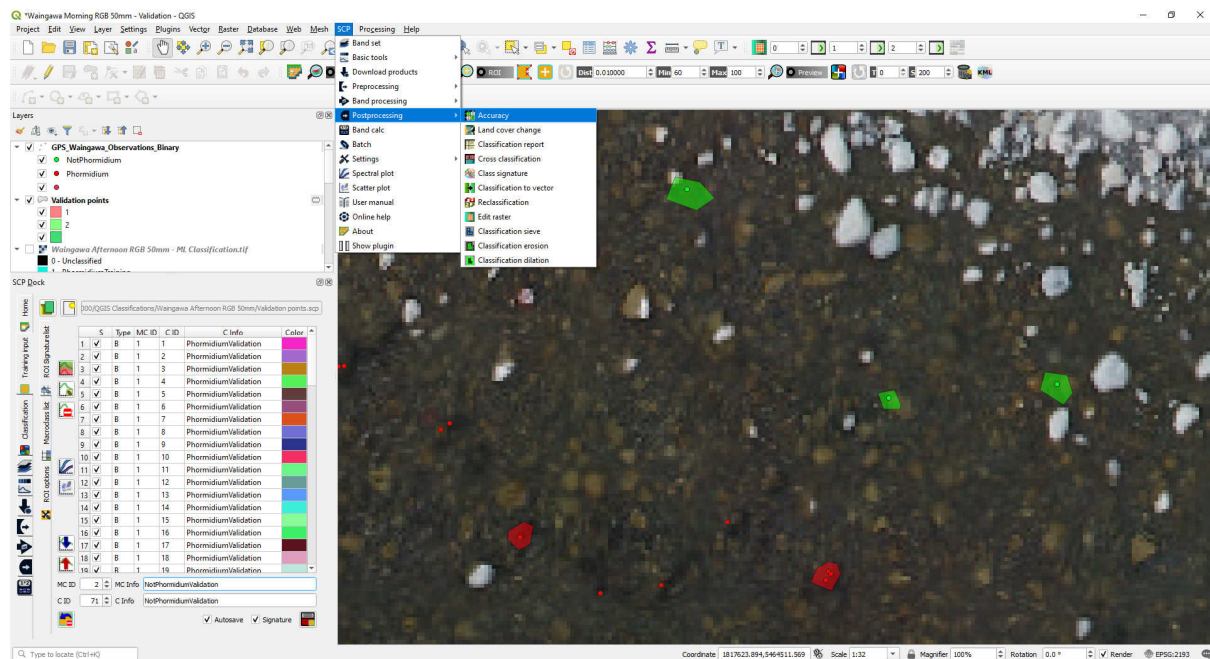
Figure 7-27:   Selecting validation pixels in QGIS from polygons around RTK GPS ground truth measurements and accuracy assessment.
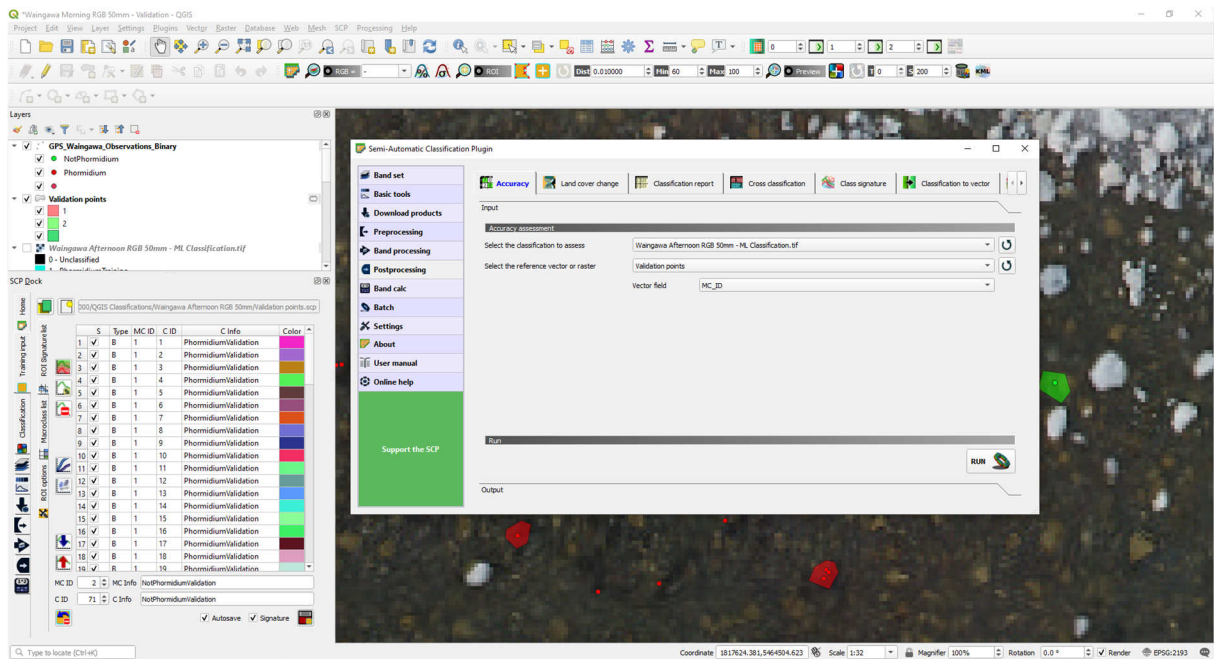
Figure 7-28: **Accuracy assessment of classification maps in QGIS from validation data to produce an error matrix.**

The accuracy assessment will then produce an error matrix comparing the classified and ground truth pixels (Table 7-2).

Table 7-2: Example Error Matrix for the two classes *Microcoleus* (Class 1) and Not *Microcoleus* (Class 2).[6]

	Ground truth pixels Class 1	Ground truth pixels Class 2	Total
Classified pixels Class 1	1410 [C1G1]	402 [C1G2]	1812 [C1$_T$]
Classified pixels Class 2	105 [C2G1]	2300 [C2G2]	2405 [C2$_T$]
Total	1515 [G1$_T$]	2702 [G2$_T$]	4217 [T]

The error matrix show the number of pixels classified as each class, then what their actual ground truth class was (Table 7-2). Correctly classified pixels are shown in green (i.e., C1G1 and C2G2), while pixels that were incorrectly classified are shown in red (i.e., C1G2 and C2G1). The overall accuracy is quantified as the number of correctly classified pixels, divided by the total number of pixels (C1G1+C2G2)/T, which is commonly expressed as a percentage.

While the overall accuracy is a useful metric for the performance of the classification, it doesn't provide specific information about the accuracy of the classification for each class, which is often more important. For example, we need to quantify how well *Microcoleus* (Class 1) was detected. For this, the 'user accuracy' and 'producer accuracy' for each class are computed (Table 7-3). The user accuracy is a measure of how many ground truth pixels were correctly classified, and how many pixels of other classes were incorrectly assigned to that class (errors of commission). The producer accuracy is a measure of how many ground truth pixels were correctly classified, and how many ground truth pixels

---

[6] Green are correctly classified pixels and red are incorrectly classified pixels.

were missed (errors of omission). For example, if user accuracy for class 1 is low, then many ground truth pixels from class 2 were misclassified as class 1, leading to an over-estimation of class 1. However, if producer accuracy is low, then many ground truth pixels from class 1 were misclassified as class 2, leading to under-estimation of class 1.

Table 7-3:   Example user accuracy and producer accuracy for the two classes *Microcoleus* (Class 1) and Not *Microcoleus* (Class 2).

	User accuracy	Producer accuracy
Class 1	77.8% [C1G1/C1$_T$]	93.1% [C1G1/G1$_T$]
Class 2	95.6% [C2G2/C2$_T$]	85.1% [C2G2/G2$_T$]

For the example user accuracy and producer accuracy in Table 7-3 (calculated from the error matrix in Table 7-2) the producer accuracy of 93.1% for class 1 shows that most of the ground truth pixels for class 1 were successfully classified as class 1. However, the user accuracy of 77.8% for class 1 shows that the classification was overpredicting class 1, with class 2 pixels being misclassified as class 1. Interpretation of these results indicate that the area of class 1 is being overestimated in the study reach. This information can be included in the final interpretation and implementation of the classification results, or the classification could be repeated after adding more training data to class 2 in order to improve its spectral signature descriptor to try to increase the accuracy of classification of class 2.

8 Post processing classification maps and combining with ground truth data for reach and river scale biomass

8.1 Cover, biomass and cell count estimates in the surveyed reach

After performing the classification and exporting a classification report (Section 7.9) the data is ready for interpretation. The classification report is a table with the 'MacroClass' ID (i.e., *Microcoleus* or Not *Microcoleus*), the number of pixels in each class, the percentage cover of each class, and the area in m² of each class (Table 7-1). It contains the estimated percentage cover of *Microcoleus* in the study reach C_M, which is currently the key metric of interest for determining alert levels and responses.

Table 8-1: Example classification report from QGIS for the binary classification of *Microcoleus* and Not *Microcoleus*.

Class	PixelSum	Percentage (%)	Area (m²)
Microcoleus	1493459	25.05 (C_M)	3733.65 (A_M)
Not *Microcoleus*	4467905	74.95	11169.76

If biomass ground truth data has been collected, then further parameters of interest can also be calculated. For example, by multiplying the area of *Microcoleus* in the study reach A_M by the Ash-Free Dry Mass Areal Density of *Microcoleus* AFDMAD$_{Microcoleus}$ (Section 5.5.2), it is possible to estimate the total biomass of *Microcoleus* in the study reach, $\text{AFDM}_{Microcoleus,Total} = \text{AFDMAD}_{Microcoleus} \times A_M$. Likewise, the Cell Count Areal Density of *Microcoleus* CCAD$_{Microcoleus}$ (Section 5.5.1) can be multiplied by the area of *Microcoleus*, to estimate the total cell count in the study reach,

$$\text{CC}_{Microcoleus,Total} = \text{CCAD}_{Microcoleus} \times A_P.$$

8.2 Cover, biomass and cell count estimates at the river scale

If the site where MAM was undertaken is representative of the whole river, then the cover estimated in Section 8.1 is also a valid estimate for the whole river. However, the total biomass and total cell counts of *Microcoleus* at the river scale are dependent on the size of the river. For example, a wider river (with suitable habitat) may have higher total numbers of *Microcoleus* cells and biomass than an equivalent smaller river. This is important, since *Microcoleus* mats commonly detach and drift downstream, accumulating at the river margins where they pose a health risk for dogs and people (particularly children). Since accumulation occurs along a one-dimensional line (i.e., a riverbank) the accumulation length is independent of the river width (i.e., the same for a river or small stream); however, *Microcoleus* production occurs over a 2D area (i.e., river upstream distance multiplied by average river width). Hence, wider rivers pose a higher risk, when considering *Microcoleus* production, drift, and riverbank accumulation.

To estimate the total upstream risk, the first step is to calculate Ash-Free Dry Mass Linear Density (AFDMLD) of *Microcoleus* at the study site, or the Cell Count Linear Density (CCLD) of *Microcoleus* at the study site. Linear density is the metric expressed per unit river length, rather than areal density, which is per unit river area. AFDMLD has units of g AFMD/m and is calculated as $\text{AFDMLD}_{Microcoleus} = \text{AFDMAD}_{Microcoleus} \times \frac{A_M}{L_T}$, where A_M is the area (m²) of *Microcoleus* in the study reach (i.e., total area of *Microcoleus* in the classification region), and L_T is the total length of the study reach (i.e., total length of the classification region). In practice, L_T can simply be found using the distance measurement

tool in QGIS (or any other GIS software) and measuring along the centreline of the study reach from the upstream end of the classification region, to the downstream end. Likewise, Cell Count Linear Density is calculated as: $\text{CCLD}_{Microcoleus} = \text{CCAD}_{Microcoleus} \times \frac{A_M}{L_T}$ and has units of cells/m.

If *Microcoleus* abundance in the study reach is representative of that in the whole river, then the upstream exposure risk at any location along the river can be quantified as Ash-Free Dry Mass Upstream Risk (AFDMUR), where $\text{AFDMUR}_{Microcoleus} = \text{AFDMLD}_{Microcoleus} \times L_U$ where L_U is the length of channel upstream from which *Microcoleus* can drift. Likewise, Cell Count Upstream Risk (CCUR) is calculated as $\text{CCUR}_{Microcoleus} = \text{CCLD}_{Microcoleus} \times L_U$.

The above methods can be used to make rough estimates, however more rigorous scientific study is required to better describe *Microcoleus* mat detachment, drift, accumulation at river margins, toxin concentrations, and toxin degradation times. This work is highly recommended, since AFDMUR and CCLD may be important risk metrics to consider for the safety of dogs and river users.

8.3   Average biomass and cell counts

The final metrics of interest for assessment of river safety are average biomass and average cell counts per m². These represent the instream risk to dogs and river users from attached mats. These metrics account for the cover of *Microcoleus*, the thickness of mats and the taxonomic composition of mats. These metrics are Ash-Free Dry Mass Areal Density Average ($\text{AFDMAD}_{Average}$) and Cell Count Areal Density Average ($\text{CCAD}_{Average}$) and are quantified as $\text{AFDMAD}_{Microcoleus,Average} = \text{AFDMAD}_{Microcoleus} \times \frac{Cover\%}{100\%}$ and $\text{CCAD}_{Microcoleus,Average} = \text{CCAD}_{Microcoleus} \times \frac{Cover\%}{100\%}$. These metrics are more accurate than simple cover assessments, since they account for heterogeneity in mat thickness (i.e., thin films vs thick mats) and taxonomic composition of mats (i.e., varying abundance of *Microcoleus*).

9 MAM Case study #1 Hutt River

Microcoleus poses a significant public health risk and management challenge in many rivers within Greater Wellington Regional Council's jurisdiction. To develop and test the methods contained within this user guide, two MAM campaigns were undertaken. The first was in the Hutt River (this section) and the second was in the Waingawa River (see Section 10).

9.1 Site location

The Hutt River site was upstream of Silverstream Bridge (-41.139804, 175.005552, [WGS84]), the site was ~500 m long, with abundant mats of *Microcoleus*. Finding a suitable site for aerial monitoring on the Hutt River illustrated some of the challenges with aerial monitoring in urban areas, such as airspace restrictions (Figure 9-1) and not flying over people or property without their consent (CAA Part 101 regulations).
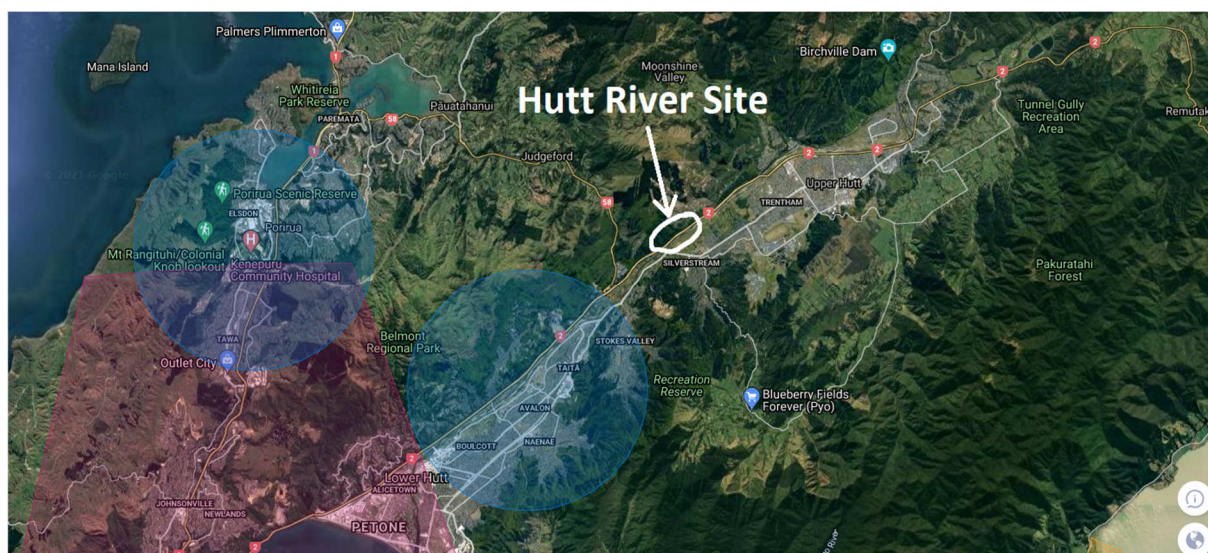
Figure 9-1: **Map showing the Hutt River site and nearby airspace restrictions.[7]**

9.2 Data collected

Data collection in the Hutt River occurred on the 12th of February 2020 at a discharge of 3.2 m^3/s. Aerial imagery data was collected with RGB, RGN, multispectral and hyperspectral cameras, with flights at two times of the day to investigate the effect of lighting and environmental conditions. Ground truth measurements consisted of 260 RTK GPS observations, 61 biomass samples, and 71 underwater views (Figure 9-2).

---

[7] Blue circles are restricted airspace due to helicopter landing pads at hospitals, while the red area is restricted airspace due to Wellington airport.
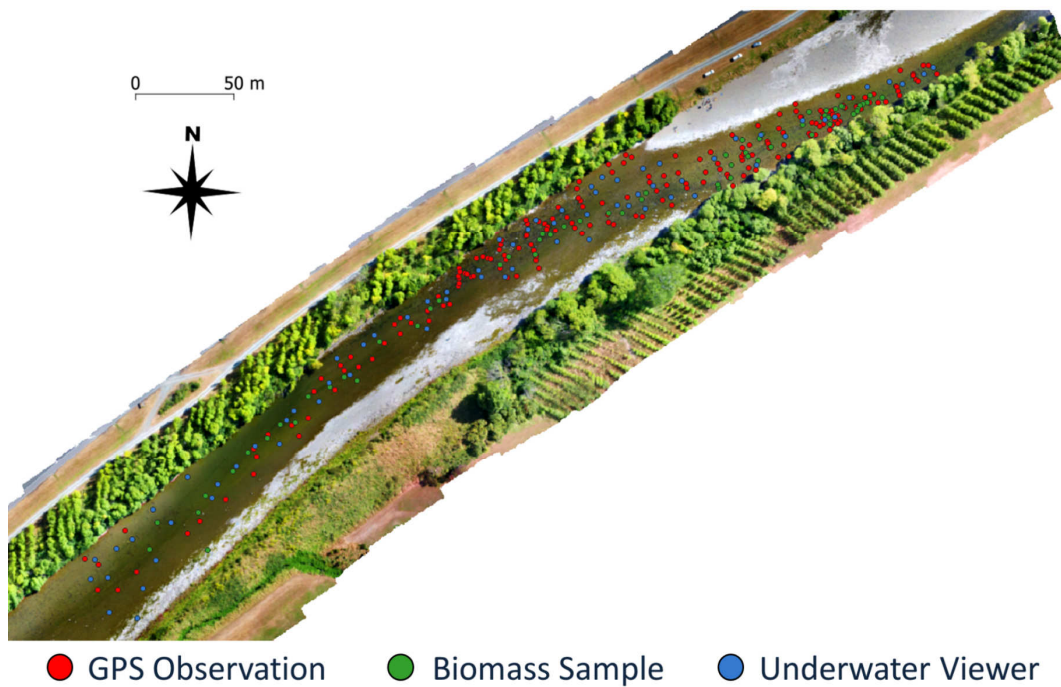
Figure 9-2: **Ground truth measurements in the Hutt River (260 GPS Observations, 61 Biomass Samples, 71 Underwater Views).**

RTK GPS observation points were combined into the binary classes of Not *Microcoleus* and *Microcoleus* (Figure 9-3).
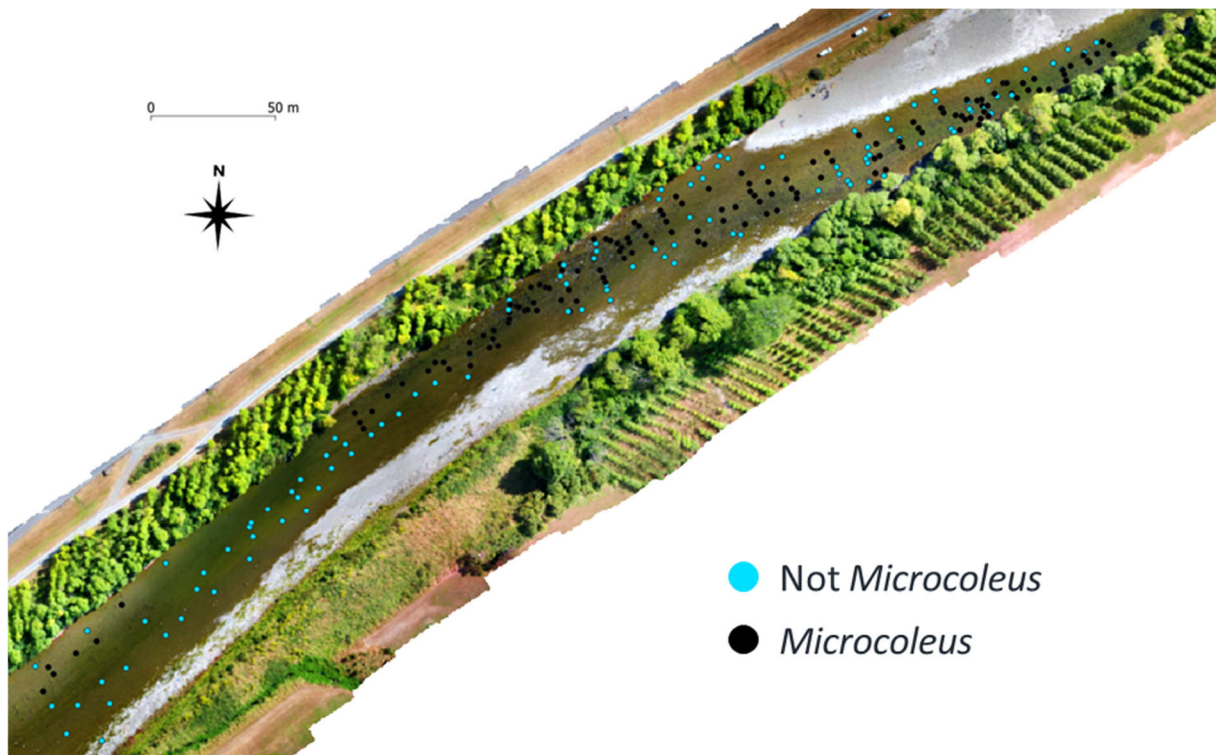
Figure 9-3: **Hutt River GPS ground truth points for *Microcoleus* presence and absence.**

9.3   Results

9.3.1   Biomass: Taxonomic composition of *Microcoleus* dominated mats

Ground truth biomass samples from the cyanobacterial mats were analysed following the methods in Section 5. Cell counts distinguished 62 different taxa, with cell counts performed, then the biovolume of each genus calculated. The relative abundance by biovolume for each sample was then determined as the biovolume of each taxon, divided by the total biovolume.

Calculation of the average taxonomic composition of the sampled mats required incorporation of mat thickness, rather than simply taking the arithmetic mean of relative abundance of each of the samples, which would have provided too much weighting to thin films compared to thick mats. The study reach averaged relative abundance was then calculated as:

$$RA_{i,average} = \frac{1}{AFDM_T} \sum_{s=1}^{s=N} AFDM_s \times RA_{i,s}$$

where $RA_{i,average}$ is the average relative abundance of taxa i, $AFDM_T$ is the total ash-free dry mass of all the samples, s is the sample index, N is the total number of samples, $AFDM_s$ is the ash-free dry mass of sample s, $RA_{i,s}$ is the relative abundance of taxa i in sample s and total ash-free dry mass is calculated as $AFDM_T = \sum_{s=1}^{s=N} AFDM_s$.

Cyanobacterial mats in the Hutt River were dominated by *Microcoleus autumnalis* (54.8%), but also included a large proportion of *Bacillariophyceae* diatoms (41.4%), with 23 other taxa making up the remaining 3.7%.
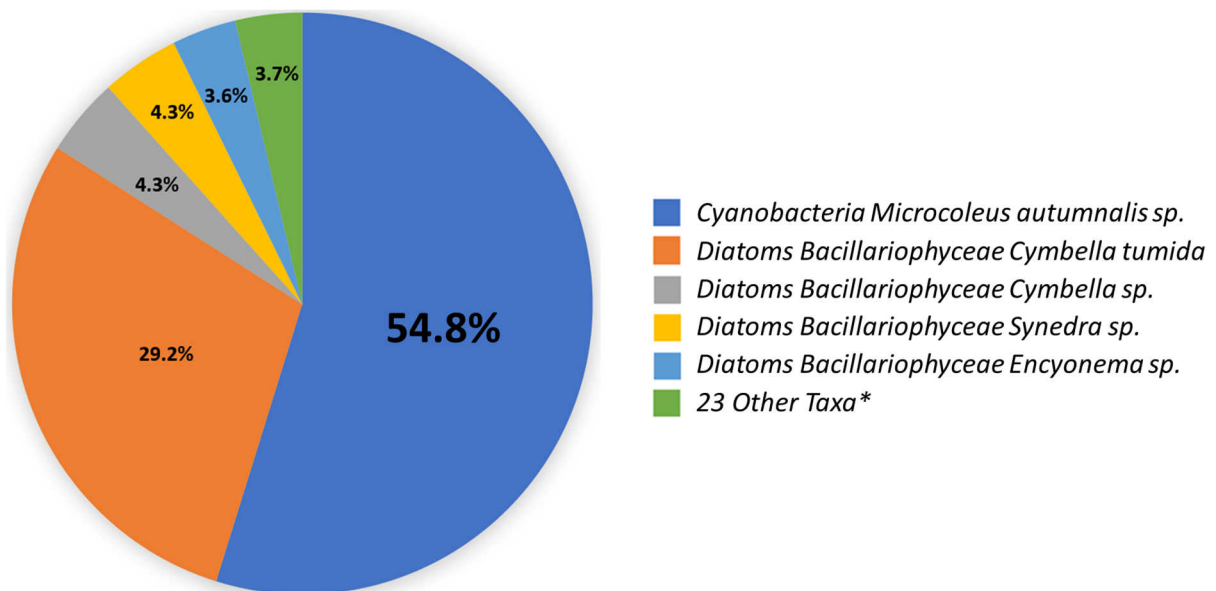
Figure 9-4:   **The taxonomic composition of cyanobacterial mats sampled from the Hutt River.[8]**

9.3.2   Biomass: AFDM and Chl-a of *Microcoleus* dominated mats

The average AFDMAD of *Microcoleus* dominated mats in the Hutt River was 30.2 g/m². The average chl *a* areal density of *Microcoleus* dominated mats in the Hutt River was 254.7 mg/m². By combining the taxonomic composition of the mats (i.e., 54.8% *Microcoleus*) (Section 9.3.1) and the ash-free dry

---

[8] Taxonomic composition is calculated as the average of relative abundance by biovolume weighted by sample AFDM.

mass of each sample, then averaging the results, the average AFDMAD of *Microcoleus* in the *Microcoleus* dominated mats can be calculated (Table 9-1). Yielding an average AFDMAD of *Microcoleus* of 16.5 g/m^2.

Table 9-1: **Ash-Free Dry Mass Aerial Density of Microcoleus dominated mats, with biomass separated by taxonomic composition of samples.**

Taxa	AFDMAD (g/m^2)
Microcoleus autumnalis	16.5
Cymbella tumida	8.8
Cymbella sp.	1.3
Synedra sp.	1.3
Encyonema sp.	1.1
Other (23 taxa with low abundance)	1.1
Total	30.1

9.3.3   Biomass: Pigment composition of *Microcoleus* dominated mats

Biomass samples were processed at Cawthron Institute using High Performance Liquid Chromatography (HPLC) and fluorescence methods to determine pigment composition of *Microcoleus* dominated mats. Samples were analysed for: alloxanthin, alpha-carotene, beta-carotene, canthaxanthin, chlorophyll-a, chlorophyll-b, diadinoxanthin, diatoxanthin, echinenone, fucoxanthin, lutein, peridin, phycocyanin, phycoerythrin, violaxanthin, and zeaxanthin. The main pigments of interest for *Microcoleus* are phycocyanin and phycoerythrin. The average pigment composition of the *Microcoleus* dominated mats are presented as % by mass (Figure 9-5). In the Hutt River phycocyanin comprised 67.5% of the total pigment mass, with phycoerythrin comprising 16.1% and other pigments comprising the remaining 16.4%. This pigment information is useful for interpreting the reflectance spectra for the *Microcoleus* dominated mats (Section 9.3.4) and selecting band pass filters for multispectral cameras to target the pigments in the mats that are specific to *Microcoleus* (Rowan, 1989).
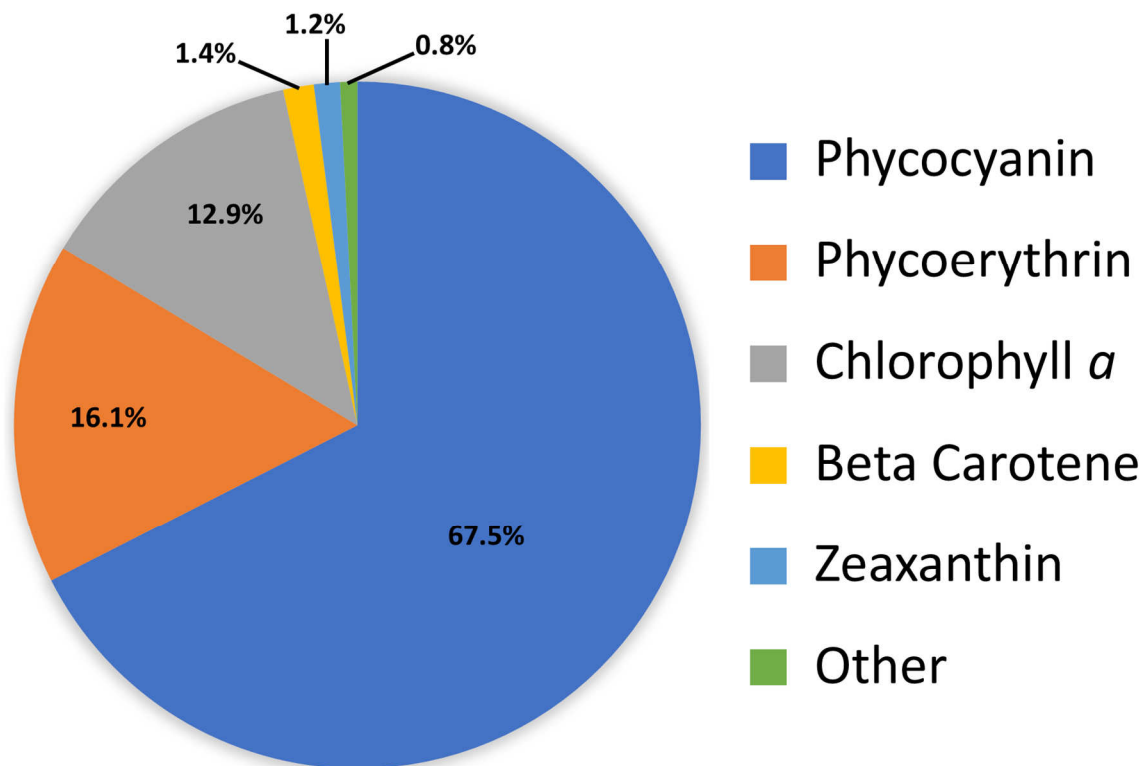
Figure 9-5: Hutt River pigment composition of *Microcoleus* dominated mats (% by mass).

9.3.4 Reflectance spectra: *Microcoleus* dominated mats and other classes

Hyperspectral aerial imagery data in the Hutt River was used to extract reflectance spectra for the classes: Dry Stones, Filamentous Green Algae, *Microcoleus*, Riparian Vegetation, and Wet Stones (Figure 9-6). There was low reflectance and minimal separability of the instream classes (compared to terrestrial classes). When directly comparing the instream classes (Figure 9-7), there is the most separability in the 500-650 nm range. Above 700 nm, the shape of the reflectance curve for *Microcoleus* closely matches that of Wet Stones and Filamentous Green Algae. Above 750 nm, the reflectance curves for Filamentous Green Algae and *Microcoleus* are nearly identical. The Wet Stones may have had some very thin periphyton film on them, yet they retained slight separation from *Microcoleus* above 750 nm. This information provides a useful indication that remote sensing *Microcoleus* with multispectral camera bands in the 500–650 nm range are the most likely to provide separability and accurate classifications. For our Airphen multispectral camera, this corresponds to bands B1, B2, B3, which are 10 nm bands, centred on the wavelengths 530, 570, and 622 nm.
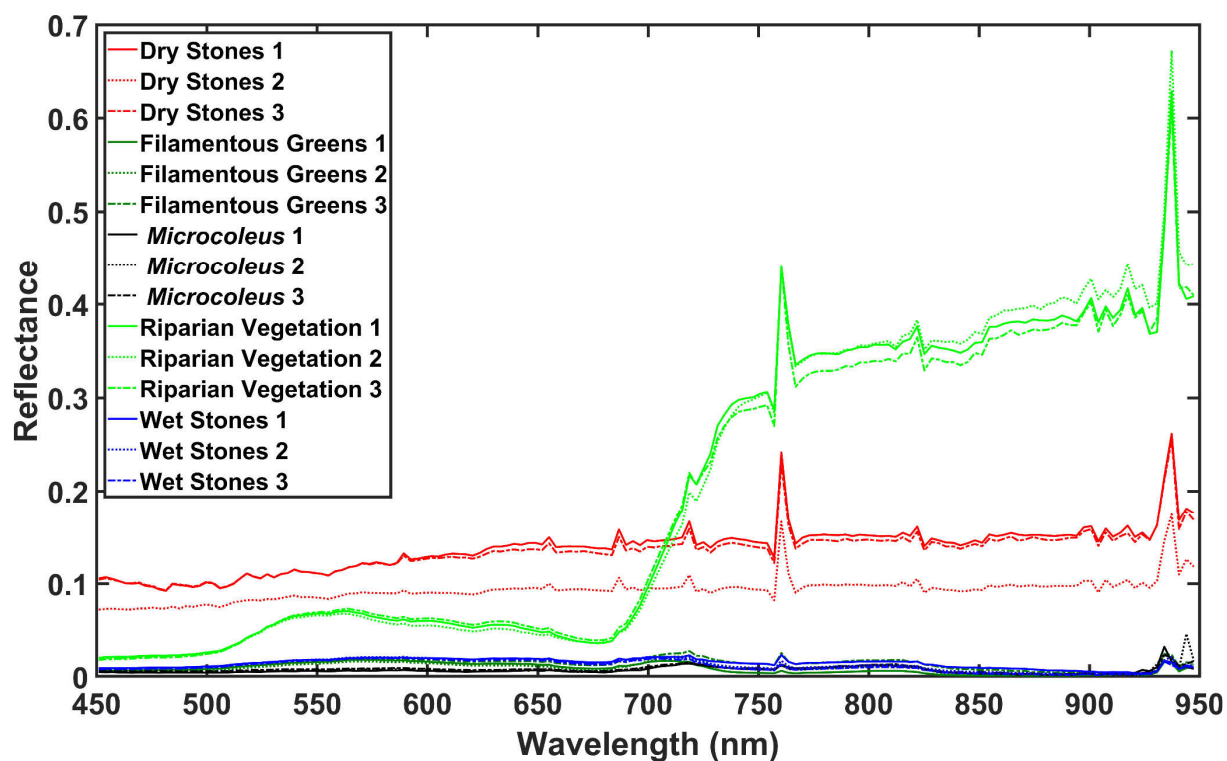
Figure 9-6: Reflectance spectra in the Hutt River for five classes of interest, with three sample polygons for each class.
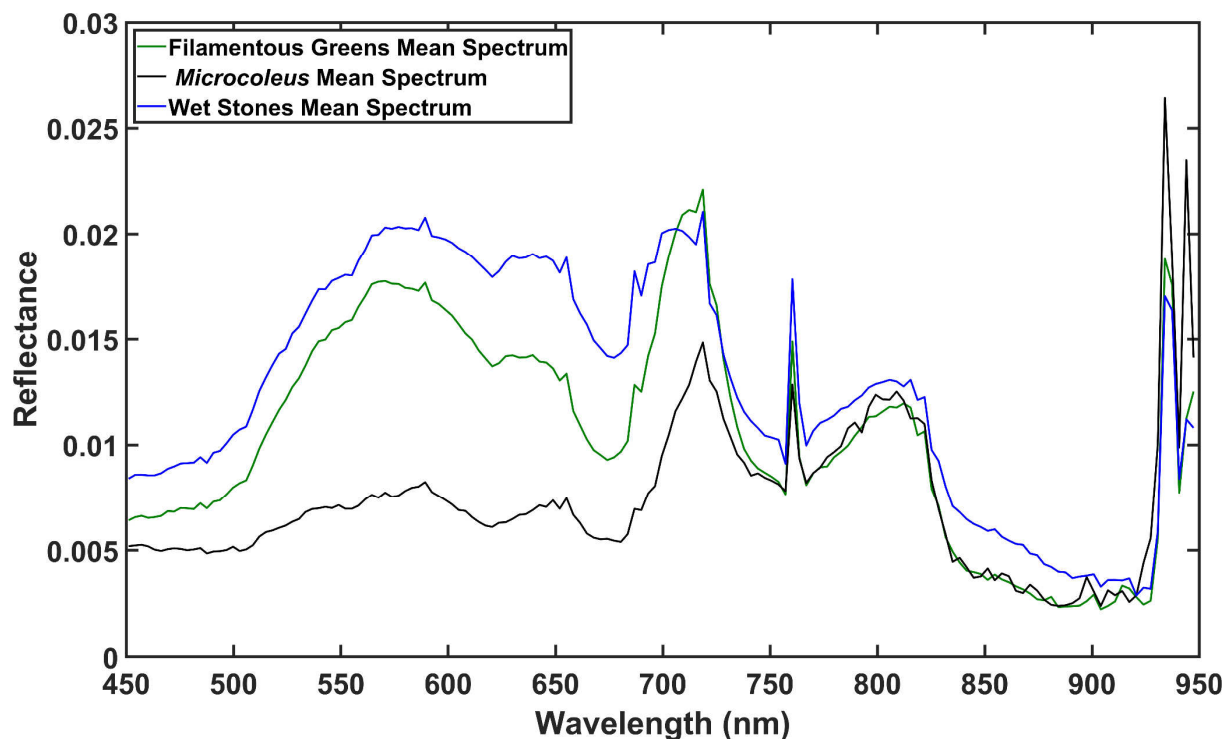
Figure 9-7: Mean reflectance spectra in the Hutt River for three instream classes: Filamentous Green Algae, *Microcoleus*, and Wet Stones.

9.3.5 Aerial imagery classifications

Aerial imagery classifications were performed in QGIS using Minimum Distance (MD), Maximum Likelihood (ML), and Spectral Angle Mapper (SAM) algorithms (Section 7). Classifications of the multispectral camera data were performed on bands 1-6, then repeated on only bands 1-3 as a comparison. The length of the classification reach was 517 m and the area of the classification reach was 13640 m^2. The cover estimates and accuracy metrics (Section 7.11) for the different types of imagery and classifications are summarised in Table 9-2. Flights were performed in the morning and repeated in the afternoon, to investigate any differences in classifications due to lighting, shadows, and reflections from cloud cover. Flights were performed at 50 m altitude, with the RGB morning flights repeated at 100 m altitude, to investigate any differences in classifications due to altitude. Orthomosaics were output with a consistent resolution of 50 mm pixels, then an extra orthomosaic from the RGB morning flights was produced (15 mm pixels), to investigate any differences in classifications due to resolution.

Training data consisted of 11 polygons of *Microcoleus* and 39 polygons of Not *Microcoleus*. There was plentiful RTK GPS ground truth data of *Microcoleus*, however there was insufficient coverage of the class Not *Microcoleus* to cover all of the spectrally distinct regions of the orthomosaics. Hence, some of the Not *Microcoleus* training polygons had to be inferred from regions that were visually distinctive as being very different from the pixels at *Microcoleus* RTK GPS ground truth locations.

Validation data consisted of 50 polygons of *Microcoleus* and 50 polygons of Not *Microcoleus* centred around RTK GPS ground truth locations.

Table 9-2: Hutt River aerial imagery classifications and accuracy (%) for *Microcoleus* (Class 1) and Not *Microcoleus* (Class 2).[9]

Aerial imagery type and time of day	Classification Type	*Microcoleus* Cover (%)	Class 1 User Accuracy	Class 2 User Accuracy	Class 1 Producer Accuracy	Class 2 Producer Accuracy	Total Accuracy
RGB Morning	MD	16.29	85.87	89.39	75.00	94.46	88.44
RGB Morning	ML	17.67	87.82	90.01	76.42	95.24	89.42
RGB Morning	SAM	17.22	56.03	76.93	43.35	84.74	71.93
RGB Morning (100 m altitude)	MD	7.61	90.16	95.37	89.43	95.71	93.79
RGB Morning (100 m altitude)	ML	7.08	96.29	95.17	88.62	98.50	95.48
RGB Morning (100 m altitude)	SAM	18.43	74.85	84.77	62.93	90.71	82.22
RGB Morning (15 mm pixels)	MD	24.47	69.05	88.05	73.68	85.45	81.85

---

[9] The classification algorithms used were: Minimum Distance (MD), Maximum Likelihood (ML) and Spectral Angle Mapper (SAM). All imagery was flown at 50 m altitude above ground level, with an orthomosaic pixel size of 50 mm (unless otherwise stated).

Aerial imagery type and time of day	Classification Type	*Microcoleus* Cover (%)	Class 1 User Accuracy	Class 2 User Accuracy	Class 1 Producer Accuracy	Class 2 Producer Accuracy	Total Accuracy
RGB Morning (15 mm pixels)	ML	17.66	82.95	89.33	74.72	93.23	87.57
RGB Morning (15 mm pixels)	SAM	17.51	49.73	74.92	36.29	83.84	69.30
RGB Afternoon	MD	12.76	38.63	70.47	19.62	86.02	65.46
RGB Afternoon	ML	17.96	58.35	79.31	51.42	83.53	73.59
RGB Afternoon	SAM	12.19	58.54	72.81	22.78	92.76	71.09
RGN Morning	MD	5.32	91.33	87.24	68.35	97.09	88.19
RGN Morning	ML	6.40	89.42	89.02	73.58	96.10	89.12
RGN Morning	SAM	7.66	93.71	89.88	75.47	97.73	90.84
RGN Afternoon	MD	16.52	63.44	81.43	56.28	85.53	76.51
RGN Afternoon	ML	16.16	64.93	82.57	59.46	85.67	77.59
RGN Afternoon	SAM	12.73	72.06	81.70	54.53	90.57	79.45
Multispectral Morning (6 Bands)	MD	1.95	99.05	95.25	88.79	99.62	96.30
Multispectral Morning (6 Bands)	ML	13.01	83.51	98.22	96.26	91.57	93.01
Multispectral Morning (6 Bands)	SAM	1.96	99.43	95.53	89.47	99.77	96.61
Multispectral Morning (3 Bands)	MD	2.32	95.61	95.19	88.79	98.19	95.31
Multispectral Morning (3 Bands)	ML	3.85	93.84	96.93	93.04	97.29	95.99
Multispectral Morning (3 Bands)	SAM	19.94	40.90	74.76	46.52	70.20	62.93

Aerial imagery type and time of day	Classification Type	*Microcoleus* Cover (%)	Class 1 User Accuracy	Class 2 User Accuracy	Class 1 Producer Accuracy	Class 2 Producer Accuracy	Total Accuracy
Multispectral Afternoon (6 Bands)	MD	8.15	81.06	93.51	85.74	91.12	89.47
Multispectral Afternoon (6 Bands)	ML	17.64	79.80	97.06	93.89	89.47	90.82
Multispectral Afternoon (6 Bands)	SAM	8.17	80.93	93.51	85.74	91.05	89.42
Multispectral Afternoon (3 Bands)	MD	5.35	87.83	93.26	84.55	94.81	91.66
Multispectral Afternoon (3 Bands)	ML	9.34	84.07	94.47	87.78	92.63	91.14
Multispectral Afternoon (3 Bands)	SAM	15.37	47.80	76.46	46.01	77.73	67.99

The classification that performed the best in the Hutt River was the Minimum Distance algorithm, on the six band multispectral aerial imagery from the morning flight (Figure 9-8), with estimated cover of 1.95% and area of 265.98 m^2 (Figure 9-9). This classification had user accuracy of 99.05%, and producer accuracy of 88.79% for the *Microcoleus* class. The user accuracy of 99.05% is very high, indicating that there were few ground truth pixels of the Not *Microcoleus* class that were misclassified as *Microcoleus*, however the producer accuracy of 88.79% indicates that there were some *Microcoleus* ground truth pixels being misclassified as Not *Microcoleus* leading to a slight underestimate of *Microcoleus* cover. Classification results for the Minimum Distance algorithm were very similar between the 6 band and 3 band Hutt morning multispectral data. However, there were significant differences between those produced with the Maximum Likelihood and Spectral Angle Mapper algorithms. Due to this discrepancy the Minimum Distance classification results were selected over those produced with MD or SAM.

Visual inspection of the aerial imagery and classification maps indicated that there was a significant overestimate of *Microcoleus* cover for most of the imagery types. This overestimate of cover was also reflected in the low values of user accuracy for class 1 (*Microcoleus*). To illustrate this difference the Hutt Morning multispectral orthomosaic is shown in Figure 9-8, with the high accuracy Minimum Distance classification (Figure 9-9) and the low accuracy Maximum Likelihood classification in Figure 9-10. These differences are illustrated for a zoomed in section of the Hutt River in Figure 9-11, Figure 9-12 and Figure 9-13.
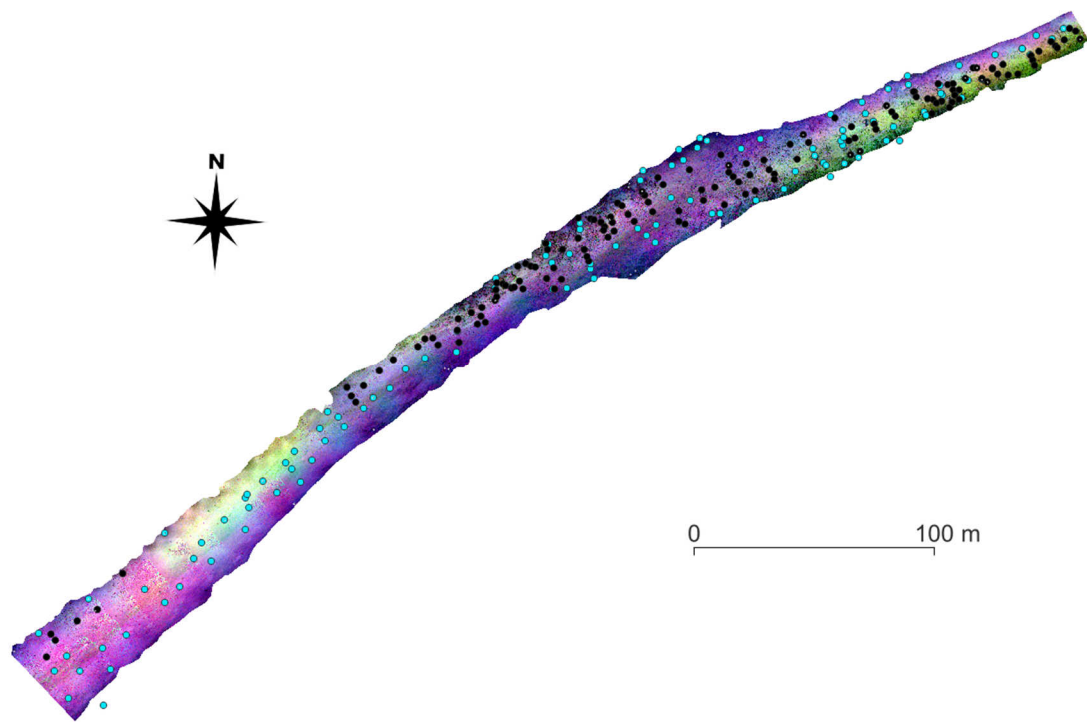
Figure 9-8: **Multispectral aerial imagery in the Hutt River (morning flights) with RTK GPS ground truth measurements.[10]**
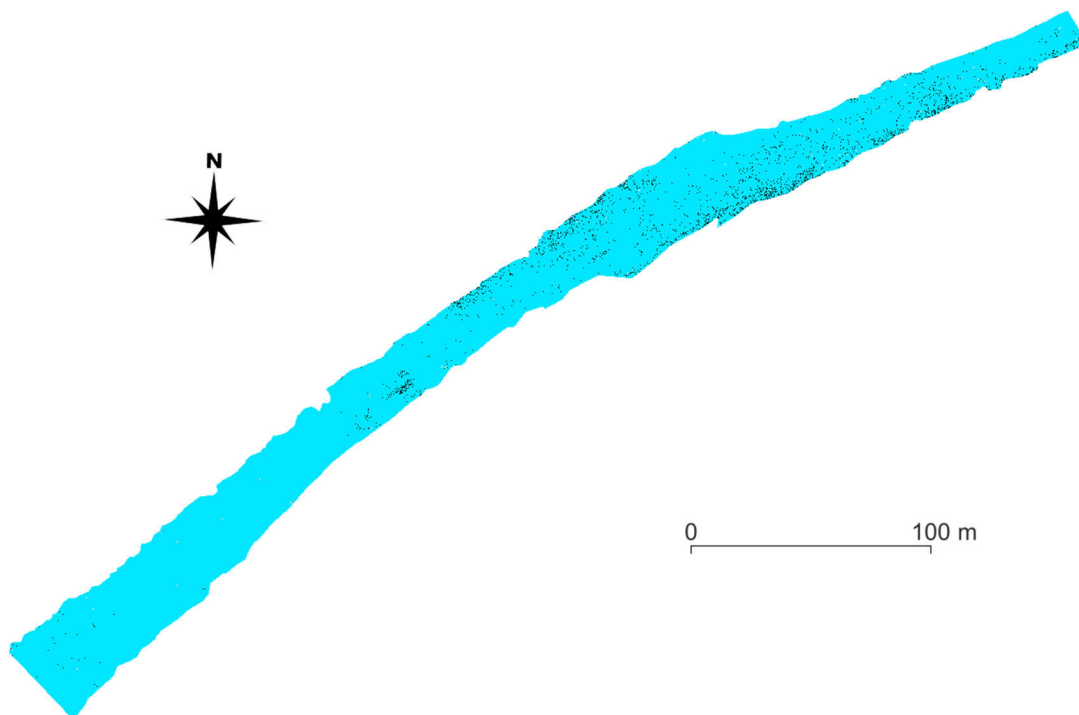
---

[10] Black dots are *Microcoleus* and blue dots are Not *Microcoleus*.
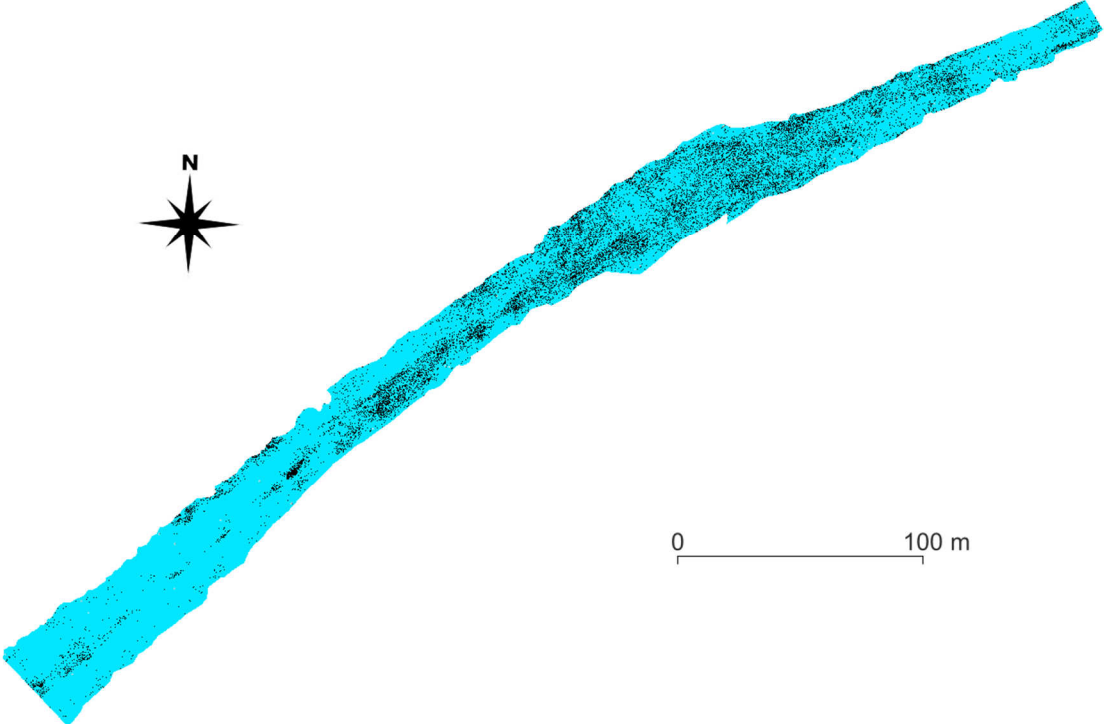
Figure 9-10: Maximum likelihood classification of the Hutt multispectral aerial imagery (morning flights).[11]
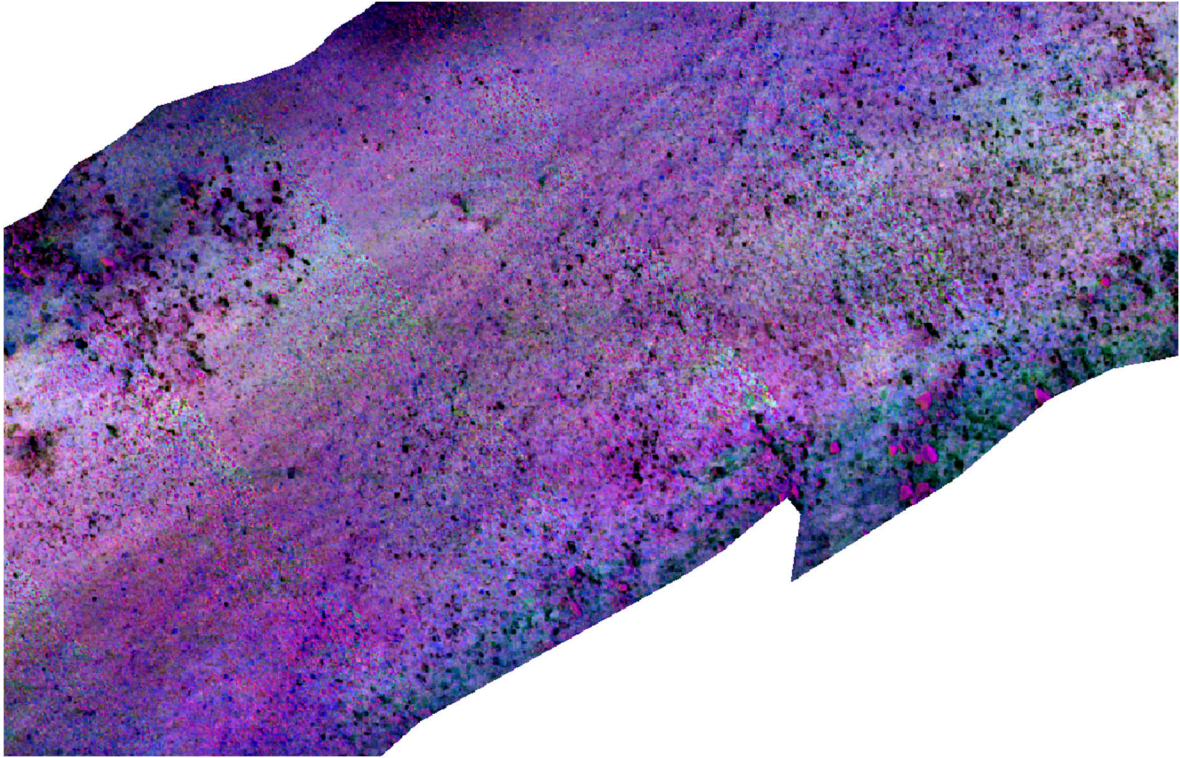
Figure 9-11: Zoomed in multispectral aerial imagery in the Hutt River (morning flights).

---

[11] Black is classified as *Microcoleus* and blue is Not *Microcoleus*.
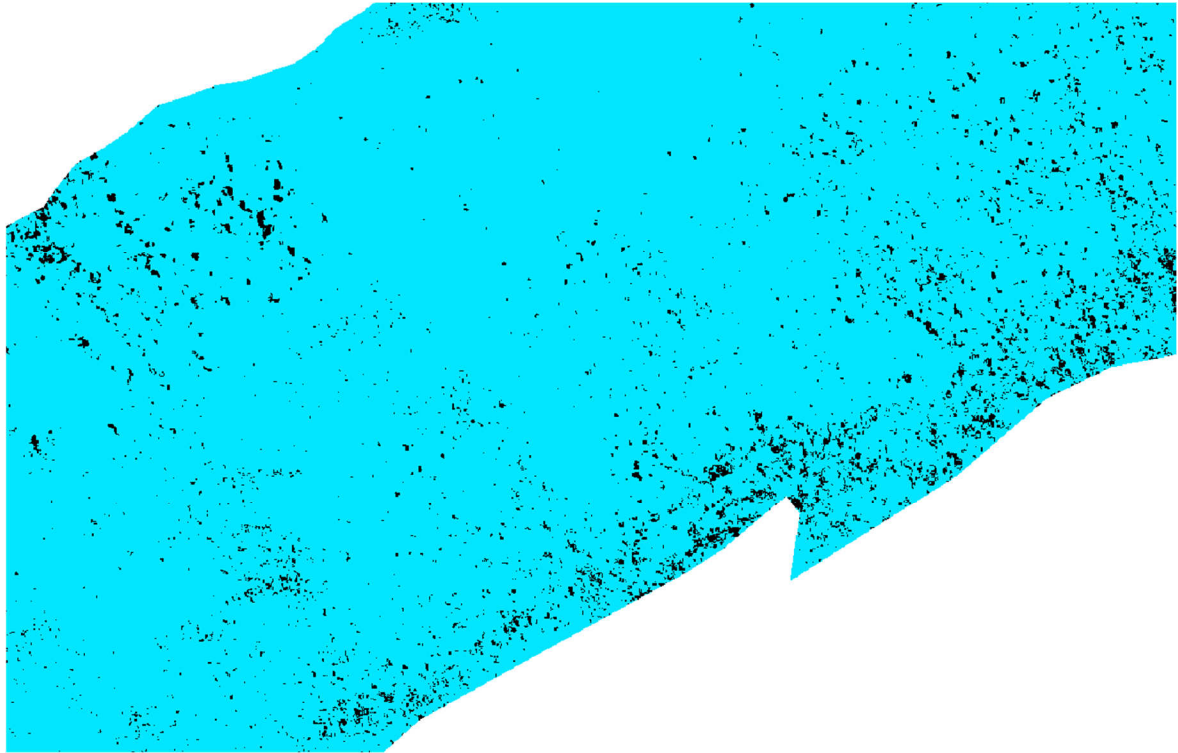
Figure 9-12: **Zoomed in Minimum Distance classification of the Hutt multispectral aerial imagery (morning flights).[11]**
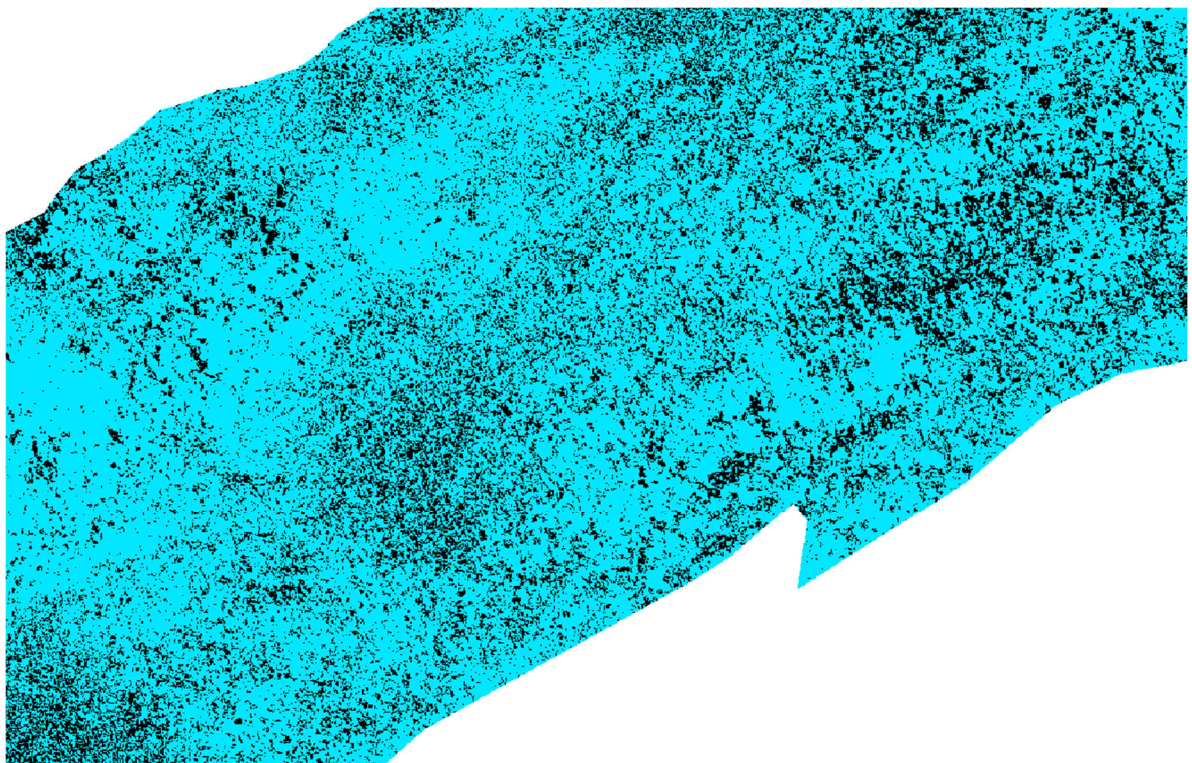
Figure 9-13: **Zoomed in Maximum Likelihood classification of the Hutt multispectral aerial imagery (morning flights).[11]**

There was also interesting variability in the accuracy of the RGB aerial imagery classifications, with the RGB morning 100 m imagery performing well (Table 9-2), however visual inspection showed substantial overestimation of cover (particularly in the upstream part of the reach) and this classification was discounted as an outlier. Outliers such as this illustrate the importance of selecting large numbers of validation points from throughout the study reach, as well as performing visual inspections of classifications. Overall, there was significant variability in the classifications between imagery type, time of day, and classification algorithm used (Table 9-2); these differences are discussed further in Section 9.4, along with strategies to improve the accuracy of classifications.

Estimated *Microcoleus* cover of 1.95% and area of 265.98 m^2 from the 6 band multispectral data (Figure 9-9) was used for subsequent biomass calculations. For practical implementation of MAM (Section 11.1), it would be prudent to multiply the classification cover estimate by a Factor of Safety to account for any underestimate of cover.

9.3.6 *Microcoleus* cover estimates from underwater viewers

There were 71 underwater views collected from throughout the Hutt River (Figure 9-2). However, these were unfortunately biased by searching for *Microcoleus* and other periphyton, yielding an estimate of *Microcoleus* cover of 26.6% that was far too high. There were insufficient views near the edges of the river and in areas without periphyton cover, with only 6.6% of the riverbed classified as having no algae, and 33.0% classified as having thin film. Even in the most densely covered part of the river reach (Figure 9-14) *Microcoleus* cover would have been less than 26.6%, let alone the whole river reach having this cover level, since most of it had no *Microcoleus* cover at all (Figure 9-3). At 26.6% cover, every 4th step in the river would be standing on *Microcoleus*, which was certainly not the case in the Hutt River. This illustrates the challenges of using underwater viewers to obtain a representative cover estimate in a whole reach (Section 5.1.2) and the challenges in general of providing an accurate reference cover level to compare aerial imagery classifications with. For this reason, the standard methods of quantifying aerial imagery accuracy through validation polygons around RTK GPS survey presence/absence points is recommended.

9.3.7 Biomass of *Microcoleus* at the reach and river scale

The biomass measurements for *Microcoleus* dominated mats (Section 9.3.2) can be combined with cover and area estimates (Section 9.3.5) to estimate reach and river averaged biomass. The average AFDMAD of *Microcoleus* in the *Microcoleus* dominated mats was 16.5 g/m^2 (i.e., AFDMAD$_{Microcoleus}$). By multiplying this with the estimated area of *Microcoleus* from aerial imagery classifications of 265.98 m^2 yields an estimated total biomass of *Microcoleus* in the classification area of 4,389 g AFDM (Section 8.1). Dividing the total biomass by the length of the classification reach (517 m) yields an Ash-Free Dry Mass Linear Density (AFDMLD) for *Microcoleus* of 8.49 g AFDM/m (Section 8.2). Combining the cover estimate of 1.95% (Section 9.3.5) and the AFDMAD$_{Microcoleus}$ yields AFDMAD$_{Microcoleus,Average}$ of 0.322 g/m^2 in the study reach (Section 8.3). Assuming that the study reach is representative of cover and biomass in the river in general, then AFDMLD$_{Microcoleus}$ and AFDMAD$_{Microcoleus,Average}$ are also valid estimates at the river scale. These metrics provide an estimate of toxin production risk, which is proportional to the number of cells (three-dimensional biomass), rather than cover (which could be a thin film).

9.4 Discussion

In the Hutt River aerial imagery, there was a significant difference in surface reflections between imagery collected in the morning (blue sky) and afternoon (cloud cover). This difference is easily visible in the aerial imagery (Figure 9-14, Figure 9-15) and is also quantified as decreased classification

accuracy for the afternoon RGB, RGN and multispectral aerial imagery (Table 9-2). This occurs due to diffuse light originating from many angles (scattered by clouds) being reflected off the water surface and illustrates the importance of deployment conditions (Section 4.1.3). When cloud cover is present, there is also less light illuminating the bed and *Microcoleus*. By contrast, when deploying in blue sky conditions there is only a small bright patch of sunglint in imagery due to specular reflection of the sun's rays directly off the water surface, however by flying aerial imagery with 80% front and 60% side overlap, these small patches are usually removed automatically and not included in stitched orthomosaics. Alternatively, aerial imagery can be pre-processed and any sunglint automatically masked before processing in Agisoft Metashape or Pix4D.
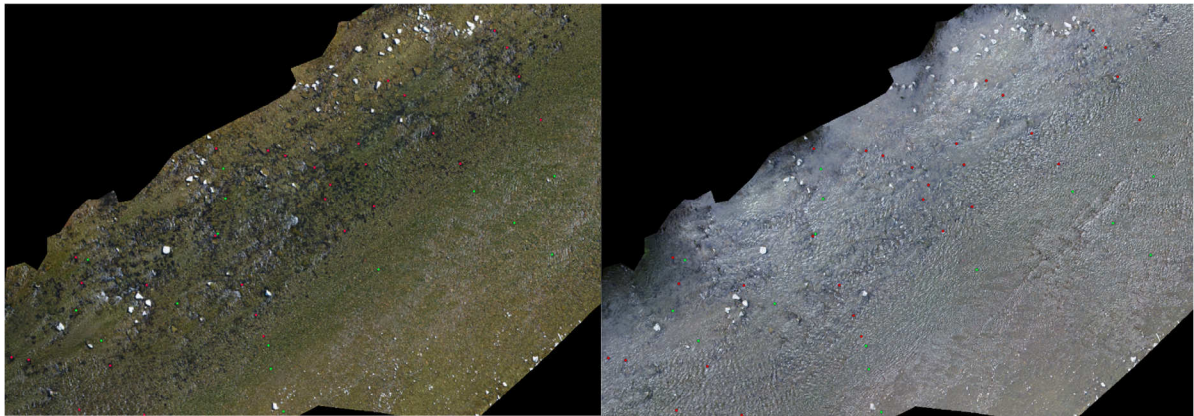
Figure 9-14: Hutt River RGB aerial imagery: morning flights (left) and afternoon flights (right).
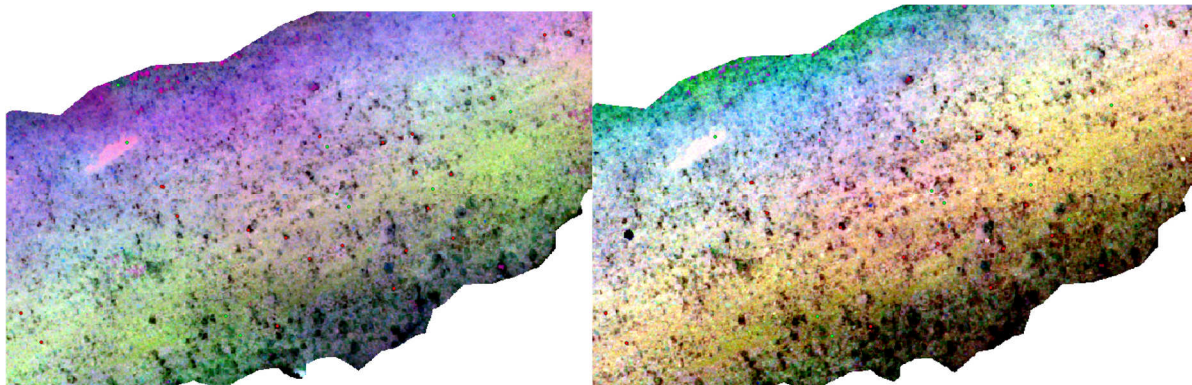
Figure 9-15: Hutt River multispectral aerial imagery: morning flights (left) and afternoon flights (right).

Other challenges in the Hutt River that likely decreased the quality of aerial imagery and thus classifications were: greater depth than the Waingawa River, shadows from tall riparian vegetation, reflections of green light from riparian vegetation, increased abundance of filamentous green algae in the Hutt River, and higher diversity of taxa in Hutt River *Microcoleus* mats (e.g., 54.8% *Microcoleus* in the Hutt River mats Section 9.3.1, compared to 85.6% *Microcoleus* in the Waingawa River, see Section 10.3.1). Overall, there appears to be an overestimate of *Microcoleus* cover estimated for most of the algorithms and imagery types in Table 9-2 compared to visual assessment of the imagery. There were also surprising discrepancies between the classifications of morning RGB aerial imagery (i.e. altitude and pixel resolution), potentially these differences are due to the sensitivity of MAM to small georeferencing errors due to the small size of *Microcoleus* patches. Higher accuracy may be obtained by: using more advanced classification algorithms; using more training polygons; specifically selecting training polygons for each type of imagery; better aligning training polygons to *Microcoleus* patches;

and iterating training polygon selection for each imagery type after each classification. The reflectance spectra obtained from hyperspectral aerial imagery provided useful input information for assessing the spectral separability of *Microcoleus* from other classes of interest (Figure 9-6 and Figure 9-7). This indicated that remote sensing in the 500 to 650 nm range is the most promising, which makes the use of RGN cameras not recommended. Near infrared wavelengths are good for remote sensing of riparian vegetation but provide little separation of instream classes. This is illustrated by little variation between the Minimum Distance classification for 6 band, or 3 band morning multispectral aerial imagery in the Hutt River (Table 9-2). Overall classification accuracies for most imagery types (other than multispectral) were not very good, yet classifications were time consuming to produce and are difficult to standardise. There are many ways to prepare the input imagery, select training and validation points, and many classification algorithms to choose from (with a wide range available beyond the three traditional ones used here). Classification algorithms can also be tuned in multiple ways, providing more challenges for developing standardised and efficient approaches. The case study in the Hutt River illustrates the potential of MAM for detailed scientific studies where 2D maps of cover are needed, but also highlights many of the challenges of this approach for routine monitoring. In general the Minimum Distance classification algorithm was the most consistent of the three tested (Table 9-2) and is the algorithm recommended for MAM classification in QGIS. Likewise, multispectral cameras are recommended for remote sensing of *Microcoleus*.

10 MAM Case study #2 Waingawa River

10.1 Site location

The Waingawa River site was located near Skeets Road (-40.941453, 175.586655, [WGS84]), the site was ~400 m long, with abundant mats of *Microcoleus*. The Waingawa River site was upstream from Masterton and outside of the restricted airspace from Masterton Airport and Wairarapa Hospital (Figure 10-1).
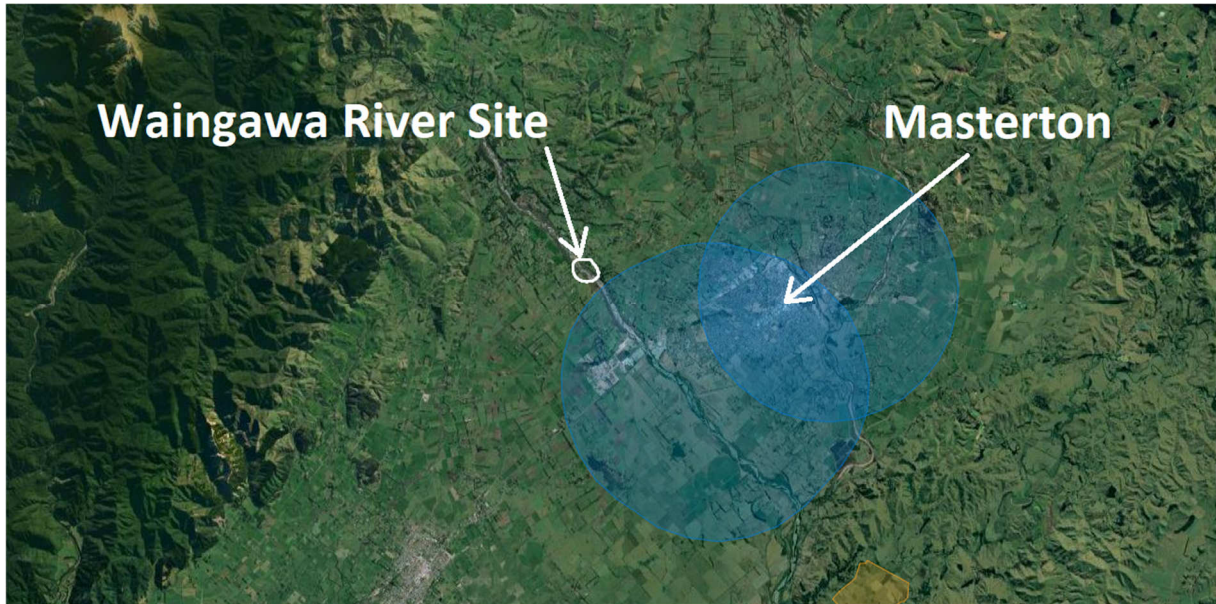
Figure 10-1:   Map showing the Waingawa River site and nearby airspace restrictions.

10.2 Data collected

Data collection in the Waingawa River occurred on the 13th of February 2020 at a discharge of 0.84 m^3/s. Aerial imagery data was collected with RGB, RGN, multispectral and hyperspectral cameras, with flights at two times of the day to investigate the effect of lighting and environmental conditions. Ground truth measurements consisted of 396 RTK GPS observations, 55 biomass samples, and 54 underwater views (Figure 10-2).
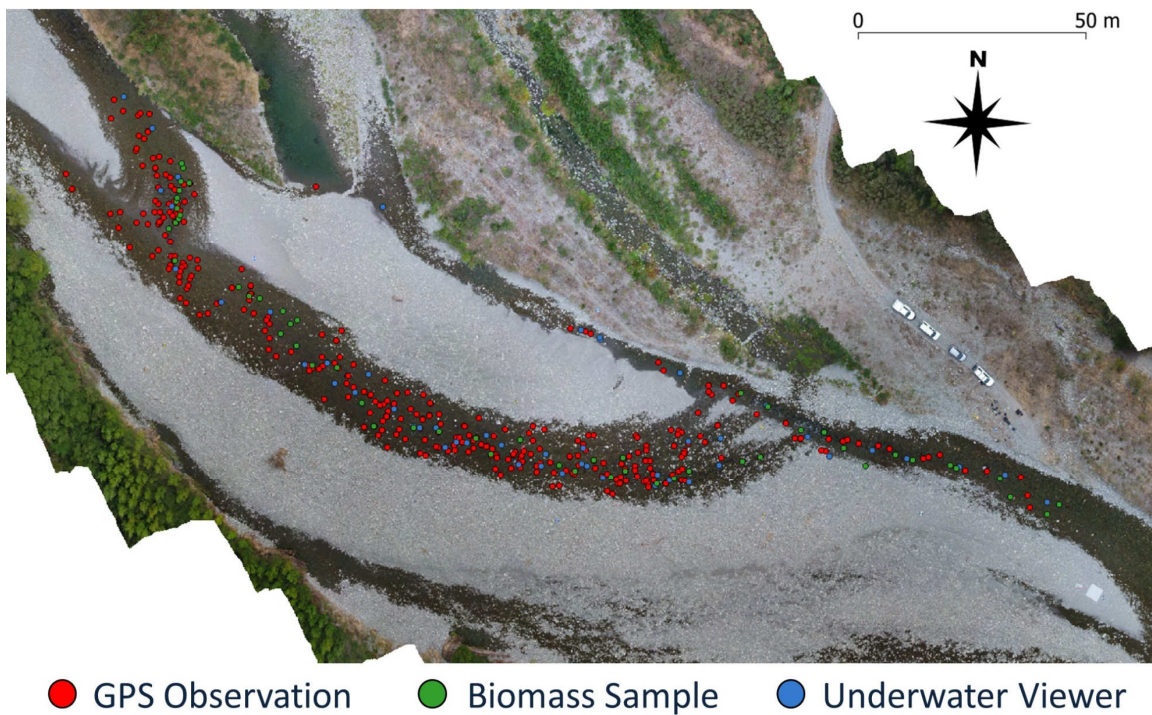
Figure 10-2: **Ground truth measurements in the Waingawa River (396 GPS Observations, 55 Biomass Samples, 54 Underwater Views).**

RTK GPS observation points were combined into the binary classes of Not *Microcoleus* and *Microcoleus* (Figure 10-3).
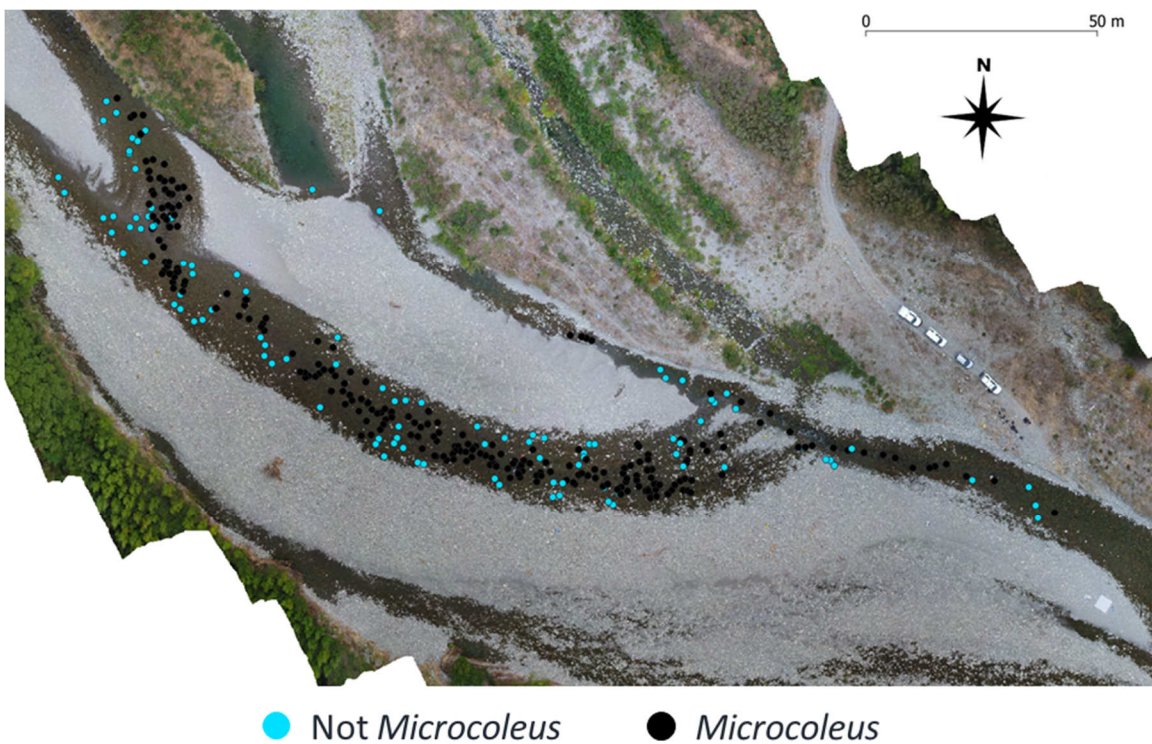
Figure 10-3: **Waingawa River GPS ground truth points for *Microcoleus* presence and absence.**

10.3   Results

10.3.1 Biomass: Taxonomic composition of *Microcoleus* dominated mats

Ground truth data for the Waingawa River were processed in the same way as those in the Hutt River (Section 9.3.1). In the Waingawa River, cyanobacteria mats were dominated by *Microcoleus autumnalis* (85.6%), with *Cymbella tumida* diatoms (12%), and a small proportion of other taxa (Figure 10-4). This contrasts with the Hutt River (Section 9.3.1), where mats were more diverse.
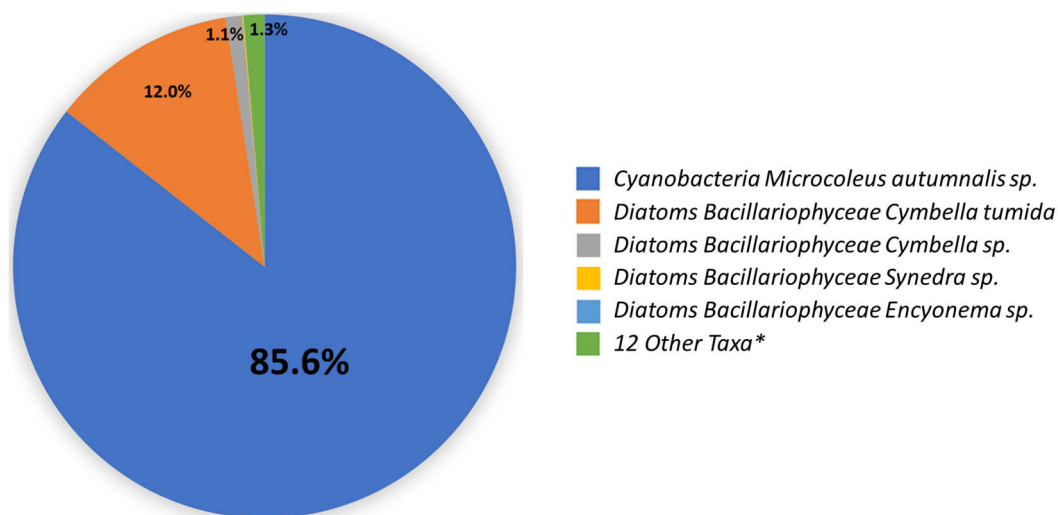
Figure 10-4:   The taxonomic composition of cyanobacterial mats sampled from the Waingawa River.[12]

10.3.1 Biomass: AFDM and Chl-a of *Microcoleus* dominated mats

The average AFDMAD of *Microcoleus* dominated mats in the Waingawa River was 25.6 g/m^2. The average chl *a* areal density of *Microcoleus* dominated mats in the Waingawa River was 155.4 mg/m^2. By combining the taxonomic composition of mats (i.e., 85.6% *Microcoleus*) (Section 10.3.1) and the ash-free dry mass of each sample, then averaging the results, the average AFDMAD of *Microcoleus* in the *Microcoleus* dominated mats was calculated (Table 10-1), yielding an average AFDMAD of *Microcoleus* of 21.9 g/m^2.

Table 10-1:   Ash-Free Dry Mass Aerial Density of *Microcoleus* dominated mats, with biomass separated by taxonomic composition of samples.

Taxa	AFDMAD (g/m^2)
Microcoleus autumnalis	21.9
Cymbella tumida	3.1
Cymbella sp.	0.3
Other (12 taxa with low abundance)	0.3
Total	25.6

---

[12] Taxonomic composition is calculated as the average of relative abundance by biovolume weighted by sample AFDM.

10.3.2 Biomass: Pigment composition of *Microcoleus* dominated mats

Biomass samples from the Waingawa River were processed for pigment composition in the same way as those from the Hutt River (Section 9.3.3). In the Waingawa River, phycocyanin comprised 52.5% of the total pigment mass, with phycoerythrin comprising 7.7% and other pigments comprising the remaining 31.1% (Figure 10-5). The proportion of phycocyanin and phycoerythrin was lower in the Waingawa River samples than those from the Hutt River (Figure 9-5), even though the proportion of the mats comprising *Microcoleus* was higher in the Waingawa River.
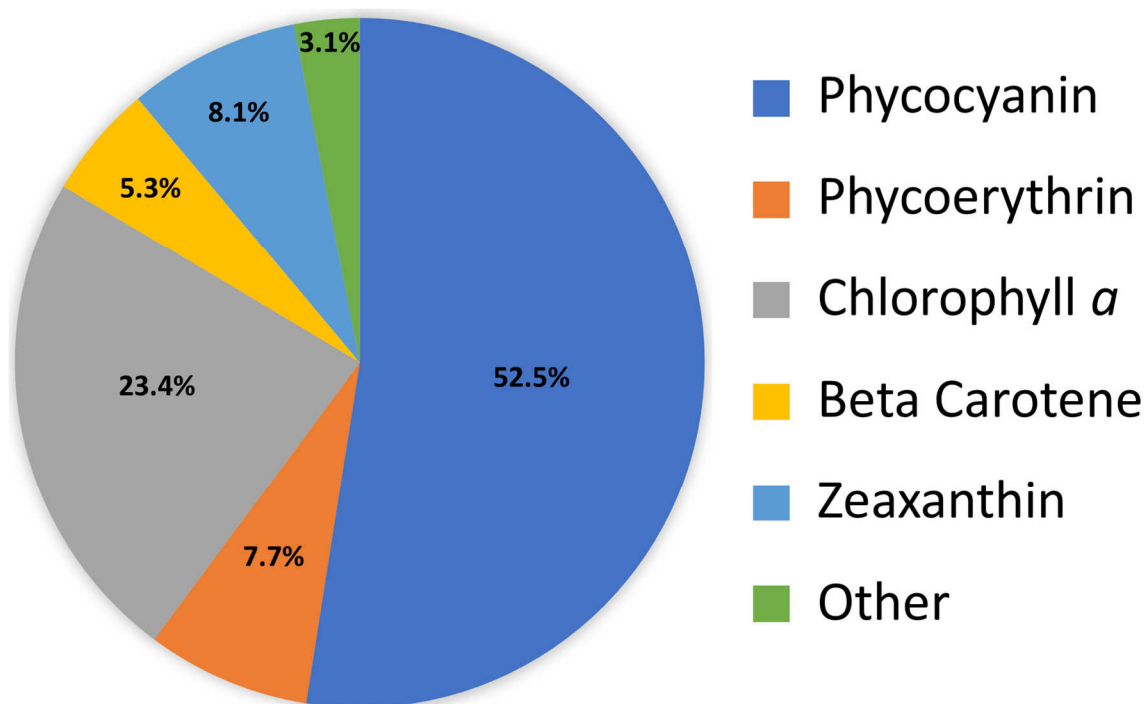
Figure 10-5:   Waingawa River pigment composition of *Microcoleus* dominated mats (% by mass).

10.3.3 Reflectance spectra: *Microcoleus* dominated mats and other classes

Hyperspectral aerial imagery data in the Waingawa River was used to extract reflectance spectra for the classes: Dry Stones, *Microcoleus*, Riparian Vegetation, and Wet Stones (Figure 10-6). Similar to the imagery from the Hutt River, this shows the low reflectance and minimal separability of the instream classes (compared to terrestrial classes). When directly comparing the instream classes (Figure 10-7), there is the most separability in the 500-650 nm range (similar to the Hutt River). Above 700 nm, the shape of the reflectance curve for *Microcoleus* closely matches that of Wet Stones, and differences may be related to river depth (due to attenuation of longer wavelengths) because the polygons of Wet Stones without *Microcoleus* were in shallower areas than those for *Microcoleus*. This information provides a useful indication that remote sensing *Microcoleus* with multispectral camera bands in the 500–650 nm range are the most likely to provide separability and accurate classifications. For our Airphen multispectral camera, this corresponds to bands B1, B2, B3, which are 10 nm bands, centred on the wavelengths 530, 570, and 622 nm.
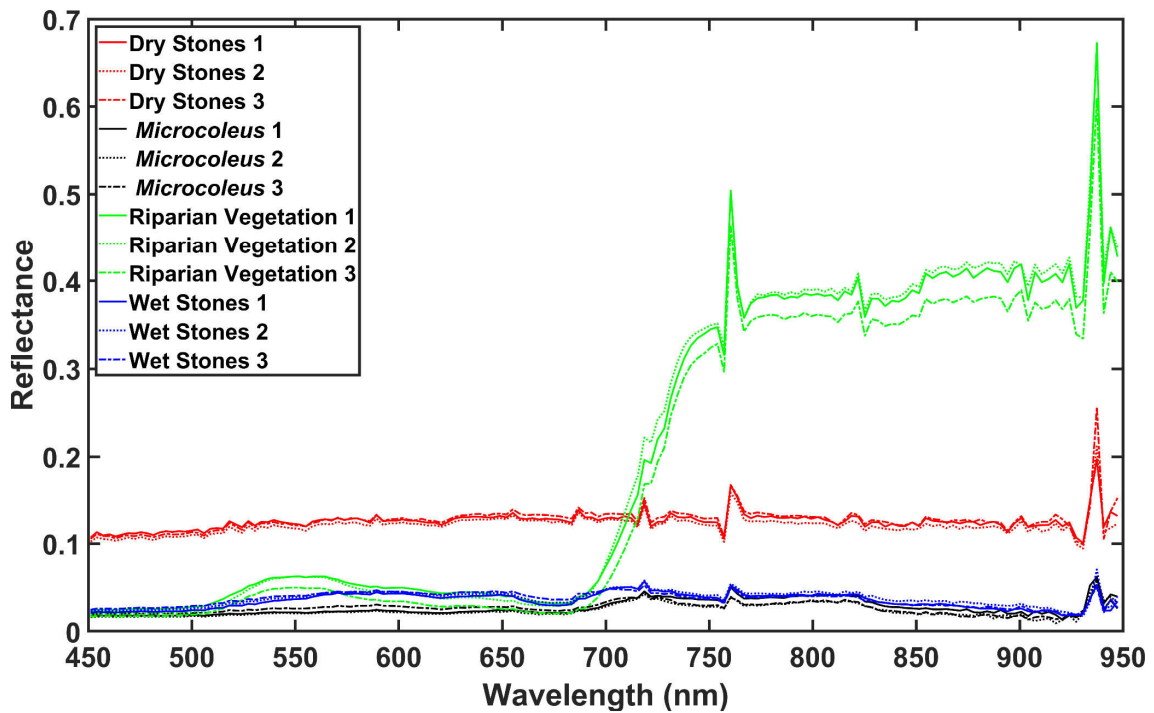
Figure 10-6: Reflectance spectra in the Waingawa River for four classes of interest, with three sample polygons for each class.
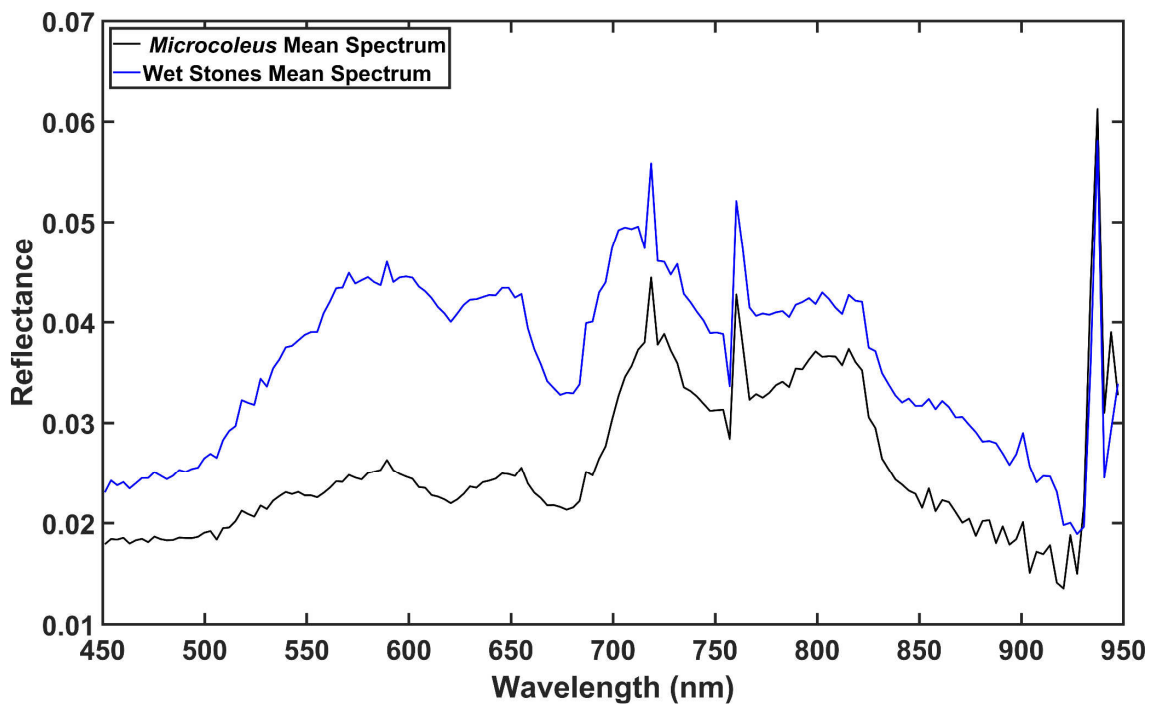
Figure 10-7: Reflectance spectra in the Waingawa River for two instream classes: *Microcoleus* and wet stones.

The reflectance spectra for Wet Stones from Figure 10-8 and Figure 10-9 may have had a thin film of periphyton covering them, so additional reflectance spectra were investigated from specific locations with (and without) film to investigate any spectral differences between Film, Wet Stones and *Microcoleus* (Figure 10-8, Figure 10-9).
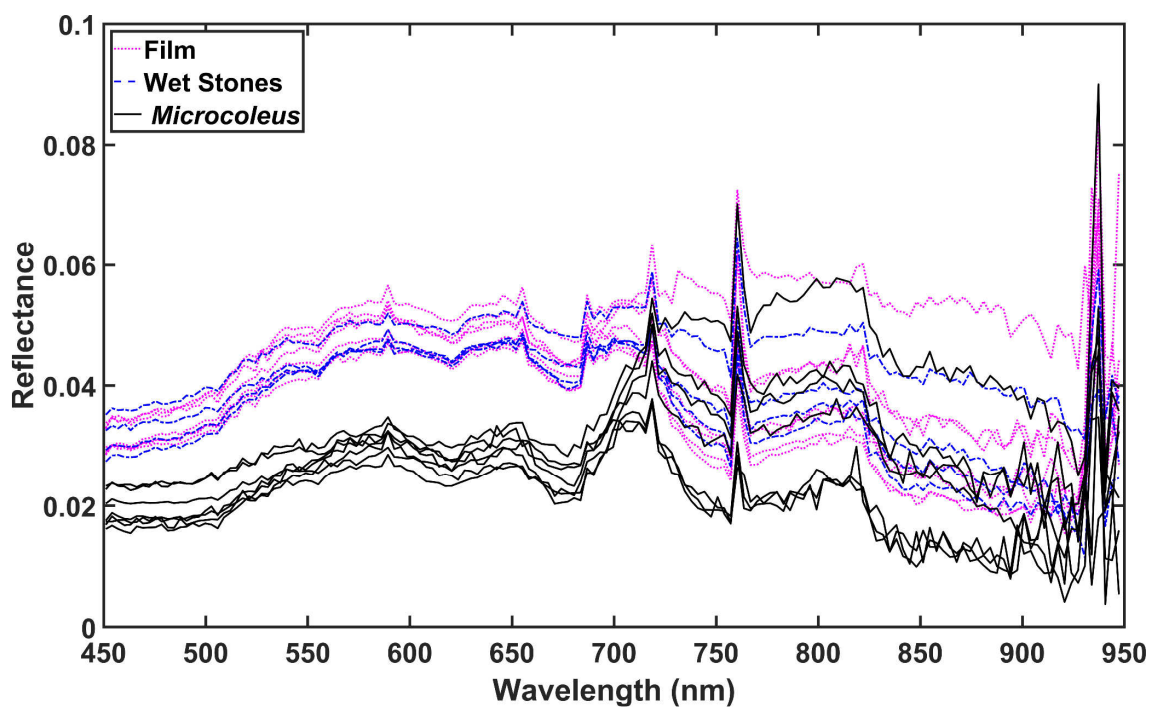
Figure 10-8: Reflectance spectra in the Waingawa River for three instream classes: Film, Wet Stones (without Film) and *Microcoleus*.
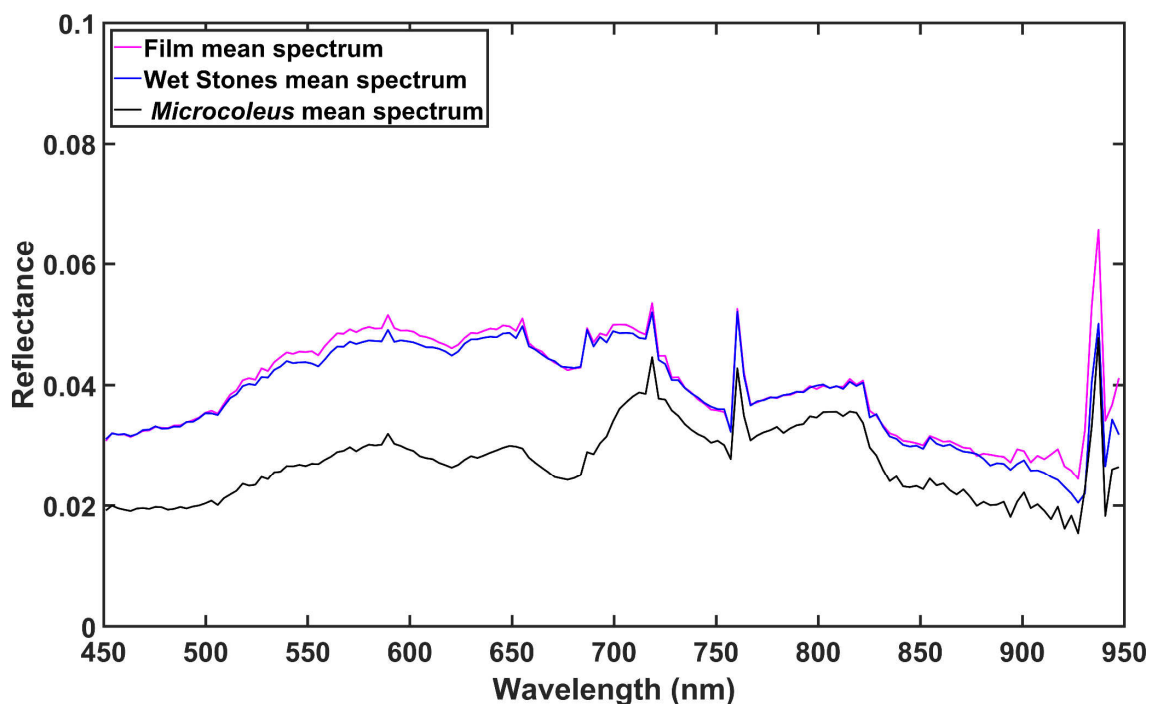
Figure 10-9: Mean reflectance spectra in the Waingawa River for three instream classes: Film, Wet Stones (without Film) and *Microcoleus*.

There was little difference in the mean spectra between Film and Wet Stones (Figure 10-8), however there was a lot of scatter in the individual spectra above 700 nm (Figure 10-9). It was important to further investigate the source of this scatter, since it could seriously impact the accuracy of remote sensing classifications if using data from above 700 nm. This investigation was undertaken by plotting

the individual spectra as a function of depth for Film (Figure 10-10), Wet Stones (Figure 10-11), *Microcoleus* (Figure 10-12), and all the samples together (Figure 10-13).
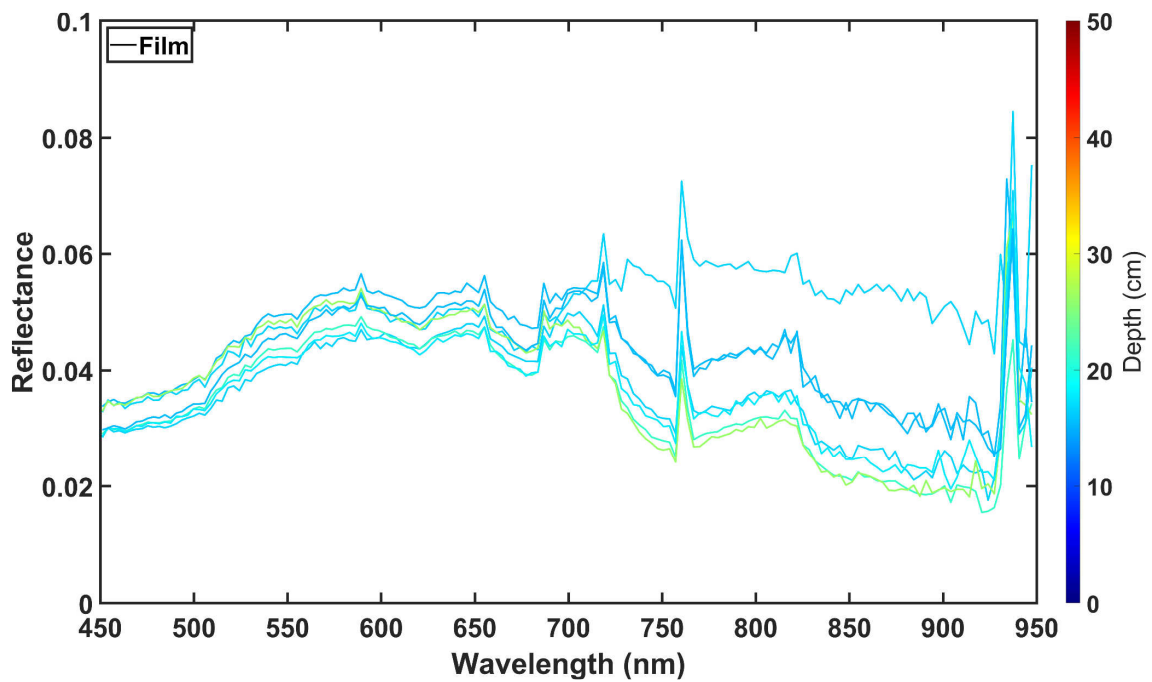
Figure 10-10: Reflectance spectra in the Waingawa River for Film as a function of depth.
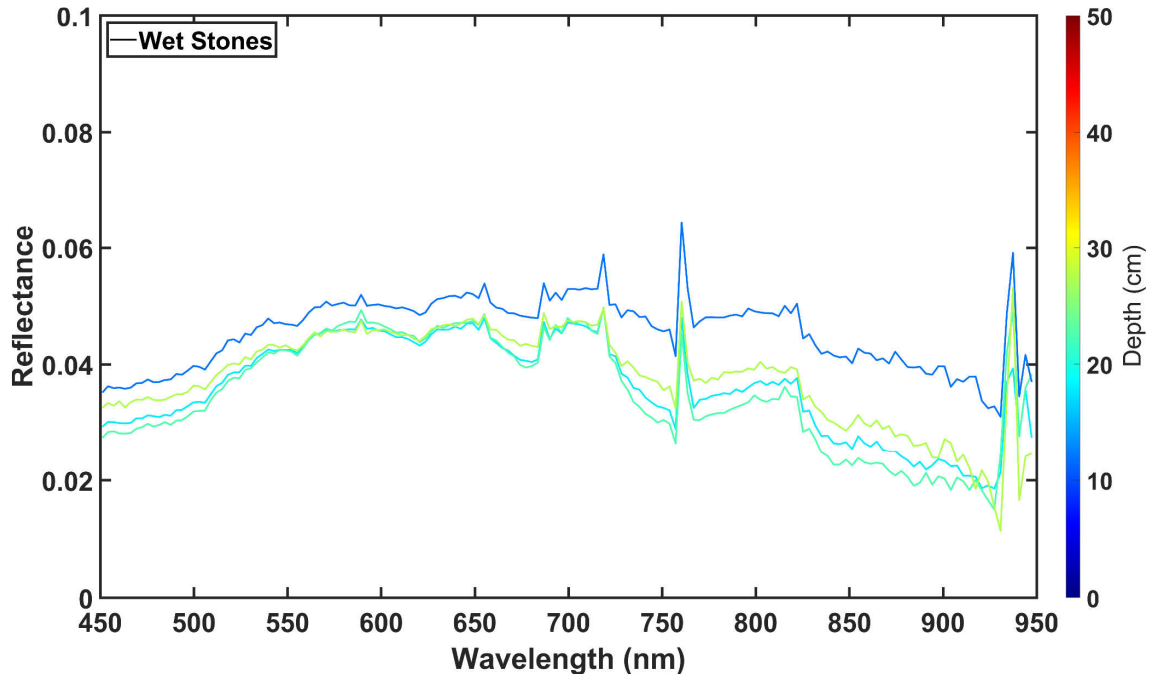
Figure 10-11: Reflectance spectra in the Waingawa River for Wet Stones as a function of depth.
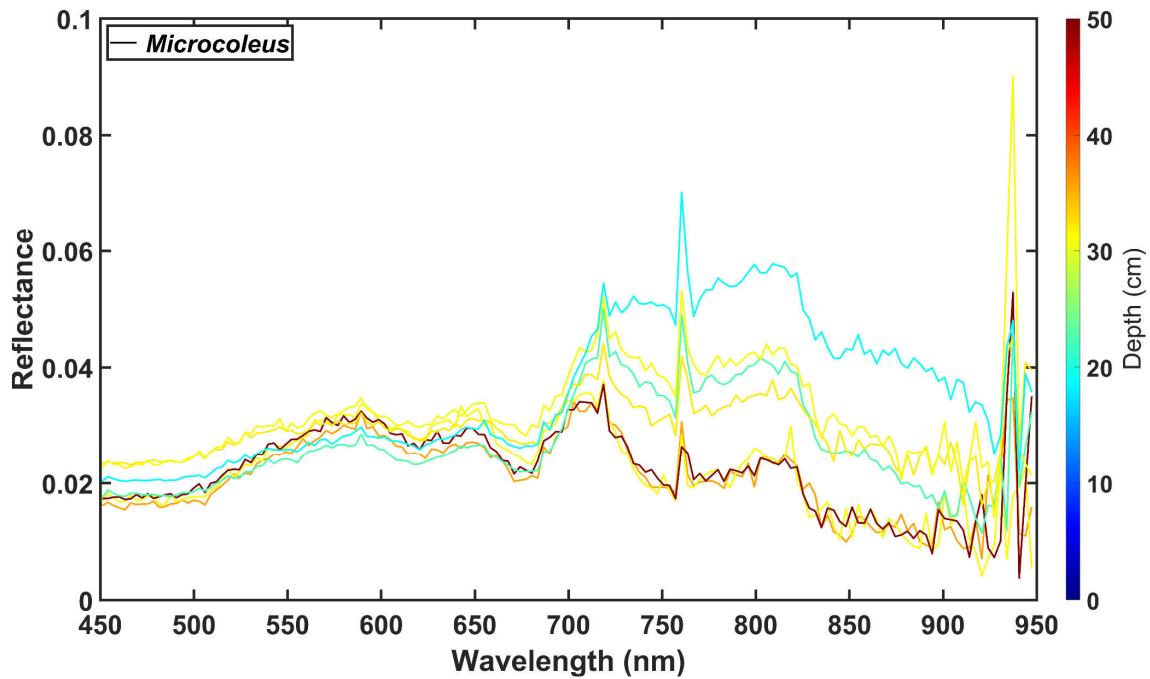
Figure 10-12: Reflectance spectra in the Waingawa River for *Microcoleus* as a function of depth.
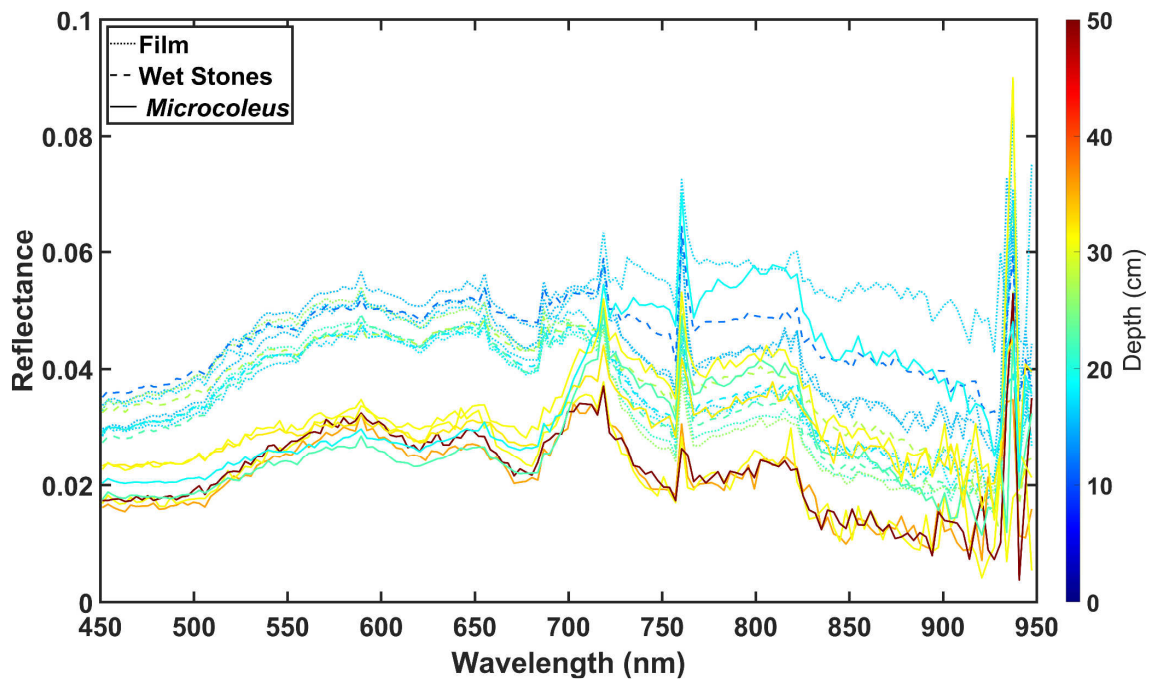
Figure 10-13: Reflectance spectra in the Waingawa River for Film, Wet Stones and *Microcoleus* as a function of depth.

There was found to be depth dependence in reflectance spectra above 700 nm (Figure 10-13). Due to this depth dependence caution should be applied if using wavelengths above 700 nm for through water remote sensing of *Microcoleus*. This contrasts with remote sensing of terrestrial targets (such as riparian vegetation), where near infrared is a very useful part of the spectrum for detection and classification.

10.3.4 Aerial imagery classifications

Aerial imagery classifications were performed in QGIS using Minimum Distance (MD), Maximum Likelihood (ML), and Spectral Angle Mapper (SAM) algorithms (Section 7). Classifications of the multispectral camera data were performed on bands 1–6, then repeated with only bands 1–3 for comparison. The length of the classification reach was 281 m and the area of the classification reach was 4281 m^2. The cover estimates and accuracy metrics (Section 7.11) for the different types of imagery and classifications are summarised in Table 10-2. Flights were performed in the morning and repeated in the afternoon, to investigate any differences in classifications due to lighting, shadows, and reflections from cloud cover. Flights were performed at 50 m altitude, with the RGB morning flights repeated at 100 m altitude, to investigate any differences in classifications due to altitude. Orthomosaics were output with a consistent resolution of 50 mm pixels, then an extra orthomosaic from the RGB morning flights was produced (15 mm pixels), to investigate any differences in classifications due to resolution.

Training data consisted of 17 polygons of *Microcoleus* and 88 polygons of Not *Microcoleus*. There was plentiful RTK GPS ground truth data of *Microcoleus*, however there was insufficient coverage of the class Not *Microcoleus* to cover all of the spectrally distinct regions of the orthomosaics. Hence, some of the Not *Microcoleus* training polygons had to be inferred from regions that were visually distinctive as being very different from the pixels at *Microcoleus* RTK GPS ground truth locations.

Validation data consisted of 50 polygons of *Microcoleus* and 50 polygons of Not *Microcoleus* centred around RTK GPS ground truth locations.

Table 10-2: **Waingawa River aerial imagery classifications and accuracy (%) for *Microcoleus* (Class 1) and Not *Microcoleus* (Class 2).[13]**

Aerial imagery type and time of day	Classification Type	*Microcoleus* Cover (%)	Class 1 User Accuracy	Class 2 User Accuracy	Class 1 Producer Accuracy	Class 2 Producer Accuracy	Total Accuracy
RGB Morning	MD	15.52	72.08	89.17	60.82	93.19	85.93
RGB Morning	ML	18.08	70.15	89.61	62.98	92.25	85.69
RGB Morning	SAM	12.16	28.95	78.57	16.95	87.98	72.06
RGB Morning (100 m altitude)	MD	18.83	54.74	87.91	59.69	85.60	79.74
RGB Morning (100 m altitude)	ML	15.86	62.24	87.71	56.84	89.93	82.46
RGB Morning (100 m altitude)	SAM	17.94	24.19	77.76	19.62	82.05	67.95
RGB Morning (15 mm pixels)	MD	13.22	75.23	90.20	64.62	93.86	87.32

---

[13] The classification algorithms used were: Minimum Distance (MD), Maximum Likelihood (ML) and Spectral Angle Mapper (SAM). All imagery was flown at 50 m altitude above ground level, with an orthomosaic pixel size of 50 mm (unless otherwise stated).

Aerial imagery type and time of day	Classification Type	Microcoleus Cover (%)	Class 1 User Accuracy	Class 2 User Accuracy	Class 1 Producer Accuracy	Class 2 Producer Accuracy	Total Accuracy
RGB Morning (15 mm pixels)	ML	12.62	79.74	91.12	67.89	95.03	88.95
RGB Morning (15 mm pixels)	SAM	15.66	31.11	79.58	25.53	83.70	70.68
RGB Afternoon	MD	18.25	70.84	89.86	63.94	92.39	86.01
RGB Afternoon	ML	17.90	72.91	89.42	61.78	93.37	86.28
RGB Afternoon	SAM	14.87	21.67	77.45	14.06	85.31	69.33
RGN Morning	MD	6.22	82.66	87.64	53.27	96.74	86.92
RGN Morning	ML	6.88	85.13	87.97	54.46	97.22	87.56
RGN Morning	SAM	7.99	84.58	90.01	63.26	96.63	89.09
RGN Afternoon	MD	7.79	91.19	94.00	78.46	97.80	93.46
RGN Afternoon	ML	8.26	91.07	94.66	80.99	97.70	93.94
RGN Afternoon	SAM	12.17	84.11	94.87	82.19	95.50	92.51
Multispectral Morning (6 Bands)	MD	2.31	98.23	98.01	93.04	99.51	98.06
Multispectral Morning (6 Bands)	SAM	2.32	98.10	98.05	93.16	99.48	98.06
Multispectral Morning (3 Bands)	MD	2.34	97.70	97.64	91.72	99.37	97.65
Multispectral Morning (3 Bands)	ML	2.92	97.78	98.55	94.96	99.37	98.38
Multispectral Morning (3 Bands)	SAM	13.84	40.93	81.26	30.61	87.17	74.46
Multispectral Afternoon (6 Bands)	MD	4.11	95.21	95.40	83.53	98.78	95.36

Aerial imagery type and time of day	Classification Type	*Microcoleus* Cover (%)	Class 1 User Accuracy	Class 2 User Accuracy	Class 1 Producer Accuracy	Class 2 Producer Accuracy	Total Accuracy
Multispectral Afternoon (6 Bands)	SAM	4.12	95.08	95.40	83.53	98.75	95.33
Multispectral Afternoon (3 Bands)	MD	4.19	95.84	95.28	83.05	98.96	95.39
Multispectral Afternoon (3 Bands)	ML	3.09	97.42	94.95	81.73	99.37	95.41
Multispectral Afternoon (3 Bands)	SAM	14.00	41.71	82.04	35.10	85.81	74.43

The most consistent classifications in the Waingawa river were obtained from the multispectral morning flight data using the Minimum Distance classification algorithm (Table 10-2). The six band multispectral imagery estimated *Microcoleus* cover of 2.31% and area of 98.89 m^2, with 98.23% user accuracy, and 93.04% producer accuracy. These accuracies are high, and only indicate a slight underestimate of cover. There was little difference between Minimum Distance classifications with 6 bands or 3 bands, however there were substantial discrepancies between classification algorithms, and the Maximum Likelihood algorithm failed completely for 6 band multispectral data and was not included in Table 10-2. Classifications of the imagery were highly sensitive to selection of sufficient training polygons of the Not *Microcoleus* class to account for all of the spectrally distinctive areas of the orthomosaics. However, even with 88 training polygons in the Not *Microcoleus* class, most of the imagery types (i.e., RGB and RGN) overpredicted *Microcoleus* cover throughout the study reach and had poor accuracy (Table 10-2).

Multispectral aerial imagery and Minimum Distance classifications of the Waingawa River reach are show in Figure 10-14 and Figure 10-15. *Microcoleus* cover was concentrated in an upstream riffle, with zoomed in images from this region shown in Figure 10-16 and Figure 10-17. Differences between the classification algorithms, imagery types, and times of the day are discussed in Section 10.4.
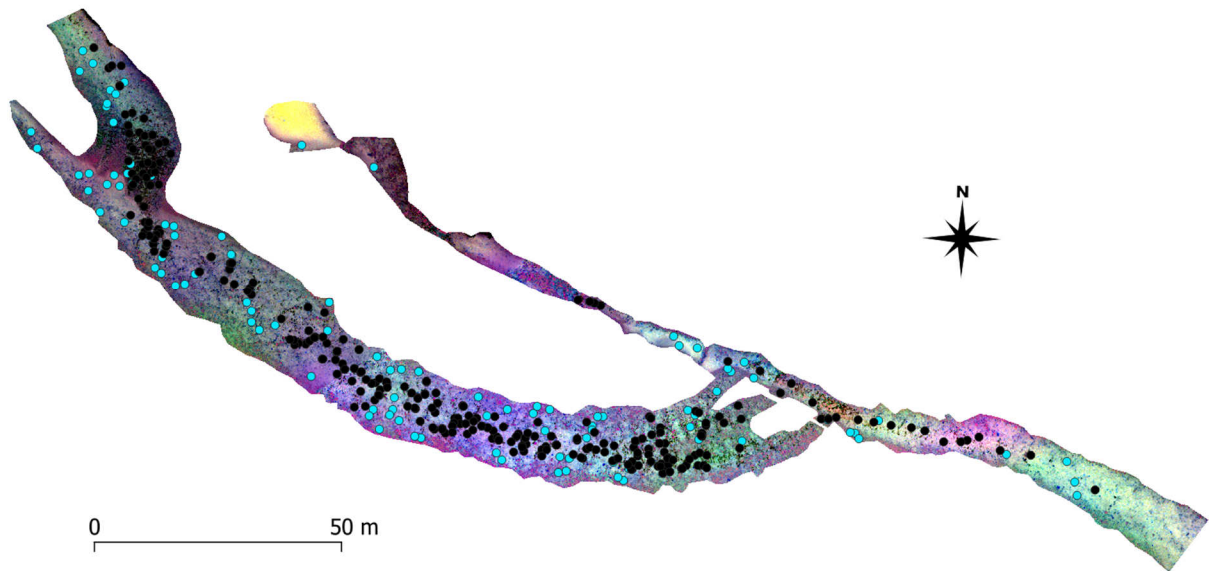
Figure 10-14: Multispectral aerial imagery in the Waingawa River (morning flights) with GPS ground truth measurements.[14]
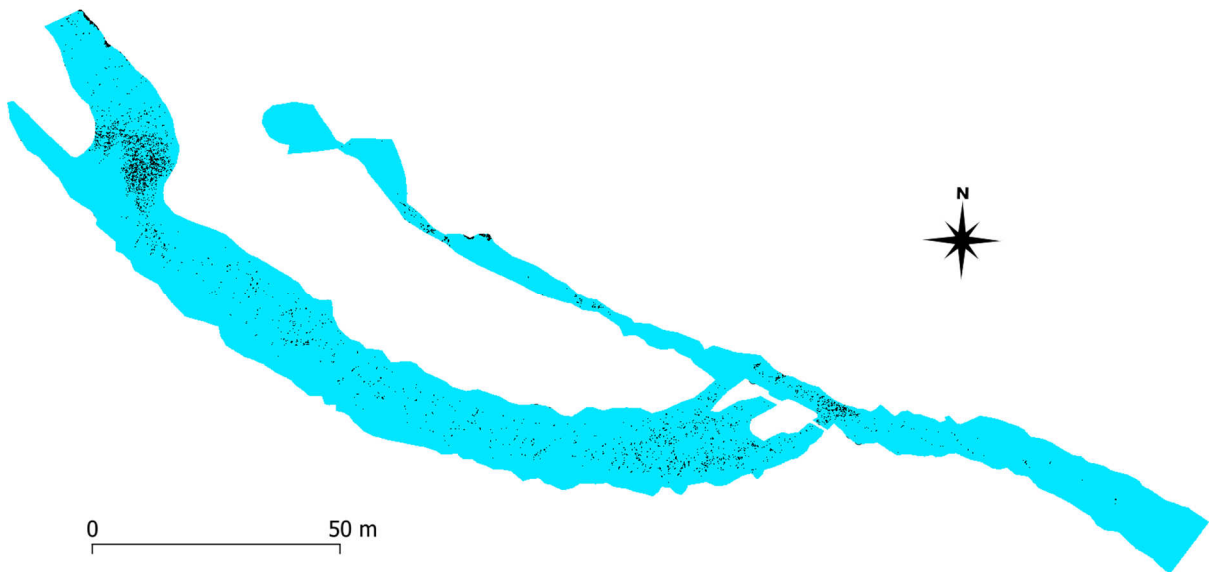
Figure 10-15: Minimum distance classification of the Waingawa River 6 band multispectral aerial imagery (morning flights).[15]

---

[14] Black dots are *Microcoleus* and blue dots are Not *Microcoleus*.
[15] Black is classified as *Microcoleus* and blue is Not *Microcoleus*.
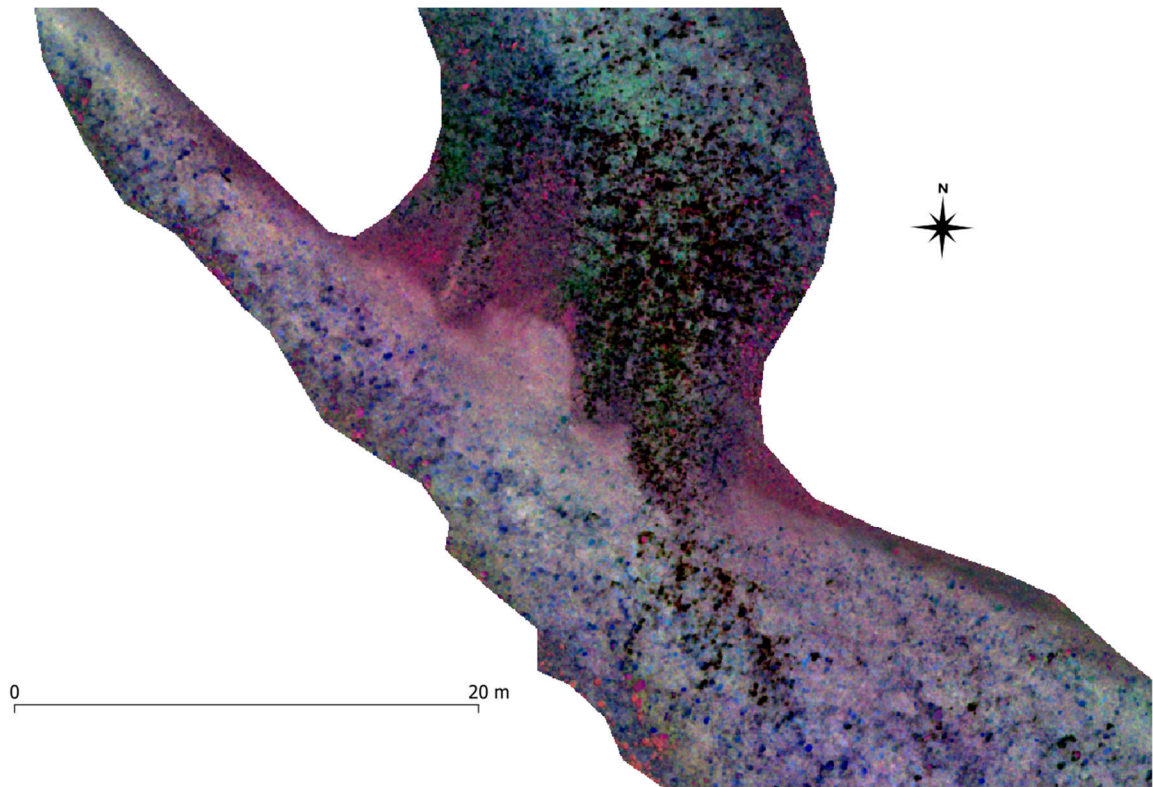
Figure 10-16: Waingawa River 6 band multispectral aerial imagery (morning flights) showing the upstream riffle where *Microcoleus* was the most abundant.
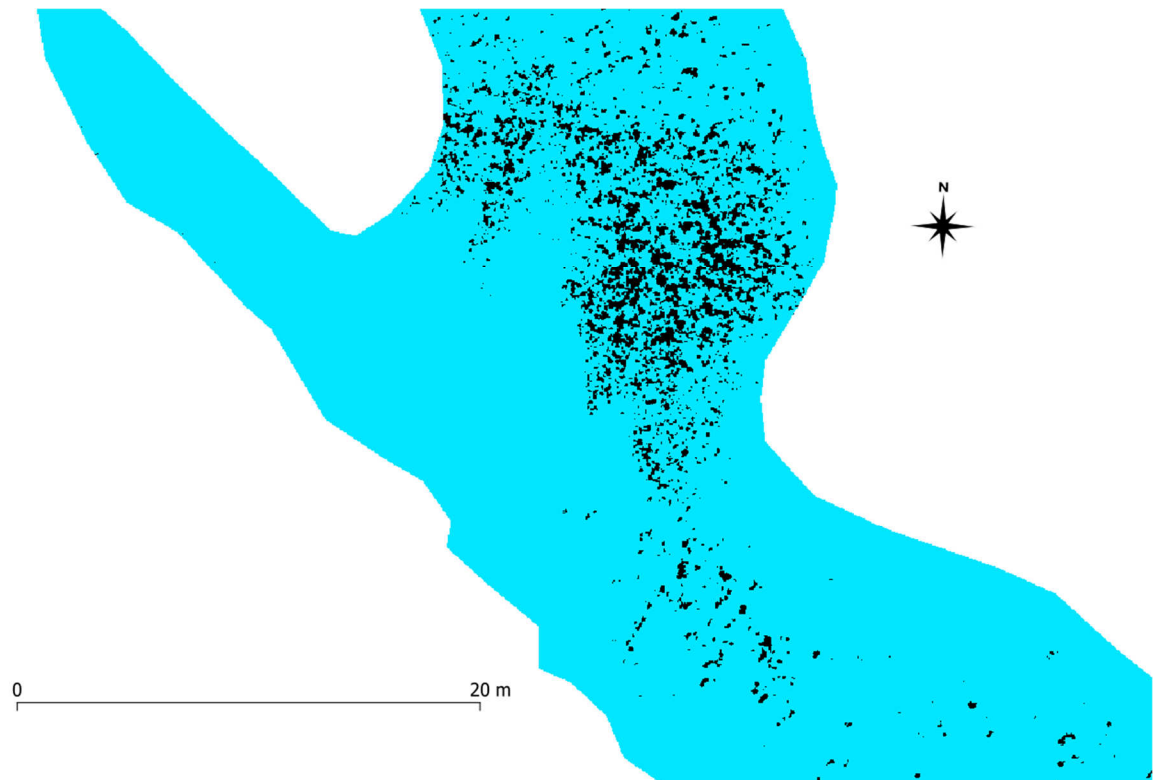
Figure 10-17: Minimum distance classification of the Waingawa River 6 band multispectral aerial imagery (morning flights) from the upstream riffle.[15]

10.3.5 *Microcoleus* cover estimates from underwater viewers

There were 55 underwater views collected from throughout the Waingawa River (Figure 10-2). However, these were unfortunately biased by searching for *Microcoleus* and other periphyton, yielding an average *Microcoleus* cover estimate of 47.0%, which was clearly a substantial overestimate. There were insufficient views in sections of the reach without periphyton cover, with only 9.3% of the riverbed classified as having no algae, and 37.7% classified as having thin film. Only in the most densely covered part of the reach (the upstream riffle) would cover have approached or exceeded 47%, let alone the whole river reach having this cover level. At 47.0% cover every 2nd step in the river would be standing on *Microcoleus*, which was certainly not the case. This illustrates the challenges of using underwater viewers to obtain a representative cover estimate in a whole reach (Section 5.1.2) and the challenges in general of providing an accurate reference cover level to compare aerial imagery classifications with. For this reason, the standard methods of quantifying aerial imagery accuracy through validation polygons around RTK GPS survey presence/absence points is recommended.

10.3.6 Biomass of *Microcoleus* at the reach and river scale

The biomass measurements for *Microcoleus* dominated mats (Section 10.3.1) can be combined with cover and area estimates (Section 10.3.4) to estimate reach and river averaged biomass. The average AFDMAD of *Microcoleus* in the *Microcoleus* dominated mats was 21.9 g/m^2 (i.e., AFDMAD$_{Microcoleus}$). By multiplying this with the estimated area of *Microcoleus* from aerial imagery classifications of 98.9 m^2 yields an estimated total biomass of *Microcoleus* in the classification area of 2,165.7 g AFDM (Section 8.1). Dividing the total biomass by the length of the classification reach (281 m), yields an AFDMLD for *Microcoleus* of 7.7 g AFDM/m (Section 8.2). Combining the cover estimate of 2.31% (Section 10.3.4) and the AFDMAD$_{Microcoleus}$ yields AFDMAD$_{Microcoleus,Average}$ of 0.51 g/m^2 in the study reach (Section 8.3). Assuming that the study reach is representative of cover and biomass in the river in general, then AFDMLD$_{Microcoleus}$ and AFDMAD$_{Microcoleus,Average}$ are also valid estimates at the river scale. These metrics provide an estimate of toxin production risk, which is proportional to the number of cells (three-dimensional biomass), rather than cover (which could be a thin film).

10.4 Discussion

Cloud cover also changed in the Waingawa during aerial surveys, from blue sky in the morning to sparse high cloud in the afternoon. This resulted in minor changes in the visibility of *Microcoleus* in the aerial imagery (Figure 10-18). However, the effect was much less pronounced than that in the Hutt River (Figure 9-14), likely due to differences in cloud height and thickness. Differences in cloud cover during the afternoon multispectral flights may have also yielded some differences in the multispectral orthomosaics (Figure 10-19), with classifications of the morning multispectral imagery having higher accuracy (Table 10-2). The accuracy of classifications of most imagery types in the Waingawa River (Table 10-2) were generally better than those in the Hutt River (Table 9-2), likely due to: shallower water, less riparian vegetation and shadows, less effect of cloud cover, collection of more training polygons, and less taxonomic diversity in the *Microcoleus* mats (Section 10.3.1). However, there were still significant discrepancies between the aerial imagery classifications for the different imagery types, with RGB and RGN tending to overpredict *Microcoleus* cover. RGB classification results in the Waingawa river were more consistent with altitude and pixel resolution, so they did not provide an explanation for the discrepancies found in the Hutt River. Overall, higher accuracy may be obtained by: using more advanced classification algorithms; using more training polygons; specifically selecting training polygons for each type of imagery; and iterated training polygon selection for each imagery type after each classification.

Figure 10-18: Waingawa River RGB aerial imagery: morning flights (left) and afternoon flights (right).

Figure 10-19: Waingawa River multispectral aerial imagery: morning flights (left) and afternoon flights (right).

There were insufficient RTK GPS ground truth measurements of the Not *Microcoleus* class in the Waingawa River (Figure 10-3). This demonstrates the risk of 'search bias' due to hunting for *Microcoleus* and other periphyton, rather than recording a similar proportion of Not *Microcoleus* GPS points (Section 5.1.1). In general the Minimum Distance classification algorithm was the most consistent of the three tested (Table 10-2) and is the algorithm recommended for MAM classification in QGIS. Likewise, multispectral cameras are recommended for remote sensing of *Microcoleus*.

The hyperspectral aerial imagery in the Waingawa River showed similar spectral separation of *Microcoleus* from other classes of interest (Figure 10-6 and Figure 10-7) as that observed in the Hutt River (Figure 9-6 and Figure 9-7), with the main separation being in the 500–650 nm range. However, there were very small difference in reflectance between *Microcoleus* and wet stones/gravel, illustrating the challenges of reliable classifications from aerial imagery. Similar to the Hutt River, the case study in the Waingawa River illustrates the potential of MAM for detailed scientific studies where 2D maps of cover are needed, but also highlights the challenges of MAM for routine monitoring.

10.5   General comment on case studies

Hyperspectral remote sensing of toxic cyanobacteria is a promising technology, due to the high spectral resolution of the sensors. Progress has been made remote sensing planktonic cyanobacteria (Hunter et al. 2010; Kudela et al. 2015; Shi et al. 2019), yet limited progress has been made with

hyperspectral remote sensing of benthic cyanobacteria. Our case studies illustrated the utility of hyperspectral remote sensing to resolve the spectral signature of benthic cyanobacteria mats and assess the spectral separability from other classes of interest, providing valuable information for the selection of band pass filters for multispectral cameras for remote sensing at larger scales. It is also possible to use hyperspectral data directly for classification mapping, however this is more challenging for benthic than planktonic cyanobacteria. The difficulties mainly arise from the small spatial scale of benthic cyanobacteria, requiring low altitude very high spatial resolution hyperspectral data (since the data resolution decreases during the georectification processing step). The high spectral resolution (i.e., 200 bands) results in the collection and processing of enormous amounts of data. Further challenges are the accuracy of the georectification of the hyperspectral aerial imagery (i.e., push broom scanner data) rather than 2D RGB or multispectral aerial imagery, where highly accurate structure from motion techniques are used for georeferencing and orthorectification. This results in much lower spatial accuracy for the georeferenced hyperspectral aerial imagery, making it challenging to align with the RTK GPS ground truth data. Overcoming these challenges and reliably stitching hyperspectral aerial imagery hypercubes together is needed before reach scale classifications and mapping based on hyperspectral aerial imagery are feasible.

11 Future outlook

11.1 Practical implementation of MAM and limitations

This user guide details methods for remote sensing *Microcoleus* using drones. Doing this work is not straightforward, and requires specialist equipment, software, and training. Data collection and processing are time consuming and expensive. There are many options for equipment to use for data acquisition (i.e., RGB, RGN, multispectral and hyperspectral cameras) and likewise many ways to process the data, with more advanced classification algorithms available through expensive commercial software such as ENVI or Erdas Imagine.

This variety of feasible approaches (and levels of investment) also makes it challenging to collect standardised data that can be legislated for, or to compare data between regions. There are also many sources of uncertainty and error due to how data are collected and processed. Environmental conditions can significantly affect the quality of input data, for example: sunglint, cloud cover, waves, wind, turbidity, refraction, depth effects, and shadows. Other potential sources of error may arise from incorrectly georeferencing or processing the imagery, and inherent variability in training polygon selection, which impacts the accuracy of classification algorithms.

Sections 9 and 10 provide some real-world case studies to demonstrate this variability and sources of error. Detailed MAM is likely very useful for scientific studies, but may be more challenging to use for routine monitoring (106Section 11.2). If it is used for routine monitoring, then a Factor of Safety (FoS) should be included into interpretation of data derived from MAM (if it is being used as an input for setting alert levels). The use of a FoS is common practice in engineering (for example structural design) and could be implemented into MAM to account for any underestimation of *Microcoleus* in aerial classifications [better to be on the safe side]. Likewise, this would be prudent if simply comparing *Microcoleus* aerial images with reference images of *Microcoleus* cover (Appendix D).

It is also possible to combine the techniques and calculations in this user guide with traditional methods for assessing *Microcoleus* cover. For example, an underwater viewer can be used to estimate average cover in a study reach. To do this accurately requires many underwater views throughout the study reach, to provide a spatially representative average. At least 20 views are recommended (Kilroy et al. 2013), although the number of views used is a trade-off between effort and precision/accuracy. This can be achieved by either a structured grid approach, or a random walk approach. The structured grid approach tries to place equidistant measurement points throughout the study reach; for example, if a river is 20 m wide, the river reach could be divided into 3 along stream sampling lines (e.g., at 5 m, 10 m and 15 m from the left bank). A team member would then walk downstream following each of these sampling lines and making underwater views every 5 or 10 m. The random walk approach is similar to a 'Wolman count', which is commonly used for estimating grain size distributions. This approach entails a random walking path downstream throughout the study reach, stopping every 5 or 10 steps to take an underwater view. When using these approaches, it is just as important to take views of areas without any *Microcoleus* cover as it is to take views of *Microcoleus* and avoid the bias introduced by 'hunting' for *Microcoleus* patches. The transect-based methods for assessing periphyton cover with underwater viewers from the New Zealand cyanobacteria guideline (MfE and MOH, 2009) can also be used. It is important to cover riffles as well as runs (unlike NEMS Periphyton, 2020), since cyanobacterial mats tend to proliferate initially in riffles.

After collecting underwater views, they are averaged to get a 'representative cover' estimate of *Microcoleus* in the study reach, and thus the full river (if the study reach is representative of the full river). Likewise, if biomass samples are taken in the study reach and processed following the procedures in Section 5, then all of the same metrics from Sections 8.1, 8.2, 8.3 can be calculated. The only other information that is needed is the total area of the study reach A_T (m^2) and the total length of the study reach L_T (m). For many rivers A_T and L_T can be estimated from satellite imagery in Google Earth (or similar). For rivers where the wetted area is significantly different during the survey than that in the aerial imagery (i.e., due to different river levels, or morphodynamic changes), then another approach may be needed. A simple estimate can be provided by manually measuring the average wetted width of the river in the study reach, then multiplying it by the length of the study reach (obtained from Google Earth or measured directly), to obtain A_T. *Microcoleus* cover, mat thickness, and mat taxonomic composition is highly heterogeneous through river reaches (i.e., riffles, runs, pools, depth and shade from riparian vegetation). Although more time consuming than simple cover estimates following MfE and MoH, (2009), the cover and particularly biomass estimation techniques provided here provide more accurate results.

All metrics in this user guide relate to either cover, biomass or cell counts, rather than toxin concentrations. This is because toxin production by *Microcoleus* is irregular and currently hard to predict (Quiblier et al. 2013; McAllister et al. 2016). Thus, it must be assumed that any *Microcoleus* mat has the potential to produce potent neurotoxins (Wood et al. 2018). The total biomass of *Microcoleus* in a river is important, because the risk of toxin production is proportional to the number of *Microcoleus* cells (three-dimensional biomass), rather than cover (which could be a thin film). Legislation and regulation should largely be based around the abundance of *Microcoleus* in a river.

11.2   Progressing MAM to routine monitoring

The framework of MAM described in this user guide could be expanded into a programme of routine monitoring of *Microcoleus* cover at various monitoring sites. While it requires some investment into initial setup, the routine monitoring process could be streamlined.

This section outlines, how such a programme could be established and structured.

11.2.1 Imagery requirements for repeatable surveys – 'reflectance'

To compare aerial surveys from different dates and lighting conditions, it is important to work with normalised data that is illumination invariant. What the sensor 'sees' is generally referred to as *radiance* data and is dependent on solar illumination. For example, *radiance* data will vary with time of the day, time of the year, cloud cover and more. This means that a spectral signature collected from training samples of *radiance* data will be difficult (or impossible) to transfer to a dataset collected under different conditions. A way around this problem is to normalise the data to *reflectance*. *Reflectance* is the ratio of reflected light to incoming light. Therefore, it is a spectral property of the material and is independent of illumination and atmospheric conditions. Spectral signatures are generally a set of normalised *reflectance* spectra and can be applied to datasets from different geographic and temporal settings. To normalise data from *radiance* to *reflectance*, there are generally two viable options: (1) using a *reflectance* tarp with a known spectral response, (2) employing a downwelling irradiance sensor. Generally, multispectral or hyperspectral cameras are deployed if reflectance data are needed (see Sections 3.2, 3.3, 6.2, and 6.3). We recommend the use of multispectral cameras for *Microcoleus* aerial monitoring.

In theory, a set of *reflectance* spectra need only be collected once for each of the classes included in the classification. The same spectral signatures can then be used for different sites and different monitoring visits. However, it is likely that different sites have different algal communities and might have different sediment composition (rock colour). Therefore, it would be recommended to develop spectral signatures specific to each site. The spectra for classes that are found at multiple sites could be combined to create a more robust spectral library.

11.2.2 Site selection and preparation

Suitable sites for routine monitoring with MAM require the same characteristics as described in Sections 2.1 and 4.1. However, to enable routine, repeat aerial surveys the installation of fixed GCPs is recommended. These GCPs will differ from those described in Section 3.5, and will likely be coloured wooden stakes (or similar) that can be driven into the river bed and banks, then left in place for months (or years). These GCPs are then surveyed once when the site is established (Section 11.2.4), but do not require repeat surveying every time a monitoring flight is conducted.

11.2.3 River conditions during surveys

For repeatable surveys that use the same library of spectral signatures, it is important that deployment conditions are equivalent. In practice this means that depth, turbidity, surface waves, surface reflections and shadows should not vary significantly between surveys. In practice it is recommend to only record data at equivalent low flows. This will avoid issues with depth changes and turbidity. It is also recommended to fly all surveys at similar times of the day (i.e. between 10 am and 2 pm).

11.2.4 First deployment (detailed) for ground truth and spectral signatures

To establish an ongoing monitoring site, an initial high-resolution MAM deployment is recommended. During this deployment the permanent GCPs will be installed and surveyed with RTK GPS. MAM is then performed to obtain the aerial imagery and illumination calibration data (i.e., tarpaulin or downwelling irradiance sensor), to enable conversion to *reflectance*. During this visit detailed ground truth measurements should be undertaken to collect sufficient training and validation points for spectrally distinctive classes. For example, a detailed RTK GPS ground truth survey (Section 5.1.1) covering *Microcoleus* and all other classes present in the study reach (i.e., wet rocks, dry rocks, green algae, film, and any other distinctive classes). It is important to collect large numbers of points that are 'Not *Microcoleus*' so that their spectral signatures can also be established.

After returning from the field, the data is processed following this user guide, with training polygons based on the RTK GPS ground truth data to create spectral signatures for all the relevant classes. An accuracy assessment is then performed using validation polygons from the same reach (but sampled at different locations from the training polygons). This process can be iterated if initial accuracy is low to include any misclassified regions/classes in the training polygons. Once sufficiently accurate, the spectral signatures from the training polygons are saved for reuse during subsequent routine monitoring surveys.

Biomass sampling is optional during this process, since routine monitoring is focused on changes in cover. Biomass will change during the season, so any conversion metrics from cover to biomass would need to be established for each subsequent survey. As discussed throughout this user guide, biomass is more accurate, but is much more intensive (expensive) and is probably only suitable for detailed scientific studies, or less frequent 'benchmark' surveys during a season.

11.2.5 Routine monitoring

After a site has been prepared properly and spectral libraries have been developed, a monitoring visit does not require the use of surveying equipment. The fieldwork would only consist of repeating a predetermined flight path to collect aerial imagery and recording solar irradiance (i.e. calibration tarpaulin, or downwelling irradiance sensor).

Back in the office, most of the data processing through Agisoft Metashape can be batch processed. However, it is important to identify and select GCPs to enable the calculation of area covered by *Microcoleus* (if only percentage coverage is required, then a completely scripted workflow is possible). If GCPs are used, manually follow the steps outlined in Section 6.1 until step 3 'Add markers'. The subsequent steps can all be added to a batch processing script (accessible through Agisoft Metashape under Workflow -> Batch Process), including exporting the resulting orthomosaics.

Classification is then conducted following the procedure described in Section 7. However, instead of collecting a new set of training samples and spectral signatures, an existing .scp training file is loaded (from Section 11.2.4) with these spectral signatures used for classification.

If *Microcoleus* cover exceeds pre-defined thresholds, decisions could then be made to either perform biomass sampling, validate the results with a detailed survey, or issue public notifications and warnings.

It may also be possible to apply libraries of spectral signatures at multiple rivers and sites, however for the first season it is recommended to do a detailed survey at each site. Ideally this survey would be repeated mid-season, and end of season to prove that spectral libraries are consistent. The spectra of *Microcoleus* are not likely to be problematic, but the spectra that make up the 'Not *Microcoleus*' class are more likely to vary between sites, or may change throughout the year with overall periphyton growth. If spectral libraries are found to be consistent, then routine aerial surveying will be relatively easy and efficient. External specialists may be used for establishing monitoring sites at the start of the season, and to undertake the development of spectral libraries, with testing of their consistency and broader applicability between sites.

12   Conclusions and recommendations

The development of the *Microcoleus* Aerial Monitoring user guide was requested in response to increased use of unmanned aerial vehicles by councils around New Zealand. It provides an overview of the hardware, software, field methods, lab methods and data analysis needed for remote sensing benthic cyanobacteria cover and biomass.

Most of the methods and equipment in this user guide are equally applicable to other remote sensing tasks. Through the detailed case studies in this user guide (Sections 9 and 10), the potential of MAM for quantification of 2D cover and biomass is demonstrated. Yet, undertaking this work is not trivial, and there are many potential sources of uncertainty, which may make it challenging to apply for routine monitoring. Examples of challenges specific to through-water remote sensing of *Microcoleus* are: turbidity/visual clarity, depth, shadows, reflections off the water surface, limited spectral separability from wet bed material, and the small spatial scale of patches. Examples of challenges general to remote sensing of cover are: collection of sufficient ground truth data, precise alignment of processed aerial imagery and ground truth data, the time taken to collect and process data. One of the biggest challenges for standardising these methods is the wide range of choices for classification algorithms, with inherent variability in the classification predictions between algorithms, and significant time to train and tune the classifications.

The use of MAM is recommended for detailed scientific studies where 2D maps of cover are needed, particularly for investigation of change vs time, as a function of environmental conditions (Wood et al. 2020). For routine monitoring, we recommend the use of underwater viewers (MfE and MOH 2009), visual comparison of aerial imagery with reference cover levels (Appendix D), or establishing monitoring sites with fixed ground control points and libraries of reflectance spectral signatures (Section 11.2). In situations when the use of MAM is considered appropriate, we recommend the use of multispectral aerial imagery focused on the spectral range from 500–650 nm. For the three classification algorithms tested in QGIS we found that Minimum Distance was the most accurate and consistent. If routine monitoring with MAM is undertaken, then it is recommended to invest in proprietary image analysis software that has more advanced classification algorithms and features.

For biomass assessment at the reach and river scale, the methods in this user guide can be combined with cover estimates from aerial imagery, or rigorous surveys with underwater viewers (Section 11.1). However, the detailed biomass and cover assessment techniques provided in this user guide will have an associated higher cost for data collection and processing (including lab analysis), compared to simple cover assessment with underwater viewers and sampling transects. Ultimately the question of which approach is appropriate will come down to the accuracy of data needed, and the frequency of monitoring needed. The main advantage of the approaches in this user guide is the combination of biomass samples with cover data to provide a more rigorous assessment of the abundance of *Microcoleus*, which can provide a risk to river users either as attached mats, or downstream risk from detachment and potential accumulation at river banks. Further work is needed to investigate mat detachment, drift, accumulation, as well as toxin production, concentration, and degradation in detached mats.

13   Acknowledgements

14   Glossary of abbreviations and terms

ACE	Adaptive Cosine Estimator (image classification algorithm).
AFDM	Ash-Free Dry Mass. Also known as Ash-Free Dry Weight (AFDW), or loss on ignition.
Agisoft Metashape	Software for creating georeferenced orthomosaics and DEMs from input imagery. Agisoft Metashape was previously known as Agisoft Photoscan.
Band-pass filter	A filter that allows transmission only within a narrow band. In the context of optics and multispectral cameras this corresponds to transmission of specific wavelengths of light, while wavelength outside this band are blocked.
BV	Biovolume.
CAA	Civil Aviation Authority.
chl a	Chlorophyll a (usually in mg/m^2).
CIELab	Colour space for processing RGB imagery that more closely matches human vision.
CNN	Convolutional Neural Network (used for image classification).
DM	Dry mass (usually in mg/m^2).
DEM	Digital Elevation Model.
Drone	Synonym for Unmanned Aerial Vehicle (UAV).
DSM	Digital Surface Model. Provides the elevation of the top of the landscape (i.e., tree canopies, water surface, and land) as opposed to a DEM which typically provides ground elevation underneath vegetation.
FoV	Field of View.
FWHM	Full Width at Half Maximum. Optical filters have a wavelength where maximum light is transmitted, the bandwidth between the lower wavelength that provides half the maximum transmission and the upper wavelength that provides half the maximum transmission is the FWHM.
GCP	Ground Control Point.

Georeferenced Orthomosaic	2D photo map that is accurately scaled and in real world coordinates. Georeferenced orthomosaics can then be opened in software such as ArcMap, ENVI, QGIS, or Matlab for image classification and further processing.
Gimbal	Device under a drone that holds a camera and maintains its orientation (usually nadir/vertical) independently of the UAV orientation. This avoids changes in camera orientation as the UAV flies, or in response to atmospheric turbulence.
GPS	Global Positioning System.
GWRC	Greater Wellington Regional Council.
HSV	Hue Saturation Value colour space for processing RGB imagery.
IMU	Inertial Measurement Unit. Used to determine orientation of hyperspectral camera.
LAWA	Land, Air, Water Aotearoa
MD	Minimum Distance (classification algorithm).
MfE	Ministry for the Environment.
Microcoleus autumnalis	New name of the of the toxic cyanobacterium originally known as *Phormidium autumnale* (Strunecký et al. 2013; Wood et al. 2018). The original name has also been used throughout this user guide for consistency with the body of literature on toxic cyanobacteria management in New Zealand and regional council monitoring policies.
MoH	Ministry of Health.
ML	Maximum Likelihood (classification algorithm).
MP	Mega Pixels (how many million pixels a camera sensor has).
Nadir	Vertically oriented (i.e., parallel with the force of gravity). Nadir imagery is captured from a camera in a gimbal under an aircraft and is used to make maps.
NDVI	Normalised Difference Vegetation Index.
NEMS	National Environmental Monitoring Standards
NIR	Near Infrared.
NIWA	National Institute of Water and Atmospheric Research.

Orthomosaic	2D photo map created by SfM software.
Pix4D	SfM software for creating georeferenced orthomosaics and DEMs from input imagery.
Phormidium autumnale	Original name of the toxic cyanobacteria *Microcoleus autumnalis* (Strunecký et al. 2013; Wood et al. 2018). The original name has been used throughout this user guide for consistency with the body of literature on toxic cyanobacteria management in New Zealand and regional council monitoring policies.
Planform Area	Planform area is the XY projection of an objects area (i.e., the area of an object when viewing it on a map or georeferenced orthomosaic). This is important to understand for the projection of 3D objects such as rocks to 2D maps (i.e., a sphere has surface area $4\pi r^2$, but planform area of only πr^2).
PPK GPS	Post Processed Kinematic Global Positioning System.
RA	Relative Abundance.
Raster	A rectangular grid of data (i.e., image matrices) compared to point or vector data.
RGB	Red Green Blue. This is the standard imagery collected by digital cameras.
RGN	Red Green Near-Infrared (also known as Vis-NIR cameras).
ROI	Region Of Interest (usually a polygon from which training or validation pixels are extracted).
RTK GPS	Real Time Kinematic Global Positioning System.
SAM	Spectral Angle Mapper (image classification algorithm).
SfM	Structure from Motion. This is a technique where multiview stereo algorithms are used to stitch aerial imagery together to create georeferenced orthomosaics and digital elevation models. The software Agisoft Metashape or Pix4D are recommended.
SVM	Support Vector Machines (image classification algorithm).
UAS	Unmanned Aerial System. Synonym for UAV, Drone, RPA (Remotely Piloted Aircraft), and RPAS (Remotely Piloted Aircraft System).
UAV	Unmanned Aerial Vehicle.
Vis-NIR	Visible to Near Infrared (also known as VNIR or RGN).
VNC	Visual Navigation Chart.

15 References

Agisoft. (2021) Agisoft Metashape User Manual: Professional Edition, Version 1.7. https://www.agisoft.com/pdf/metashape-pro_1_7_en.pdf

Biggs, B., Kilroy, C. (2000) Stream periphyton monitoring manual. NIWA.

Biggs, H. (2020). Aquatic vegetation aerial monitoring. In: Unmanned Aerial Remote Sensing - UAS for Environmental Applications (Ed. D. Green). CRC Press.

Blaschke, T. (2010) Object based image analysis for remote sensing. ISPRS journal of photogrammetry and remote sensing, 65(1), 2-16.

Cao, F., Guichard, F., Hornung, H., Masson, L. (2009) Sensor information capacity and spectral sensitivities. In Digital Photography V (Vol. 7250, p. 725006). International Society for Optics and Photonics.

Congalton, R. Green, K. (2009).Assessing the Accuracy of Remotely Sensed Data: Principles and Practices. CRC Press, Boca Raton, Florida.

Congedo, L. (2021) Semi-Automatic Classification Plugin: A Python tool for the download and processing of remote sensing images in QGIS. Journal of Open Source Software, 6(64), 3172.

Edler, L., Elbrächter, M. (2010) The utermöhl method for quantitative phytoplankton analysis. In: Microscopic and Molecular Methods for Quantitative Phytoplankton Analysis (Eds. B. Karlson, C. Cusack, & E. Bresnan), UNESCO.

Hamill, K. (2001) Toxicity in benthic freshwater cyanobacteria (blue-green algae): First observations in New Zealand. New Zealand Journal of Marine and Freshwater Research, 35(5), 1057-1059.

Heath M., Wood, S., Ryan, K. (2010) Polyphasic assessment of fresh-water benthic mat-forming cyanobacteria isolated from New Zealand. FEMS Microbiology Ecology, 73(1), 95-109.

Heath, M., Wood, S., Ryan, K. (2011) Spatial and temporal variability in *Phormidium* and associated anatoxin production in two New Zealand rivers. Aquatic Microbial Ecology, 64(1), 69-79.

Heath, M., Wood, S., Brasell, K., Young, R., Ryan K. (2012) Hutt River *Phormidium* habitat suitability criteria and hydraulic habitat assessment. Report No. MH01. 2012 prepared for Greater Wellington Regional Council by the School of Biological Sciences, Victoria University of Wellington.

Heath, M., Greenfield, S. (2016) Benthic cyanobacteria blooms in rivers in the Wellington Region: Findings from a decade of monitoring and research. Greater Wellington Regional Council, Publication No. GW/ESCI-T-16/32, Wellington.

Heath, M. (2018) Learning from experience – drones in action and potential for monitoring to the Ministry for the Environment cyanobacteria guidelines review working group 07 May 2018. Greater Wellington Regional Council, Wellington.

Hempel, S., Heath, M., Olds, J., Wood, S., Seah, W., Ryan, K. (2014) Monitoring benthic *Phormidium* blooms using imagery gathered with an Unmanned Aerial Vehicle (UAV). A report prepared for Greater Wellington Regional Council by Victoria University of Wellington.

Hillebrand, H., Durselen, C.D., Kirschtel, D., Pollingher, U., Zohary, T. (1999) Biovolume calculation for pelagic and benthic microalgae. Journal of Phycology, 35(2), 403-424.

Hunter, P., Tyler, A., Carvalho, L., Codd, G., Maberly, S. (2010) Hyperspectral remote sensing of cyanobacterial pigments as indicators for cell populations and toxins in eutrophic lakes. Remote Sensing of Environment, 114(11), 2705-2718.

Husson, E., Hagner, O., Ecke, F. (2014) Unmanned aircraft systems help to map aquatic vegetation. Applied Vegetation Science, 17(3), 567-577.

Husson, E., Ecke, F., Reese, H. (2016) Comparison of manual mapping and automated object-based image analysis of non-submerged aquatic vegetation from very-high-resolution UAS images. Remote Sensing, 8(9), 724.

Ibraheem, N., Hasan, M., Khan, R. Mishra, P. (2012) Understanding color models: a review. ARPN Journal of Science and Technology, 2(3), 265-275.

Kilroy, C., Biggs, B., Death, R. (2008) A periphyton monitoring plan for the Manawatu-Wanganui region. NIWA ClientReportCHC2008-03. Christchurch, New Zealand.

Kilroy, C., Booker, D., Drummond, L., Wech, J., Snelder, T. (2013) Estimating periphyton standing crop in streams: a comparison of chlorophyll *a* sampling and visual assessments. New Zealand Journal of Marine and Freshwater Research, 47(2), 208-224.

Klemas, V. (2015) Coastal and environmental remote sensing from unmanned aerial vehicles: An overview. Journal of Coastal Research, 31(5), 1260-1267.

Kudela, R., Palacios, S., Austerberry, D., Accorsi, E., Guild, L., Torres-Perez, J. (2015) Application of hyperspectral remote sensing to cyanobacterial blooms in inland waters. Remote Sensing of Environment, 167, 196-205.

Martínez-Carricondo, P., Agüera-Vega, F., Carvajal-Ramírez, F., Mesas-Carrascosa, F., García-Ferrer, A., Pérez-Porras, F. (2018) Assessment of UAV-photogrammetric mapping accuracy based on variation of ground control points. International journal of applied earth observation and geoinformation, 72, 1-10.

McAllister, T., Wood, S., Hawes, I. (2016) The rise of toxic benthic *Phormidium* proliferations: a review of their taxonomy, distribution, toxin content and factors regulating prevalence and increased severity. Harmful Algae, 55(1), 282-294.

McAllister, T., Wood, S., Atalah, J., Hawes, I. (2018) Spatiotemporal dynamics of *Phormidium* cover and anatoxin concentrations in eight New Zealand rivers with contrasting nutrient and flow regimes. Science of the Total Environment, 612(1), 71-80.

Mez, K., Beattie, K., Codd, G., Hanselmann, K., Hauser, B., Naegeli, H., Preisig, H. (1997) Identification of a microcystin in benthic cyanobacteria linked to cattle deaths on alpine pastures in Switzerland. European Journal of Phycology, 32(2), 111-117.

Ministry for the Environment and Ministry of Health. (2009) New Zealand guidelines for managing cyanobacteria in recreational fresh waters – interim guidelines. Prepared for the Ministry for the Environment and the Ministry of Health by Wood, S., Hamilton, D., Paul, W., Safi, K. & Williamson, W. Ministry for the Environment, Wellington.

NEMS Periphyton. (2020) Sampling and measuring periphyton in wadable rivers and streams. Prepared for MfE by Hayward, S., Downs, P., Heath, M., Patterson, M., Hodson, R., Kilroy, C., Milne, J. & Greenfield, S. Ministry for the Environment, Wellington.

Overstreet, B., Legleiter, C. (2017) Removing sun glint from optical remote sensing images of shallow rivers. Earth Surface Processes and Landforms, 42(2), 318-333.

Quiblier, C., Wood, S., Echenique-Subiabre, I., Heath, M., Villeneuve, A., Humbert, J-F. (2013) A review of current knowledge on toxic benthic freshwater cyanobacteria – ecology, toxin production and risk management. Water Research, 47(15), 5464-5479.

Resonon. (2021a) Spectronon User Manual V3.4.0. Resonon Inc, Bozeman, Montana.

Resonon. (2021b) Airborne User Manual V6.3. Resonon Inc, Bozeman, Montana.

Richards, J. (2013) Remote sensing digital image analysis (5th Edition). Springer.

Rowan, K. (1989) Photosynthetic pigments of algae. Cambridge University Press.

Saini, D., Pabbi, S., Shukla, P. (2018) Cyanobacterial pigments: Perspectives and biotechnological approaches. Food and Chemical Toxicology, 120, 616-624.

Schanda, J. (2007) Colorimetry: understanding the CIE system. John Wiley & Sons. Hoboken, New Jersey.

Schlüter, L., Lauridsen, T., Krogh, G., Jorgensen, T. (2006) Identification and quantification of phytoplankton groups in lakes using new pigment ratios–a comparison between pigment analysis by HPLC and microscopy. Freshwater Biology, 51(8), 1474-1485.

Scott J., Marcarelli A. (2012) Cyanobacteria in freshwater benthic environments. In: Ecology of cyanobacteria II: their diversity in space and time (Ed. Whitton, B.). Springer.

Shi, K., Zhang, Y., Qin, B., Zhou, B. (2019) Remote sensing of cyanobacterial blooms in inland waters: present knowledge and future challenges. Science Bulletin, 64(20), 1540-1556.

Stancheva, R., Fetscher, A., Sheath, R. (2012) A novel quantification method for stream-inhabiting, non-diatom benthic algae, and its application in bioassessment. *Hydrobiologia*, 684(1), 225-239.

Štroner, M., Urban, R., Reindl, T., Seidl, J., Brouček, J. (2020) Evaluation of the Georeferencing Accuracy of a Photogrammetric Model Using a Quadrocopter with Onboard GNSS RTK. Sensors, 20(8), 2318.

Strunecký, O., Komárek, J., Johansen, J., Lukešová, A., Elster, J. (2013) Molecular and morphological criteria for revision of the genus *Microcoleus* (Oscillatoriales, Cyanobacteria). Journal of Phycology, 49(6), 1167-1180.

Tomaštík, J., Mokroš, M., Surový, P., Grznárová, A., Merganič, J. (2019) UAV RTK/PPK Method—An Optimal Solution for Mapping Inaccessible Forested Areas?. Remote sensing, 11(6), 721.

Wood, S., Selwood, A., Rueckert, A., Holland, P., Milne, J., Smith, K., Smits, B., Watts, L., Cary, C. (2007) First report of homoanatoxin-a and associated dog neurotoxicosis in New Zealand. Toxicon, 50(2), 292-301.

Wood, S., Heath, M., Kuhajek, J., Ryan, K. (2010) Fine-scale spatial variability in anatoxin-a and homoanatoxin-a concentrations in benthic cyanobacterial mats: Implications for monitoring and management. Journal of Applied Microbiology, 109(6), 2011-2018.

Wood, S., Hawes, I., McBride, G., Truman, P., Dietrich, D. (2015) Advice to inform the development of a benthic cyanobacteria attribute. Prepared for Ministry for the Environment. Cawthron Report No. 2752.

Wood, S., Puddick, J., Fleming, R., Heussner, A. (2017) Detection of anatoxin-producing *Phormidium* in a New Zealand farm pond and an associated dog death. New Zealand Journal of Botany, 55(1), 36-46.

Wood, S., Puddick, J., Thomson-Laing, G., Hawes, I., Safi, K., McBride, G., Hamilton, D. (2018) Review of the 'New Zealand Guidelines for Cyanobacteria in Recreational Fresh Waters' - 2018. Prepared for the New Zealand Ministry for the Environment. Cawthron Report No. 3233.

Wood, S., Kelly, L., Bouma-Gregson, K., Humbert, J., Laughinghouse IV, H., Lazorchak, J., Davis, T. (2020) Toxic benthic freshwater cyanobacterial proliferations: challenges and solutions for enhancing knowledge and improving monitoring and mitigation. Freshwater Biology, 65(10), 1824-1842.

Appendix A Workflow for recording and processing RGB images to quantify *Microcoleus* cover (and biomass)

Select RGB Camera and Aircraft (e.g. DJI Phantom 4 Pro). [3.1,3.4]

↓

Plan mission, obtain flight permissions and ensure flights comply with CAA regulations. [4.1]

↓

Layout and survey ground control points. [3.5, 4.2]

↓

Perform flights with image overlap of 80% front and 60% side. [4.3]

↓

Collect ground truth data for cover and biomass. [5.1, 5.2]

↓

Process biomass samples for *Microcoleus* specific abundance metrics. [5.4, 5.5]

↓

Process images and ground control point coordinates with a structure from motion software such as Agisoft Metashape to produce a georeferenced orthomosaic. [6.1]

↓

Load the georeferenced orthomosaic into an aerial imagery analysis program of choice (e.g. QGIS, ENVI, Erdas Imagine). [7.1]

↓

Demarcate wetted boundaries of the river. [7.4]

↓

Select training and validation polygons for classes of interest. [7.8]

↓

Run supervised classification algorithm (e.g. MD, ML, SAM). [7.9]

↓

Assess the accuracy of the classification with validation data. [7.11]

↓

Combine classification results with ground truth biomass data and measurements of the size of the classification area. Calculate biomass and cover estimates at the reach and river scale. [8]

Appendix B   Workflow for recording and processing multispectral to quantify *Microcoleus* cover (and biomass)

```
┌─────────────────────────────────────────────────────────────┐
│        Select Multispectral Camera and Aircraft. [3.2, 3.4]  │
└─────────────────────────────────────────────────────────────┘
                              ↓
┌─────────────────────────────────────────────────────────────┐
│   Plan mission, obtain flight permissions and ensure flights │
│            comply with CAA regulations. [4.1]                │
└─────────────────────────────────────────────────────────────┘
                              ↓
┌─────────────────────────────────────────────────────────────┐
│        Layout and survey ground control points. [3.5, 4.2]   │
└─────────────────────────────────────────────────────────────┘
                              ↓
┌─────────────────────────────────────────────────────────────┐
│  Perform flights with image overlap of 80% front and 60% side. [4.3] │
└─────────────────────────────────────────────────────────────┘
                              ↓
┌─────────────────────────────────────────────────────────────┐
│     Collect ground truth data for cover and biomass. [5.1, 5.2] │
└─────────────────────────────────────────────────────────────┘
                              ↓
┌─────────────────────────────────────────────────────────────┐
│  Process biomass samples for *Microcoleus* specific abundance │
│                    metrics. [5.4, 5.5]                       │
└─────────────────────────────────────────────────────────────┘
                              ↓
┌─────────────────────────────────────────────────────────────┐
│   Process images and ground control point coordinates with a │
│  structure from motion software such as Agisoft Metashape to │
│         produce a georeferenced orthomosaic. [6.2]           │
└─────────────────────────────────────────────────────────────┘
                              ↓
┌─────────────────────────────────────────────────────────────┐
│   Load the georeferenced orthomosaic into an aerial imagery  │
│  analysis program of choice (e.g. QGIS, ENVI, Erdas Imagine). [7.1] │
└─────────────────────────────────────────────────────────────┘
                              ↓
┌─────────────────────────────────────────────────────────────┐
│        Demarcate wetted boundaries of the river. [7.4]       │
└─────────────────────────────────────────────────────────────┘
                              ↓
┌─────────────────────────────────────────────────────────────┐
│  Select training and validation polygons for classes of interest. [7.8] │
└─────────────────────────────────────────────────────────────┘
                              ↓
┌─────────────────────────────────────────────────────────────┐
│   Run supervised classification algorithm (e.g. MD, ML, SAM). [7.9] │
└─────────────────────────────────────────────────────────────┘
                              ↓
┌─────────────────────────────────────────────────────────────┐
│  Assess the accuracy of the classification with validation data. [7.11] │
└─────────────────────────────────────────────────────────────┘
                              ↓
┌─────────────────────────────────────────────────────────────┐
│  Combine classification results with ground truth biomass data and │
│  measurements of the size of the classification area. Calculate │
│   biomass and cover estimates at the reach and river scale. [8] │
└─────────────────────────────────────────────────────────────┘
```

Appendix C Workflow for recording and processing hyperspectral imagery to obtain reference spectra for *Microcoleus* and select band pass filters for multispectral cameras

Select Hyperspectral Camera and Aircraft. [3.3, 3.4]

↓

Plan mission, obtain flight permissions and ensure flights comply with CAA regulations. [4.1]

↓

Setup Hyperspectral Camera and layout tarpaulin. [3.3.1, 3.3.2]

↓

Perform flights (50% side overlap recommended). [4.3]

↓

Collect RTK GPS ground truth data for each class of interest. [5.1.1]

↓

Process hyperspectral aerial imagery (i.e. raw data to reflectance with the downwelling irradiance sensor or calibration tarpaulin, and georectify the hyperspectral aerial imagery). [6.3]

↓

Create polygons around classes of interest and export reflectance spectra. [6.3]

↓

Interpret the reflectance spectra and use them to select band pass filters for multispectral cameras, or to inform which bands to process for larger scale surveys and classifications. [3.2.1, 7.3]

Appendix D Reference images of *Microcoleus* cover levels

Reference images of *Microcoleus* cover levels are provided below. Both RGB and multispectral images are shown, with the multispectral images showing bands B1, B2, B3 from an Airphen camera which are 10 nm bands, centred on the wavelengths 530, 570, and 622 nm. Cover levels are obtained from subsampling aerial imagery classifications and provide a best estimate.
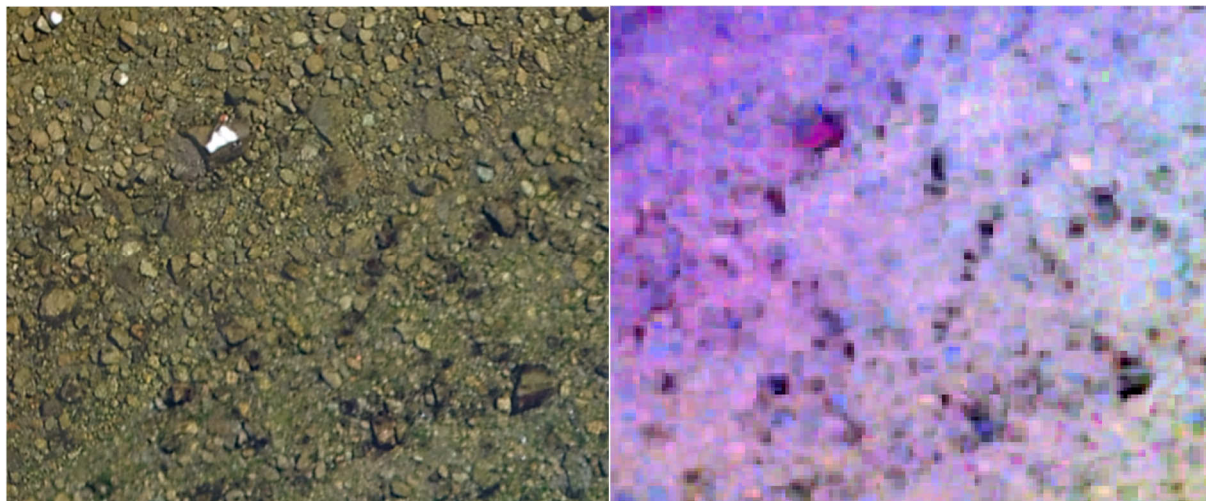
Figure D-1: **Reference cover levels 5% (Left: RGB, Right: Multispectral).**
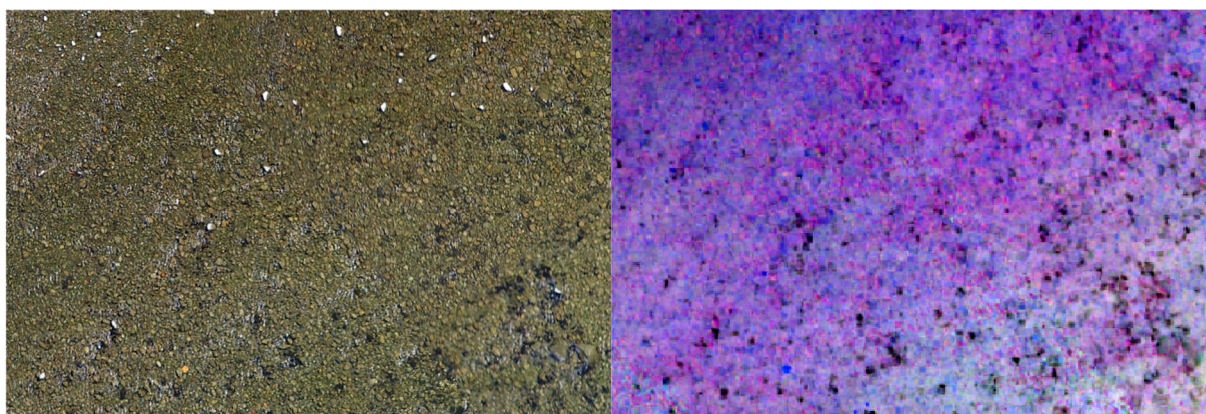
Figure D-2: **Reference cover levels 6% (Left: RGB, Right: Multispectral).**
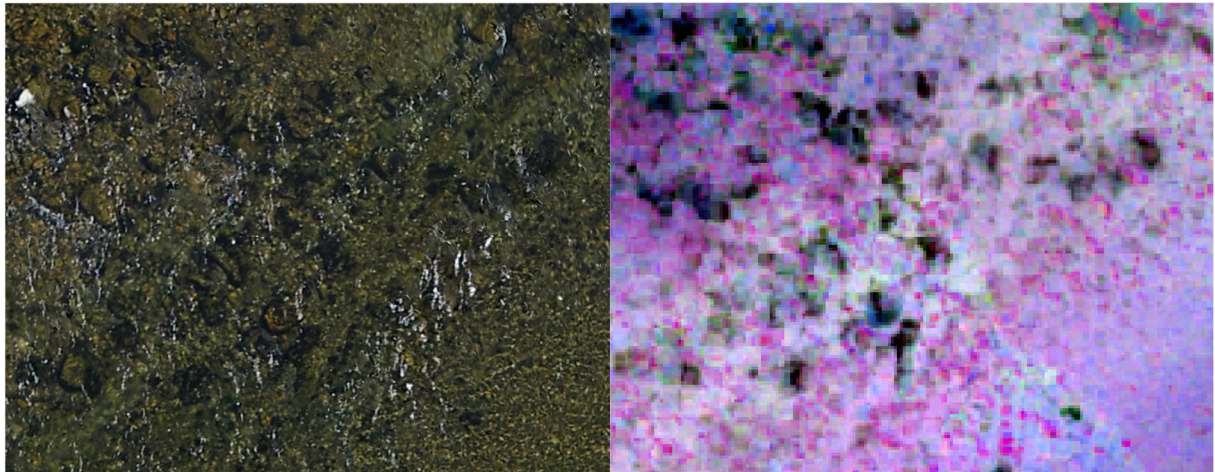
Figure D-3:   **Reference cover levels 13% (Left: RGB, Right: Multispectral).**
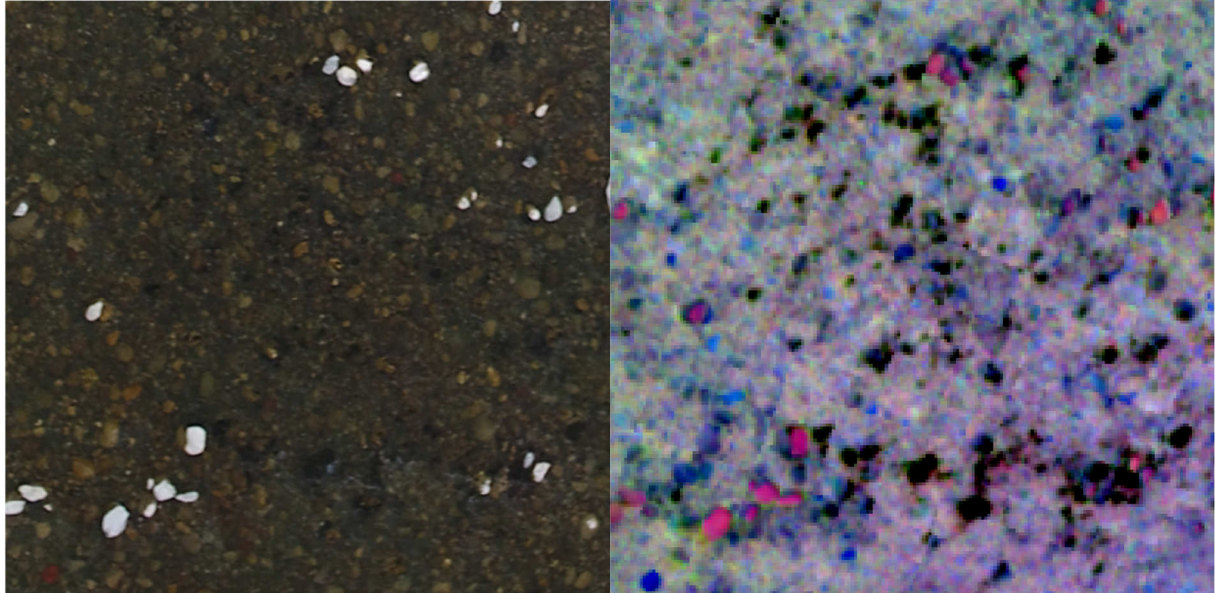
Figure D-4:   **Reference cover levels 14% (Left: RGB, Right: Multispectral).**
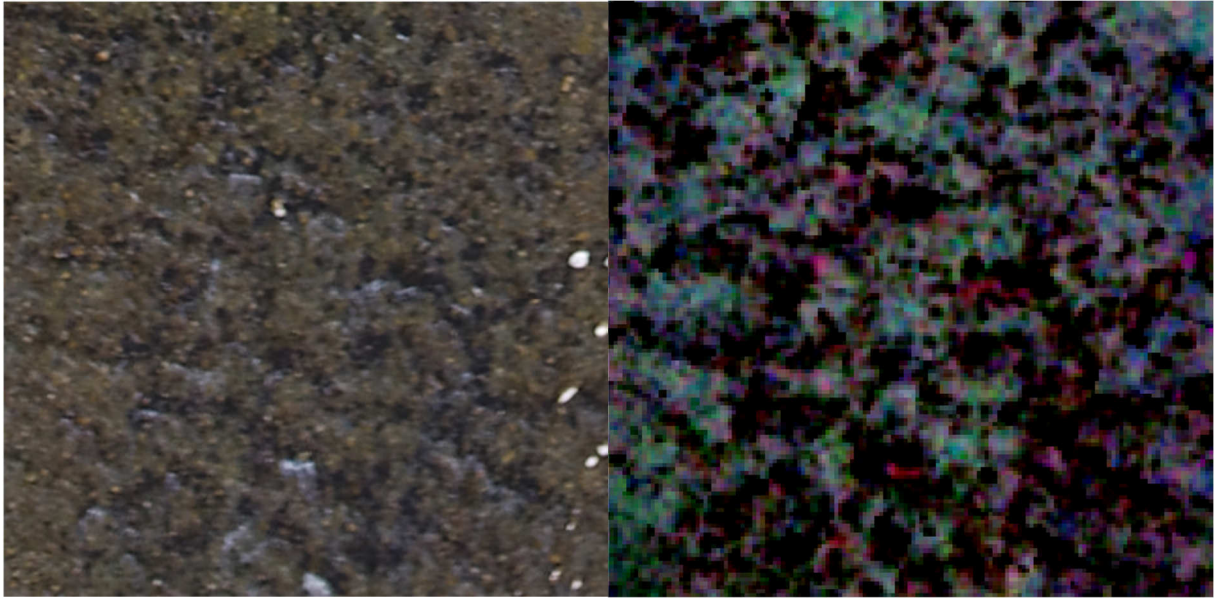
Figure D-5:   Reference cover levels >20% (Left: RGB, Right: Multispectral).

Appendix E Example of council decision tree for *Microcoleus* monitoring

An example decision tree for *Microcoleus* monitoring in the Greater Wellington region is shown below. Although MAM is not recommended for rapid routine monitoring, it does provide a useful tool for assessment of cover and/or biomass at larger spatial scales, or when nearing alert levels, or for communication of risks to the public.